INHIBITION OF AN *E*. COLI GLYCOSYLASE, MUTM, BY NON-NATIVE METALS

by

MIER AN

LAURA S. BUSENLEHNER, COMMITTEE CHAIR
STEPHEN A. WOSKI
SHANLIN PAN
CAROLYN J. CASSADY
STEVAN MARCUS

A DISSERTATION

Submitted in partial fulfillment of the requirements
for the degree of Doctor of Philosophy
in the Department of Chemistry
in the Graduate School of
The University of Alabama

TUSCALOOSA, ALABAMA

2013

ABSTRACT

Non-native metals are well recognized carcinogens; however, most exhibit low mutagenicity. One route by which metals could contribute to carcinogenesis is by inhibition of crucial DNA repair processes. The protein targets and mechanism of inhibition, however, are not fully understood. DNA repair proteins that contain zinc finger motifs are potential targets because of their high affinity for metal ions. Insight into the ability of non-native metals to displace the native metal, zinc, and the mechanism they use to inhibit protein function is needed to fully understand this pathway's contribution to metal-induced cancer. In this dissertation, we probe MutM, an *Escherichia coli* zinc finger–containing DNA glycosylase/AP lyase that excises oxidized guanine bases, 8-oxoguanine, from double stranded DNA. We identify that Zn(II)–, Cd(II)– and Co(II)–MutM complexes coordinate metal ions in the zinc finger motif in a 1:1 stoichiometric ratio. We demonstrate, for the first time, that Cd(II)binding to the MutM zinc finger affects the recognition of 8-oxoguanine containing DNA and inhibits the glycosylase activity, the first step in the mechanism. However, Co(II)–MutM retains most of the native enzymatic activity, demonstrating the specificity for certain non-native metals. Furthermore, we characterize the conformational and dynamic changes of MutM caused by Cd(II) binding that contribute to the loss of glycosylase activity. This is the first study to relate non-native metal induced changes in structure of zinc finger DNA repair proteins to the mechanism of metal inhibition.

LIST OF ABBREVIATIONS AND SYMBOLS

% v/v	Percent volume-to-volume
αKG	α-Ketoglutaric acid
ε	Extinction coefficient
ε_{280}	Extinction coefficient at 280 nm
μg	Microgram
6-4 PPs	6-4 Photoproducts
8-oG	8-Oxoguanine
A	Adenine
Å	Angstrom
AA	Atomic absorption
ADA	Adenosine deaminase A
Al	Aluminum
AP	Apurinic
Arg	Arginine
As	Arsenic
Asn	Asparagine
BER	Base excision repair
bp	Base pairs
C	Cytosine

CCHH	Cysteine-Cysteine-Histidine-Histidine
CCHC	Cysteine-Cysteine-Histidine-Cysteine
CCCC	Cysteine-Cysteine-Cysteine-Cysteine
Cd	Cadmium
CD	Circular dichroism
CHA	Continuous hyperchromicity assay
cm^{-1}	Inverse centimeter
Co	Cobalt
CPDs	Cyclobutane pyrimidine dimers
Cr	Chromium
Cu	Copper
Cys	Cysteine
D	Deuterium
DNA	Deoxyribonucleic acid
dRbl	Deoxyribitol
dsDNA	Double stranded DNA
DTNB	5,5'-Dithio-bis(2-nitrobenzoic) acid
E. coli	*Escherichia coli*
EDTA	Ethylenediaminetetraacetic acid
EMSA	Electrophoresis mobility shift assay
EPA	Environmental Protection Agency
EXAFS	Extended x-ray absorption fine structure
Fe	Iron

Fpg	Formamidopyrimidine glycosylase
G	Guanine
GDH	L-glutamic dehydrogenase
Glu	Glutamate
Gly	Glycine
H2TH	Helix2-turn-helix
HCL	Hollow cathode lamp
HDX–MS	Hydrogen/Deuterium exchange–mass spectrometry
HEPES	4-(2-hydroxyethyl)-1-piperazineethanesulfonic acid, free acid
Hg	Mercury
His	Histidine
hOGG1	Human 8-oxoguanine glycosylase
HPLC	High performance liquid chromatography
hXPA	Human xeroderma pigmentosum A protein
IARC	International Agency for Research on Cancer
IPTG	Isopropyl-β-D-thiogalactopyranoside
KCl	Potassium chloride
K_d	Dissociation constant
kDa	kilodalton
KH_2PO_4	Potassium dihydrogen phosphate monobasic
K_m	Michealis–Menton constant
LB	Luria–Burtani
LC	Liquid chromatography

LFSE	Ligand field stabilization energy
LMCT	Ligand–Metal charge transfer
Lys	Lysine
M	Molar
M^{-1}	Inverse molar
MBD	Minimalbinding domain
Met	Methionine
mg	Milligram
$MgCl_2$	Magnesium chloride
mL	Milliliter
mm	Millimeter
mM	Millimolar
mM^{-1}	Inverse millimolar
MMR	Mismatch repair
MS	Mass spectrometry
MT	Metallothionein
MutM	FormamidopyrimidineDNA glycosylase
N	Nitrogen
$NaBH_4$	Sodium borohydride
NaCl	Sodium chloride
NADH	β-Nicotinamide adenine dinucleotide 2'-phosphate
NaH_2PO_4	Sodium dihydrogen phosphate monobasic
NEM	*N*-Ethylmaleimide

NER	Nucleotide excision repair
Ni	Nickel
nm	Nanometer
nM	Nanomolar
NMR	Nuclear magnetic resonance
NTB^-	2-Nitro-5-thiobenzoate anion
O	Oxygen
OD_{600}	Optical density at 600 nanometers
PAR	4-(2-pyridylaza)resorcinol
PARP	Poly(ADP-ribose) polymerase
Pb	Lead
PEI	Polyethyleneimine
Phe	Phenylalanine
PMPS	4-(hydroxymercury)benzoic acid sodium salt
PMSF	Phenylmethylsulfonylfluoride
ppm	Parts per million
Pro	Proline
RNA	Ribonucleic acid
ROS	Reactive oxygen species
RPA	Replication protein A
rpm	Revolutions per minute
S	Sulfur
SDS–PAGE	Sodium dodecyl sulfate–polyacrylamide gel electrophoresis

ssDNA	Single stranded DNA
T	Thiamine
TBE	Tris–Borate–EDTA
TCEP	Tris (2-carboxyethyl)-phosphine hydrochloride
TE	Tris-EDTA
TFIIIA	Transcription factor–III A
Tyr	Tyrosine
UV	Ultra–Violet
V	Volts
XPAzf	Xeroderma pigmentosum A zinc finger peptide
Zn	Zinc

ACKNOWLEDGMENTS

This dissertation would not have been possible without the training and guidance of my research advisor, Prof. Laura. S. Busenlehner. I sincerely appreciate her support and encouragement throughout my studies.

I would also like to thank my committee members, Prof. Stephen A. Woski, Prof. Carolyn J. Cassady, Prof. Shanlin Pan, and Prof. Stevan Marcus for their valuable advice and suggestions throughout my graduate studies.

The financial support of the National Science Foundation is gratefully acknowledged. I am also appreciative of the support from The University of Alabama and the Chemistry Department. I would also like to acknowledge the current and past group members of Dr. Busenlehner's laboratory, in particular Harsimran Singh, Leslie Gentry and Yu Wang for their support throughout my studies. I am also grateful to Prof. Patrick A. Frantom for his advice in the enzymatic assays, Prof. Marco Bonizzoni for allowing me to use the plate reader, and Dr. Qiaoli Liang for assistance in the mass spectrometry.

Finally, I would like to thank my family for their patience, love, and support.

CONTENTS

LIST OF TABLES

LIST OF FIGURES

CHAPTER 1

INTRODUCTION

1.1 METAL-INDUCED CARCINOGENESIS

The original definition of "heavy metal" is based on the atomic weight or the specific gravity of the metal. Metals with specific gravities greater than 5 are classified as heavy metals. In recent life science studies, however, the concept of "heavy metal" includes metals and semi-metals with potential human or environmental toxicity.Here, we will refer them as non-native metals, as compared to native metals like zinc, copper, and iron. Humans may be exposed to non-native metals through ingestion, inhalation or skin absorption, which could lead to metal toxicity. Metal toxicity depends on the specific metal, the dose during exposure, whether exposure is acute or chronic, and the chemical form and/or oxidization state of the metal. Metal–induced carcinogenesis is one of the biggest concerns of chronic non-native metal exposure. Metals including As(III), Cr(VI), Cd(II) and Ni(II) are classifiedGroup 1carcinogens by the International Agency for Research on Cancer (IARC) and Environmental Protection Agency (EPA).[1] The molecular basis of non-native metal carcinogenesis has gained much attention in the last few decades.

1.1.1 Mechanisms of carcinogenesis. Carcinogenic metals can disrupt a wide range of cellular processes.[2] (*1*) They can create oxidative stress conditions in the cells by generating free

radicals. Most non-native metals induce reduction–oxidation (redox) reactions in cells like the Fenton and Haber-Weiss reactions. The produced reactive oxidative species (ROS) (*e.g.*, hydrogen peroxide and superoxide) damage DNA, proteins, and lipids.[3] (*2*) Non-native metals can also interrupt cell growth and proliferation via signal transduction pathways and dysregulation of oncogenes or tumor suppressors. For example, aluminum can bind to estrogen receptor and mimic estrogen function, giving rise to an increase in the number of cell divisions in breast tissue.[3] (*3*) Despite the widely recognized ability to transform cells, only chromium is considered a strong mutagen, while other carcinogenic metals including arsenic, nickel and cadmium are weak mutagens. Recent research suggests that functionally relevant modifications to the genome may play a role in activating or silencing the expression of certain genes to promote carcinogenesis. In this vein, arsenic and cadmium exposure are known to induce both DNA hypo- and hyper-methylation by inhibiting the DNA methyltransferase enzyme.[1,4,5] (*4*) Some carcinogenic metals interfere with DNA repair pathways. This type mechanism explains many apparently contradictory effects, such as discrepancies between low mutagenicity and high carcinogenicity, or co-carcinogenesis with other carcinogens. Individual metal ions are known to interfere with specific DNA repair pathways or steps. Non-native metals may compete with DNA repair proteins that contain zinc finger motif(s). The native zinc is tetrahedrally coordinated by Cys and/or His residues and must be considered a target for substitution by non-native metals. Zinc finger DNA repair proteins XPA, MutM, PARP, and p53 are reportedly inhibited by non-native metals, but little information into the mechanism of this inhibition has been provided.[2,3,6]

1.2 DNA DAMAGE AND REPAIR SYSTEMS

Genomic integrity is essential for DNA replication, transcription and protein expression; however, DNA molecules are continuously exposed to both exogenous (UV irradiation, chemical reagent) and endogenous (normal metabolism by-products, reactive oxygen species) damage. The genome of a typical mammalian cell accumulates thousands of lesions during a 24-hour period.However, as a result of DNA repair, less than 1 in 1000 becomes a propagated mutation. In addition, the native DNA replication process during cell division is prone to errors. While a proofreading enzyme normally recognizes and corrects most of the errors, some mutations are not repaired.[7] To minimize adverse consequences, a complex network of different DNA repair systems has evolved in all cells to maintain genomic integrity.

Distinct DNA repair pathways involve different enzymes and are specific for certain types of DNA damage(Table 1.1). Mismatch repair (MMR) corrects the rare mismatches left after replication and improves the overall fidelity of replication. DNA damage that distort the double helix like cyclobutane pyrimidine dimmer (CPDs) and 6-4 photoproducts (6-4 PPs), two common lesions caused by UV radiation, are recognized and repaired though the nucleotide excision repair (NER) pathway. Single damaged bases that are not recognized by the NER machinery are corrected by base excision repair (BER). In this process, damaged bases that are oxidized, alkylated, or hydrolyzed are excised from the genome by DNA glycosylases. These enzymes cleave the covalent bond between the bases and the sugar–phosphate backbone. These glycosylases are specific for different base alterations.[7] One such base alteration of particular interest is 8-oxoguanine (8-oG), an oxidation product of ~10^6 guanines in human DNA (Figure 1.1). Oxidation of guanine to 8-oG causes a G:C to T:A transversion mutation during replication,

Table 1.1. Types of DNA repair systems in *E. coli*.

Repair mechanism	Proteins	Damage
Mismatch	MutH methylase , MutL, MutS, DNA helicase II, SSB, DNA polymerase III, Exonuclease I/III/X, RecJ nuclease, DNA ligase	Mismatches
Base-excision	Specific DNA glycosylase, AP endonucleases, DNA polymerase I, DNA ligase	Uracil, hypoxanthine, xanthine, alkylated or oxidized bases
Nucleotide-excision	ABC exonuclease, DNA polymerase I, DNA ligase	Large DNA lesions
Direct Repair	DNA photolyases, O^6-Methylguanine-DNA methyltransferase, AlkB protein	methylguanine, methylcytosine, pyrimidine dimers

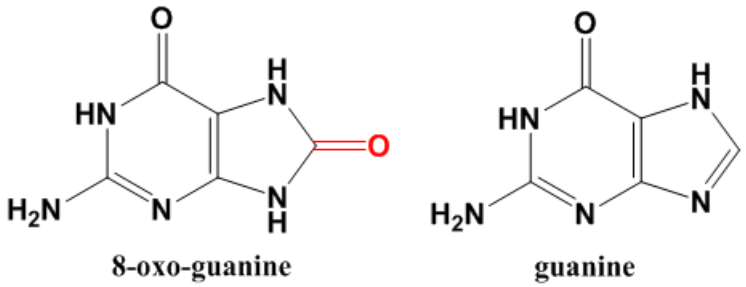

Figure 1.1. Guanine and 8-oxo-guanine. The oxidized position in 8-oxoguanine is colored red. Structures are created through ChemBioDraw Ultra.

which is frequently encountered in human cancers. To prevent genetic instability caused by 8-oG, cells express 8-oG specific DNA glycosylases that cleave the glycosidic bond of the damaged base. In humans, these enzymes are hOGG1 and hMYH, while MutM and MutYare the homologues in*E*. *coli* and other bacteria. Both MutM and hOGG1 specifically remove 8-oG in the 8-oG:C base pair, while MutY and hMYH specifically cleave the adenine base incorrectly paired with 8-oG in the 8-oG:A mismatch.[8-10]If non-native metals inhibit DNA repair processes, the increased number of mutations could lead to cancer, so understanding proteins and enzymes in these pathways that are potential targets of these metals is required. One such class of proteins called zinc finger proteins are prime candidates for this type of mechanism.

1.3 ZINC FINGER PROTEINS

The first zinc finger protein, transcription factor-IIIA (TFIIIA), was discovered in 1980 and since then multiple types of zinc fingers have been characterized. A zinc finger motif (zf) is a protein secondary structural element of 20–30 amino acid residues that coordinate with Zn(II) through side chains of Cys and/or His residues. The number of known zinc finger proteins is still increasing and but, in humans, it is predicted to be as much as 8% of total protein. Zinc fingers have a wide range of functions including DNA recognition and repair, RNA packaging, transcription activation, regulation of apoptosis, and protein folding and assembly.[11]

With the increasing number of zinc finger proteins discovered and their structures determined, there are several different motifs typified by coordinating amino acid residues, secondary structure, and cellular functions. Most zinc fingers are structural sites that only require zinc to fold correctly. Theyare constituted of mainly hydrophobic amino acid residuesand tend to

be exposed to solvent.The best characterized are the "classic zinc fingers" with $Cys_2His_2Zn(II)$ coordination, but other common zinc fingers include Cys_3His and Cys_4types. These two classes of zinc fingersare commonly found in pathways related to cell cycle and genome integrity. For example, XPA and RPA in the NER pathway have a single Cys_4 zinc finger, whilethe BER protein PARPpossesses two separate Cys_3His motifs. Classical zinc fingers possess a ββα motif, but other secondary structures like the gag knuckle, the treble clef, and zinc ribbon folds are also known.[11,12]

1.3.1 Function of zinc finger proteins. The classic zinc fingers are best known for sequence–specific binding of DNA, binding of single-stranded RNA, and mediating protein–protein interactions. DNA binding zinc fingers make sequence–specific contacts to nucleobases and can often occur as tandem repeats with two, three, or more fingers comprising the DNA binding domain of the protein. These tandem arrays usually bind in the major groove of DNA. Zinc finger proteins can also lead to assembly of multiprotein complexes on DNA that have architectural or enzymatic functions. For example, the protein XPA assembles the NER machinery to initiate repair. There are few zinc finger enzymes, but one notable example is the DNA repair protein ADA, which removes methyl group from DNA backbone phosphodiesters using a Cys_4 zinc finger motif.[11,13]

1.3.2. Zinc coordination. Due to the high metal affinity of the zinc finger, some non-native metals may compete with Zn(II) coordination. Table 1.2 presents the dissociation constants (K_d) of Zn(II), Co(II), Cd(II) and Ni(II) complexes with some well-studied zinc finger proteins and peptides.[13] The dissociation constants of Zn(II)–zinc fingers range from 10^{-13} to $10^{-8}M^{-1}$ and are

Table 1.2. Conditional dissociation constants for Zn(II), Ni(II), Co(II), and Cd(II) complexes with zinc finger proteins.

Type	Protein/peptide	K_{Zn} (M)	K_{Ni} (M)	K_{Co} (M)	K_{Cd} (M)	pH	Reference
CCHH	CP-1	$10^{-11.2}$	$10^{-5.8}$	$10^{-7.2}$	$10^{-8.7}$	7.0	14,15
	Sp1-3	$10^{-9.2}$	$10^{-5.4}$	$10^{-6.5}$		7.0	16
	TFIIIA	10^{-8}	$10^{-4.6}$		$10^{-5.6}$	7.0	14,15
	TFIIIA-zf	$10^{-8.5}$		$10^{-5.4}$	$10^{-7.7}$	7.4	15
	Ant-F	$10^{-7.9}$		$10^{-4.3}$		7.5	15
CCHC	CP1(H24C)	$10^{-11.5}$	$10^{-5.9}$			7.0	14
	Rauscher NC peptide	$10^{-9.2}$				7.0	17
	Rauscher NC protein	$10^{-12.0}$				7.0	17
	NZF-1	$10^{-9.9}$		$10^{-6.4}$		6.9	15
	Fw	$10^{-11.7}$				8.0	18
	NCp7(35-50)	$10^{-12.5}$				7.5	19
	NCp7(34-51)	$10^{-13.2}$				7.5	20
	NCp10	$10^{-13.1}$				7.5	21
CCCC	CP1(H20C, H24C)	10^{-12}		$10^{-6.5}$	$10^{-13.4}$	7.0	15
	DNA-bound ER	$10^{-8.2}$				7.9	14
	XPAzf	$10^{-9.8}$	$10^{-6.5}$	$10^{-7.8}$	$10^{-12.8}$	7.4	14,15

generally higher than that for other metals, except for Cd(II) binding to the Cys_4 motif. Although there is generally no relationship between the number of Cys residues and the strength of Zn(II) binding, it appears as though Cd(II) affinity is related to the number of coordinating thiolates. This preference is partly due the Cd–S bond strength and the preference for tetrahedral geometry. Cd(II) is also significantly larger than Zn(II) and often leads to distortion of the zinc finger conformation, which could also affect binding affinities. Co(II) on the other hand is isostructural with Zn(II) but the dissociation constants are 10^2–10^5 fold higher than Zn(II) regardless of the number of coordinating Cys residues. Ni(II) substitution of Zn(II) in zinc fingers is not isostructural and often results in distortion of the preferred coordination geometry. Both distorted tetrahedral (Cys_2His_2) and nearly square planar (Cys_4) coordination environments have been identified for Ni(II) substituted zinc fingers. As a result, the affinities of Ni(II) to zinc fingers are even lower than that of Co(II). Heavy metals like Hg(II) and Pb(II) with high affinities to thiolate ligands, may also replace Zn(II) in zinc fingers. [22]

1.4 METAL INHIBITION OF ZINC FINGER DNA REPAIR PROTEINS.

1.4.1 Zinc finger proteins inhibited by metals.

The idea that zinc finger proteins in DNA repair pathways could be specifically targeted by non-native metals as one contributing factor towards metal–induced carcinogenesis was proposed shortly after the first zinc fingers were identified. For example, DNA strand break repair protein polyADP-ribose polymerase (PARP) possesses two separate Cys_3His_1 zinc fingers and detects DNA strand breaks and recruits enzymes involved in BER. PARP activity was reportedlyinhibited by As(III), Co(II), Cd(II), Cu(II) , and Ni(II), but whether inhibition is due to interactions with the zinc fingers has yet to be

determined. Another example is the tumor suppressor protein p53, a zinc finger transcription factor that is activated by multiple forms of stress signals, including DNA damage. P53–DNA binding is mediated by a single Cys_3His_1 zinc finger. Exposure of p53 protein to Cd(II), Co(II) or Ni(II) disrupted the native p53 conformation and inhibited of DNA binding.[6] However, the most well-studied zinc finger DNA repair proteins affected by non-native metals are human XPA and *E. coli* formamidopyrimidine DNA glycosylase (also known as MutM or Fpg), which both possess a single Cys_4 zinc finger. XPA recruits the repair machinery in the first steps of NER. Loss of XPA function causes the accumulation of the UV irradiation damaged DNA and eventually leads to xeroderma pigmentosum type A, a severe disease characterized by UV-hypersensitivity and enhanced cancer risk.[15] MutM, on the other hand, recognizes and removes 8-oG as a trifunctional enzyme with glycosylase, apurinic/apyrimidincylase, and 5'-termial deoxyribose phosphate–excision activities. It converts the damaged dsDNA into single strand breaks. Studies specifically geared towards a detailed understanding of how non-native metals inhibit hXPA and MutM have yet to be described.

1.4.2 Inhibition of human XPA by non-native metals. XPA is a monomeric protein that binds to DNA through a Cys_4 zinc finger in its minimal binding domain (XPA–MBD, M98–F219). This domain is also essential in recruiting RPA, TFIIIA and other proteins to assemble the NER repair machinery. Electrophoresis mobility shift assay (EMSA) showed that DNA binding is inhibited by Cu(II), Cd(II), Co(II) and Ni(II).[23] Investigation of metal coordination by extended x-ray absorption fine structure spectroscopy (EXAFS) has been performed with the XPA-MBD construct, but not the full-length protein. EXAFS revealed that Cd(II) and Co(II) form a tetrahedral coordination environment with XPA–MBD with no major

geometric distortion; however, the Cd(II)–Sbond is ~0.2 Å longer than thenative Zn(II)−S bond. Circular dichroism (CD) and nuclear magnetic resonance (NMR) spectroscopies on these metal constructs showed that the difference in the metal–S bond length does not result in any detectable structural changes to the protein domain. There is debate on whether Cd(II) can displace Zn(II) from the zinc finger.Alternative possibilities include that Cd(II) may bind to negatively charged surface residues on XPA, which may interfere with DNA binding, but not alter the structure of XPA, or that Cd(II) inhibition is the result of its association with DNA, rather than NER proteins.[24] Studies have also been performed using a 37 amino acid peptide of XPA containing only the zinc finger motif (XPAzf). This peptide was used to study the metal binding affinities. The K_{Co}/K_{Zn} ratios of all types of zinc fingers are usually in the 10^3–10^4 range, which means Zn(II) is thermodynamically favored over Co(II). The ratio obtained for XPAzf is 10^2, which is the lowest of all reported. The K_{Cd}/K_{Zn} ratio for XPAzf of 0.001 is also lower than all other published Cd(II)–zinc finger complexes.[15] Therefore, the Cys_4 zinc finger seems to be the most possible target for Cd(II) replacement.

1.4.3 Inhibition of *E. coli*MutMDNA glycosylase by metals. In human cells, the initial steps in BER are catalyzed by DNA glycosylases. Although many have activity towards specific damaged bases, the DNA glycosylases share many structural and functional features, such as a positively charged DNA binding cleft containing the active site pocketthat accommodates an extruded, damaged base for nucleophilic attack at the C1’ of deoxyribose. The formamidopyrimidine-DNA glycosylase (Fpg) family is a well–defined family of DNA glycosylases, comprising MutM, endonuclease VIII (Nei) and mammalian homologs (Neil).[25]

E. coli MutM is a 269-amino acid enzyme that recognizes and removes 8-oG using three separate catalytic activities.[26] MutM has been widely studied in terms of three-dimensional structure and recognition of 8-oG damaged dsDNA. Like most of the DNA glycosylases, MutM binds DNA through DNA binding cleft between the two domains and the damaged base is flipped into the active site, which is at the bottom of the cleft, for excision(Figure 1.2).[25] It has two domains connected by a hinge polypeptide. The structural Cys_4-type zinc finger motif (Cys_{244}-X_2-Cys_{247}-X_{16}-Cys_{264}-X_2-Cys_{267}) located at the C-terminus of the protein is involved in 8-oG recognition and DNA binding.[27]

MutM was inhibited in a dose–dependent manner by Cd(II), Cu(II), and Hg(II), but not by Co(II), As(III), Ni(II) or Pb(II) (Table 1.3).[23] Cu(II) or Hg(II) coordination to the zinc finger alters the geometry and the secondary structure of the motif. [2,6]However, similar to XPA, Cd(II) and Co(II) are isostructural (*i.e.*, tetrahedral) substitutes for Zn(II) in the zinc finger motif, and caused no significant conformational change as evidenced by CD spectroscopy.[24,28] Therefore, the inhibition mechanism of MutM by Cd(II) and other metals is not clear.

1.5 SCOPE OF THE DISSERTATION RESEARCH

The goal of the experiments presented in this dissertation is to gain insight into (1) the ability of non-native metals such as cadmium and cobalt tocoordinate the zinc finger of MutM, (2) the specific catalytic step or steps inhibited by non-native metals,(3) the ability of MutM with non-native metals to recognize and bind damaged DNA, and (4) whether non-native metals alter the conformation or dynamic motions correlated with MutM activity.

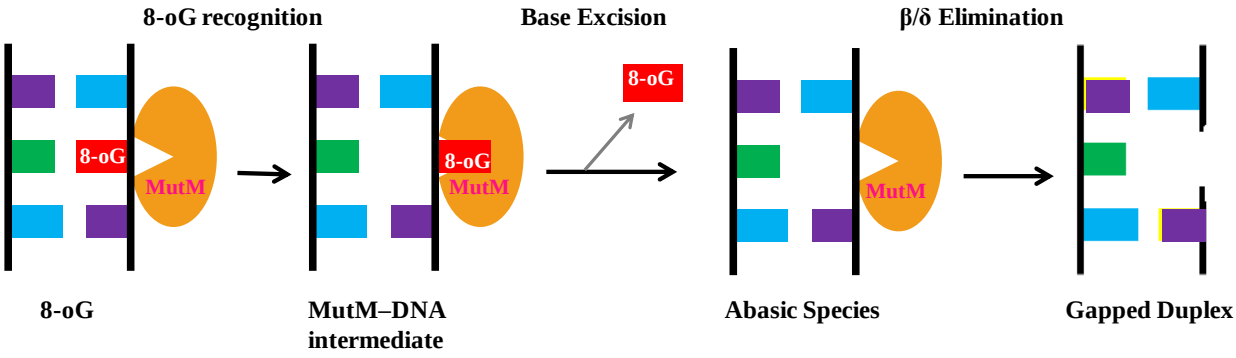

Figure 1.2. Schematic of the mechanism of MutM catalyzed 8-oG excision. MutM binds specifically to the 8-oG damaged DNA and flips the 8-oG out form the double helix for excision. After that, MutM cuts the apurinic site as an AP-lyase.

Table 1.3. Effects of non-native metals on the activity of MutM on methylene blue-damaged PM2 DNA.[23] The percentages are the ratios of activity of MutM incubated with metals over that of native MutM.

Metal concentration (μM)	Cd(II)	Cu(II)	Hg(II)	Ni(II), Pb(II), Co(II), As(III)
0.1	>90%	>90%	10%	>90%
1	>90%	>90%	<5%	>90%
10	> 90%	10%	<5%	>90%
100	20%	<5%	<5%	>90%
1000	<5%	<5%	<5%	>90%

We first characterized zinc, cadmium, and cobalt binding at the zinc finger of MutM, as described in Chapter 2. We then developed and compared two activity assays that monitor individual steps of the MutM catalyzed DNA base excision reaction. Further, we tested whether these metals interfered with DNA binding and damaged base recognition. These studies are presented in Chapter 3. We also used hydrogen–deuterium exchange mass spectrometry (HDX–MS) to characterize the structural changes that occur upon coordination of non-native metals in the MutM zinc finger and correlated these changes to the catalytic activities, as described in Chapter 4. Finally, we present a unified model of how certain non-native metals inhibit MutM, reexamining whether inhibition of zinc finger DNA repair glycosylases by heavy metals *in vivo* is a viable mechanism for metal–induced carcinogenesis.

1.6. REFERENCES

(1) Mishra, S., Dwivedi, S. P., and Singh, R. B. (2010) A review of epigenetic effect of heavy metal carcinogens on human health. *The Open Nutraceuticals Journal 3*, 188–193.

(2) Beyersmann, D., and Hartwig, A. (2008) Carcinogenic metal compounds: Recent insight into molecular and cellular mechanisms. *Arch. Toxicol.82*, 493–512.

(3) Koedrith, P., and Seo, Y. R. (2011) Advances in carcinogenic metal toxicity and potential molecular markers. *Int. J. Mol. Sci.12*, 9576–9595.

(4) Arita, A., and Costa, M. (2009) Epigenetics in metal carcinogenesis: nickel, arsenic, chromium and cadmium. *Metallomics1*, 222–228.

(5) Salnikow, K., and Zhitkovich, A. (2008) Genetic and epigenetic mechanisms in metal carcinogenesis and cocarcinogenesis: nickel, arsenic, and chromium. *Chem. Res. Toxicol.21*, 28–44.

(6) Hartwig, A., Asmuss, M., Blessing, H., Hoffmann, S., Jahnke, G., Khandelwal, S., Pelzer, A., and Burkle, A. (2002) Interference by toxic metal ions with zinc-dependent proteins involved in maintaining genomic stability. *Food. Chem. Toxicol.40*, 1179–1184.

(7) Friedberg, E. C. (2003) DNA damage and repair. *Nature421*, 436–440.

(8) Bruner, S. D., Norman, D. P., and Verdine, G. L. (2000) Structural basis for recognition and repair of the endogenous mutagen 8-oxoguanine in DNA. *Nature403*, 859–866.

(9) Hill, J. W., Hazra, T. K., Izumi, T., and Mitra, S. (2001) Stimulation of human 8-oxoguanine-DNA glycosylase by AP-endonuclease: Potential coordination of the initial steps in base excision repair. *Nucleic Acids Res.29*, 430–438.

(10) Qi, Y., Spong, M. C., Nam, K., Banerjee, A., Jiralerspong, S., Karplus, M., and Verdine, G. L. (2009) Encounter and extrusion of an intrahelical lesion by a DNA repair enzyme. *Nature462*, 762–766.

(11) Krishna, S. S., Majumdar, I., and Grishin, N. V. (2003) Structural classification of zinc fingers: Survey and summary. *Nucleic Acids Res.31*, 532–550.

(12) Laity, J. H., Lee, B. M., and Wright, P. E. (2001) Zinc finger proteins: New insights into structural and functional diversity. *Curr. Opin. Struct. Biol.11*, 39–46.

(13) Witkiewicz-Kucharczyk, A., and Bal, W. (2006) Damage of zinc fingers in DNA repair proteins, a novel molecular mechanism in carcinogenesis. *Toxicol. Lett.162*, 29–42.

(14) Bal, W., Schwerdtle, T., and Hartwig, A. (2003) Mechanism of nickel assault on the zinc finger of DNA repair protein XPA. *Chem. Res. Toxicol.16*, 242–248.

(15) Kopera, E., Schwerdtle, T., Hartwig, A., and Bal, W. (2004) Co(II) and Cd(II) substitute for Zn(II) in the zinc finger derived from the DNA repair protein XPA, demonstrating a variety of potential mechanisms of toxicity. *Chem. Res. Toxicol.17*, 1452–1458.

(16) Posewitz, M. C., and Wilcox, D. E. (1995) Properties of the Sp1 zinc finger 3 peptide: Coordination chemistry, redox reactions, and metal binding competition with metallothionein. *Chem. Res. Toxicol.8*, 1020–1028.

(17) Green, L. M., and Berg, J. M. (1990) Retroviral nucleocapsid protein-metal ion interactions: Folding and sequence variants. *Proc. Natl. Acad. Sci. U. S. A.87*, 6403–6407.

(18) Bavoso, A., Ostuni, A., Battistuzzi, G., Menabue, L., Saladini, M., and Sola, M. (1998) Metal ion binding to a zinc finger peptide containing the Cys-X2-Cys-X4-His-X4-Cys domain of a nucleic acid binding protein encoded by the drosophila Fw-element. *Biochem. Biophys. Res. Commun.242*, 385–389.

(19) Bombarda, E., Morellet, N., Cherradi, H., Spiess, B., Bouaziz, S., Grell, E., Roques, B. P., and Mely, Y. (2001) Determination of the $pK_{(a)}$ of the four Zn^{2+}-coordinating residues of the distal finger motif of the HIV-1 nucleocapsid protein: Consequences on the binding of Zn^{2+}. *J. Mol. Biol.310*, 659–672.

(20) Mely, Y., De Rocquigny, H., Morellet, N., Roques, B. P., and Gerad, D. (1996) Zinc binding to the HIV-1 nucleocapsid protein: A thermodynamic investigation by fluorescence spectroscopy. *Biochemistry35*, 5175–5182.

(21) Mely, Y., Cornille, F., Fournie-Zaluski, M. C., Darlix, J. L., Roques, B. P., and Gerard, D. (1991) Investigation of zinc-binding affinities of moloney murine leukemia virus nucleocapsid protein and its related zinc finger and modified peptides. *Biopolymers31*, 899–906.

(22) Predki, P. F., and Sarkar, B. (1994) Metal replacement in "Zinc finger" and its effect on DNA binding. *Environ. Health. Perspect.102 Suppl 3*, 195–198.

(23) Asmuss, M., Mullenders, L. H., Eker, A., and Hartwig, A. (2000) Differential effects of toxic metal compounds on the activities of Fpg and XPA, two zinc finger proteins involved in DNA repair. *Carcinogenesis21*, 2097–2104.

(24) Buchko, G. W., Hess, N. J., and Kennedy, M. A. (2000) Cadmium mutagenicity and human nucleotide excision repair protein XPA: CD, EXAFS and $^{(1)}H/^{(15)}N$-NMR spectroscopic studies on the zinc(II)- and cadmium(II)-associated minimal DNA-binding domain (M98-F219). *Carcinogenesis21*, 1051–1057.

(25) Zharkov, D. O., Shoham, G., and Grollman, A. P. (2003) Structural characterization of the Fpg family of DNA glycosylases. *DNA Repair (Amst)2*, 839–862.

(26) Li, G. M. (2010) Novel molecular insights into the mechanism of go removal by MutM. *Cell Res.20*, 116–118.

(27) Sugahara, M., Mikawa, T., Kumasaka, T., Yamamoto, M., Kato, R., Fukuyama, K., Inoue, Y., and Kuramitsu, S. (2000) Crystal structure of a repair enzyme of oxidatively damaged DNA, MutM (Fpg), from an extreme thermophile, Thermus thermophilus HB8. *EMBO J.19*, 3857–3869.

(28) Buchko, G. W., Hess, N. J., Bandaru, V., Wallace, S. S., and Kennedy, M. A. (2000) Spectroscopic studies of zinc(II)- and cobalt(II)-associated *Escherichia coli* formamidopyrimidine-DNA glycosylase: Extended X-ray absorption fine structure evidence for a metal-binding domain. *Biochemistry39*, 12441–12449.

CHAPTER 2

ASSOCIATION OF NON-NATIVE METALS WITH MUTM DNA GLYCOSYLASE

2.1 INTRODUCTION

Non–native metals including Cd(II),Cu(II), Pb(II), Hg(II), Co(II) and As(III) inhibit the nucleotide excision repair (NER) and base excision repair (BER) pathways. The mechanism of inhibition, however, is still under investigation. The presence of zinc finger containing DNA repair proteins in these pathways may be one route for metal-based inhibition.[1,2]If DNA mutations are not repaired, then this is one potential mechanism for metal induced carcinogenesis. MutM, an 8-oxoguanine (8-oG) specific DNA glycosylase, is a potential target of metal inhibition of the BER pathway. Zn(II)–MutM is inhibited in a dose–dependent manner by Cd(II), Cu(II), and Hg(II). Simultaneous treatment of MutM with Cd(II) and Zn(II) only partly prevents inhibition of activity.[3] Overall, these studies suggest that the zinc ion that binds the zinc finger motif may be replaced by some of the non-native metals, which leads to the inactivation of MutM.

Non-native metal substitution for Zn(II) in the Cys_4-type zinc finger includes isostructural substitution, substitution with altered geometry, mixed complex formation, and catalysis of thiol oxidation. Both Cd(II) and Co(II) are isostructural (*i.e.*, tetrahedral) substitutes for Zn(II). Extended x-ray absorption fine structure (EXAFS) studies of full-length Zn(II)–MutM and

Co(II)−MutM revealed that substitution of Co(II) for Zn(II) did not significantly alter the metal coordination environment and geometry.[4] This was also observed in EXAFS studies on thetruncated zinc finger motif. In that study, the Cd(II)-bound zinc finger was also described. The metal–S bond length was increased due to the larger size of the Cd(II) ion compared to Zn(II), which likely indicates structural distortion of the finger.[5] However, MutM coordination with other metal ions has yet to be described and the mechanism of MutM inhibition by these metals is still unknown.

UV–visible spectroscopy is a useful tool to investigate the metal coordination environment and relative affinities of non-native metals that MutM binds. The electronic absorption bands observed by UV–visible spectroscopy include ligand–metal charge transfer (LMCT) and *d–d* transitions. LMCT transitions are the result of electron transfer from a ligand orbital, particularly sulfur, to a low energy metal ion orbital. These are high energy electronic absorptions in the UV region of the spectrum. The energy of these LMCT transitions is dependent on the type of metal. Since metal coordination to MutM should involve the Cys_4 zinc finger, LMCT transitions from cysteine thiolate (S^-) coordination to transition metals such as Cd(II), Pb(II) and Co(II) should be observed. LMCT bands can also indicate the relative number of thiolates coordinated to the metal ion based on the molar extinction and maximum wavelength of the transition.[6,7] This could help differentiate as to whether there could be additional metal binding sites outside the zinc finger. Since Zn(II) is spectroscopically silent, Co(II) has been used for many years as a spectroscopic surrogate for investigation of zinc finger protein coordination. The Co(II) *d–d* transitions occur at lower energies than the LMCT and are usually in the visible region of the spectrum. Protein coordination leads to specific *d–d* transitions that are characteristic of the type of protein residues ligated to the metal (O/N vs. S). In addition, *d–d* transitions can reveal

information about the coordination geometry (*i.e.*, octahedral, tetrahedral) based on the molar extinction of the transition.[7,8]

In this chapter, we describe the construction and identification of the Zn(II)–, Cd(II)–, Co(II)– and apo–MutM enzyme preparations, verifying the coordination of these metal ions with the MutM zinc finger motif. We perform UV–visible spectroscopy based titration experiments, demonstrating that Zn(II) forms stable complex with MutM though the zinc finger, which is not replaced by Co(II) and Pb(II) under our experiment conditions. Cd(II), however, does show some ability to substitute for Zn(II) in MutM.

2.2 MATERIALS AND METHODS

2.2.1 Chemicals. All buffers were prepared using Milli-Q deionized water. The 4-(2-hydroxyethyl)-1-piperazineethanesulfonic free acid (HEPES), Tris (2-carboxyethyl)-phosphine hydrochloride (TCEP), and ethylenediaminetetraacetic acid (EDTA) were purchased from Calbiochem, Amresco, and VWR, respectively. *Escherichia coli* strain BL21(DE3)/pLysS (Agilent Technologies), Luria Broth and carbenicillin (purchased from Teknova), chloramphenicol (purchased from Genlantis), isopropyl-b-D-thiogalactopyranoside (IPTG, purchased from EMD) were used for MutM overexpression. Chemicals used for purification include phenylmethylsulfonylfluoride (PMSF, Biosynt), egg white lysozyme (Calbiochem), polyethyleneimine (PEI, MP Biomedicals), ammonium sulfate (Acros Organics), and SP Sepharose Fast Flow resin (GE Healthcare). Rockland 14–120 kDa protein marker, standard metal solutions for atomic absorption analysis (PerkinElmer), 5,5'-dithio-bis(2-nitrobenzoic) acid (DTNB, Biosynth Inc.), *N*-ethylmaleimide (NEM, Alfa Aesar), 4-(hydroxymercury)benzoic

acid sodium salt (PMPS, Acros Organics), 4-(2-pyridylaza)resorcinol (PAR, Alfa Aesar) were used for protein identification, metal and free thiol quantification. Trace metals in deionized water solutions were removed by passage over a Chelex-100 column (Bio-Rad). Ultrapure Cd(II) chloride, Co(II) chloride hexahydrate and Zn(II) sulfate heptahydrate were purchased from Fisher Scientific, Mallinckrodt Chemicals, and Alfa Aesar, respectively.

2.2.2 MutM purification. The gene for MutM was amplified from *E. coli* genomic DNA and cloned into *pET-21b* using *Nde*I and *Hin*dIII restriction sites and verified by DNA sequencing. Recombinant *pET-21b-MutM* was transformed into *E. coli* strain BL21(DE3)/pLysS by heat shock. The transformed cells were plated onto Luria Bertani (LB) agar plates containing 100 μg/mL ampicillin and 34 μg/mL chloramphenicol and then incubated at 37 ℃ overnight. LB media with 50 μg/mL carbenicillin and 34 μg/mL chloramphenicol was inoculated with single colonies and grown at 37 ℃ to an OD_{600} of 0.6–0.8 then induced by addition of 1 mM IPTG, followed by an additional 3 hr growth at 30 ℃. At an OD_{600} of 1.8, the cells were harvested by centrifugation and the pellet was resuspended in Buffer A (50 mM HEPES, pH 8.0, 50 mM NaCl, 1 mM TCEP) containing 100 μM PMSF and 1 mg/mL lysozyme. The following steps were carried out at 4 ℃. The cells were lysed with a Branson Sonifier 250 with an output of 4, 50% duty cycle, for a total of 15 min. The cellular debris was removed by centrifugation at 10,000 rpm for 20 min. The supernatant was incubated with 0.015 (v/v) of PEI for 1 hr with gentle stirring to precipitate nucleic acids. The precipitation was separated by centrifugation at 10,000 rpm for 20 min. MutM remained in the supernatant, which was subjected to ammonium sulfate precipitation (30% saturation) for 2 hr with gentle stirring. The precipitated proteins were removed by centrifugation as described. MutM remains in the supernatant.

The protein was loaded on a 50 mL SP Sepharose Fast Flow column pre-equilibrated with Buffer A. The column was washed with 100 mL Buffer A and the protein was eluted with a gradient of 300 mL NaCl (50 mM–500 mM) in Buffer A. The purest MutM fractions by SDS-PAGE were combined and then dialyzed against Buffer B (50 mM HEPES, pH 8, 400 mM NaCl, 1 mM TCEP, 10% glycerol) with changes every 4 hr for a total 8 hr. The purity of the isolated MutM was revealed by a 15% SDS-PAGE and the concentration was determined by UV–visible spectroscopy from the molar extinction coefficient of MutM, 39.8 $mM^{-1}cm^{-1}$ at 280 nm.

2.2.3 Apo−MutM purification. All anaerobic procedures were performed in a Vacuum Atmosphere anaerobic glove box (<1 ppm O_2). As-purified MutM was dialyzed in Buffer C (50 mM HEPES, pH 8, 400 mM NaCl) with changes every 4 hr for a total 8 hr to remove the reducing agent TCEP. Ten molar equivalents of PMPS was added to MutM and incubated for 30 min in order to release Zn(II) from cysteine thiolates.[9] Released Zn(II) ions were chelated with an excess of EDTA (2–5 mM) then removed by dialysis against Buffer C containing Chelex-100 resin, with changes every 2 hr for a total 4 hr. The thiols modified with PMPS were then reduced overnight with 20 molar equivalents of TCEP over MutM and again dialyzed against Buffer C. The Zn(II):MutM ratio was below 0.1 Zn(II) per protein according to atomic absorption (AA) spectroscopy, as described below.

2.2.4 Metal supplemented MutM purification. MutM with Zn(II)–, Cd(II)–, Co(II)– or Pb(II)–bound was obtained by supplementing the cell culture media with 100–500 μM metal ion. The proteins were also purified with metal–supplemented Buffer A and the amount of metal bound to the purified protein was determined by AA spectroscopy using a Zn hollow cathode

lamp (HCL) at 213.86 nm (slit widths of 2.7 nm/1.8 nm), a Cd HCL at 228.8 nm (slit width of 2.7/1.35 nm), a Co HCL at 240.73 nm (slit width of 1.8/1.35 nm), and a Pb HCL at 283.31 nm (slit width of 2.7/1.05 nm). Metal stoichiometry in the isolated Zn(II)–, Cd(II)–, Co(II)– and Pb(II)–MutM preparations were 1.0 (±0.11), 0.87 (±0.05), 0.95 (±0.13), and 0.43 (±0.08) per protein, respectively.

2.2.5 Tandem mass spectrometry. The identification of purified MutM was obtained through pepsin digestion and tandem MS/MS spectroscopy. MutM was diluted in the Buffer Q (10 mM potassium phosphate, pH 2.4) to obtain a 100 μL sample with 40 μg MutM. A 2 mg/mL pepsin stock was made fresh in Buffer I (10 mM potassium phosphate, pH 7.2) and 2 μL was mixed with MutM (0.1 μg/μg) and incubated on ice for 5 min. Digested MutM peptides were separated on a 50 mm × 2 mm Phenomenex C_{18} column (5 micron) using an Agilent Technologies 1200 series LC. Tandem MS/MS (CID) was performed using SmartFrag™ settings by the Bruker HCTultra PTM mass spectrometer in positive ion mode. Sequenced peptides were identified by PeaksClient 6.

2.2.6 Free thiol quantitation. The DTNB assay was carried out anaerobically at ambient temperature. MutM (apo and metallated forms) was diluted in 100 mM Tris, pH 8, 0.3 mM DTNB to obtain 150 μL samples of 2–8 μM MutM. The samples were incubated for 30 min, removed from glovebox, and their UV-visible spectra were recorded from 260–600 nm. The concentration of thiol groups was determined at 412 nm using a molar absorptivity of 14.2 $mM^{-1}cm^{-1}$.

2.2.7 PMPS titration with PAR. The preparation was carried out in a glovebox at room temperature.Zn(II)–MutM was diluted in chelexed Buffer G (20 mM HEPES, pH 7.5, 100 mM KCl) to 10 μM and 100 μM PAR (diluted from 2 mM stock in Buffer G) was added. The sample was added to a custom anaerobic cuvette, sealed, and equipped with a Hamilton gastight syringe loaded with 4 mM of PMPS in Buffer G (20 molar equivalents) before removal from the glovebox. The UV–visible spectrum (190 nm–900 nm) of Zn(II)–MutM was recorded prior to the addition of PMPS, and the concentration of MutM was determined at 280 nm using $\varepsilon_{280\ nm}$=39.8 $mM^{-1}cm^{-1}$. PMPS was titrated in 5 μL aliquots with 10 min of incubation before the spectrum was taken for each addition. The data were plotted monitoring the absorbance at 500 nm as a function of the molar ratio of PMPS over Zn(II)–MutM.[9]

2.2.8 Metal binding titrations. All metal binding experiments were carried out anaerobically at ambient temperature (25 °C) using an Agilent model 8453 spectrophotometer. For Cd(II) titrations, 10 μM MutM was diluted from the 100 μM stock with Buffer D (50 mM HEPES, pH 7, 200 mM NaCl) to obtain a 1 mL sample in an anaerobic quartz cuvette, sealed, and equipped with a Hamilton gastight syringe loaded with 350 μM of Cd(II) (3 molar equivalents) before removal from the glovebox. The UV spectrum (190 nm–600 nm) of MutM was taken prior to the addition of Cd(II) and the protein concentration was determined at 280 nm. Cd(II) was titrated in 5 μL aliquots with 3 min incubation before the spectrum was taken.[10]Co(II) titrations were performed in the same manner except that concentration of MutM and Co(II) titrant was 100 μM and 340 mM, respectively.

For the metal titrations with the presence of the Zn(II) indicator PAR, 10 molar equivalents of PAR over MutM concentration was included in the 1 mL sample. Corrected absorbance

spectra were obtained by first subtracting the original MutM spectrum from each metal–addition spectrum and then correcting each spectrum for dilution. For titrations involving PAR, control titrations of metal into PAR using the same concentration of PAR present in the MutM titrations. Additional control titrations included titration Buffer C with metal solution as for MutM.[9,11]

2.3 RESULTS

2.3.1 MutM purification. MutM was purified after over–expression in *E. coli* BL21(DE3) cells. The purity of the isolated MutM preparations is revealed by the Coomassie-stained SDS polyacrylamide gels and is estimated to be > 90% (Figure 2.1). Pepsin digestion and tandem mass spectrometry was performed and the data was submitted to Peaks for identification. The results confirm that the protein purified is *E. coli* MutM (Figure 2.2). Expression of MutM in metal supplemented media allows for different metals to be purified with MutM. Metal stoichiometry, measured by the atomic absorption analysis, in the isolated Zn(II)–, Cd(II)– and Co(II)–MutM preparations are 1.0 (±0.1), 0.87 (±0.05) and 0.95 (±0.13) molar equivalents of metal per protein, respectively. Apo–MutM contains <0.1 equivalents of Zn(II) per MutM, which is as low as possible for Zn(II) in high–affinity proteins. We also tried to purify Pb(II)–MutM in the same way; however, with 1000-fold excess Pb(II) provided in during protein expression and purification, Pb(II) stoichiometry in the preparation was less than 0.5 equivalents bound.

2.3.2 Quantification of the reduced thiols. Since apo–MutM is sensitive to cysteine oxidation, we determined the number of reduced cysteine thiolates that are capable of coordinating with metals via a DTNB assay. Free cysteine thiolates can reduce the disulfide bond

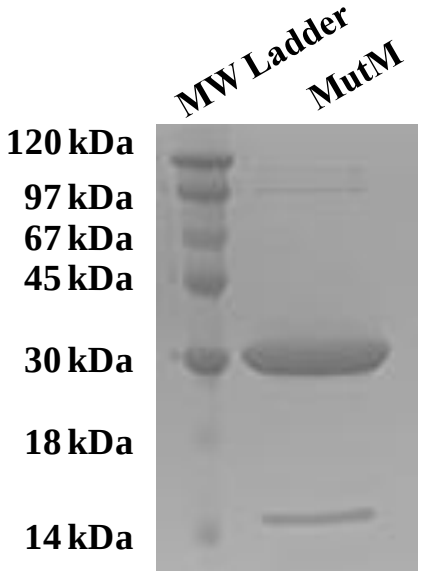

Figure 2.1. Representative SDS–PAGE of as-purified MutM. The purity of the isolated MutM with molecular weight of 31 kDa was estimated to be > 90% after Coomassie blue staining.

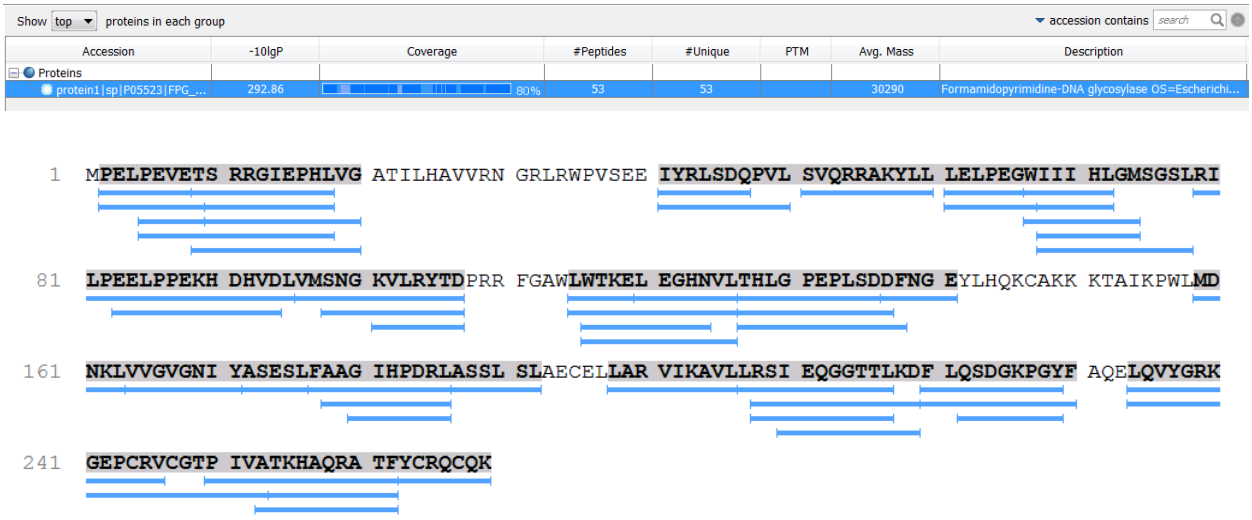

Figure 2.2. MutM identification by tandem MS/MS mapping. The full length MutM was digested by pepsin and tandem MS/MS was performed. The peptide map was created using peptides identified by Peaks giving over 80% sequence coverage.

in DTNB liberating 2-nitro-5-thiobenzoate (NTB^-), which ionizes to the yellow NTB^{2-} dianion at alkaline pH (ε_{412nm} =14.2 $mM^{-1}cm^{-1}$). This reaction is rapid and stoichiometric. The DTNB assay indicates that all six cysteines in our purified preparation of apo−MutM are reduced and, thus, available for metal coordination. The DTNB assay using the purified MutM preparations with metals bound show approximately two free thiols per protein, indicating that the cysteines in the zinc finger are protected by the metals (Cys 244, 247, 264, 267) but the two remaining cysteines (Cys 147 and Cys195) are in the reduced form. As further confirmation, Zn(II)–MutM was titrated with *p*-mercurimethyl phenylsulfonate (PMPS), a thiol specific modifying mercurial compound, in the presence of PAR, a Zn(II) indicator. As PMPS is titrated, mercury coordination to MutM cysteines releases Zn(II), which is then chelated by PAR. The Zn(II)–PAR complex absorbs at 500 nm and increases as PMPS is added (Figure 2.3A). The binding isotherm indicates ~6 molar equivalents of PMPS over MutM is required to release the Zn(II) (Figure 2.3B). This result confirms that in the Zn(II)–MutM complex, all six cysteine residues are reduced and the Zn(II) ion is coordinated with four cysteine residue(s) in the zinc finger domain.

2.3.3 Zinc binding to MutM. The stoichiometry of Zn(II) for MutM is confirmed by Zn(II) titration of apo–MutM in the presence of the indicator PAR (Figure 2.4). Clearly, MutM has a higher affinity for Zn(II) than PAR, since only after 1 equivalent of Zn(II) is added does the Zn(II)–PAR complex absorbance at 500 nm increase. This demonstrates that Zn(II) and MutM form 1:1 complex. We also tested whether excess PAR could remove Zn(II) from Zn(II)-MutM after a 3 hr incubation. No increase in absorbance at 500 nm is observed (data not shown). This confirms that PAR cannot compete with MutM for Zn(II) binding under our experimental

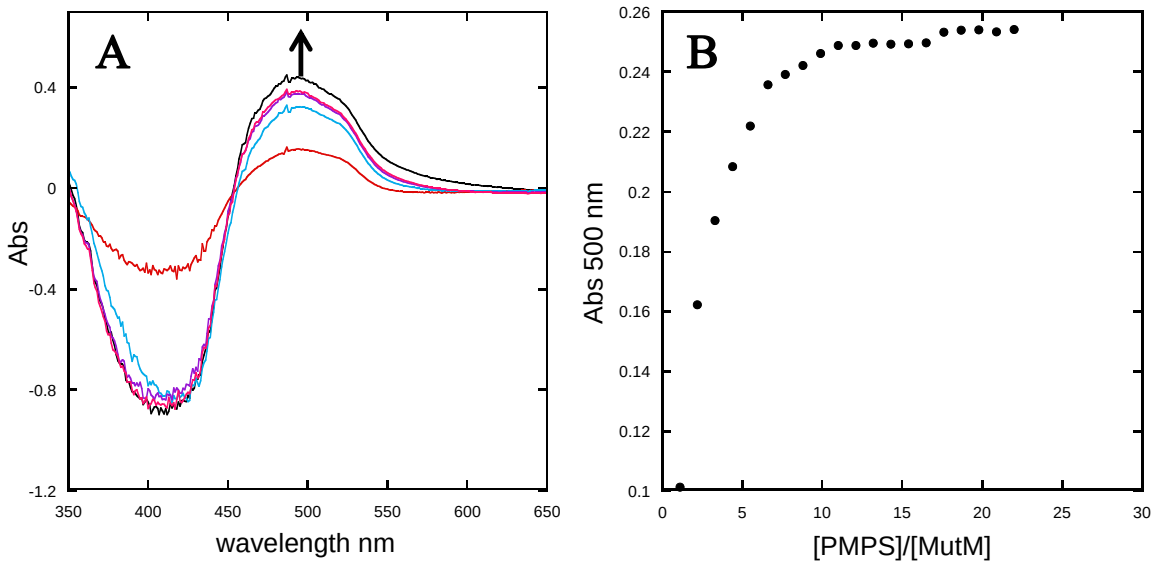

Figure 2.3. UV–visible titration of Zn(II)–MutM with PMPS. (A) As PMPS is titrated, the released Zn(II) coordinates to PAR leading to an absorbance at 500 nm for the Zn(II)-PAR complex. Spectra is corrected for Zn(II) titration with PMPS. (B) Zn(II)–PAR absorbance at 500 nm is plotted as a function of the equivalents of PMPS over MutM.

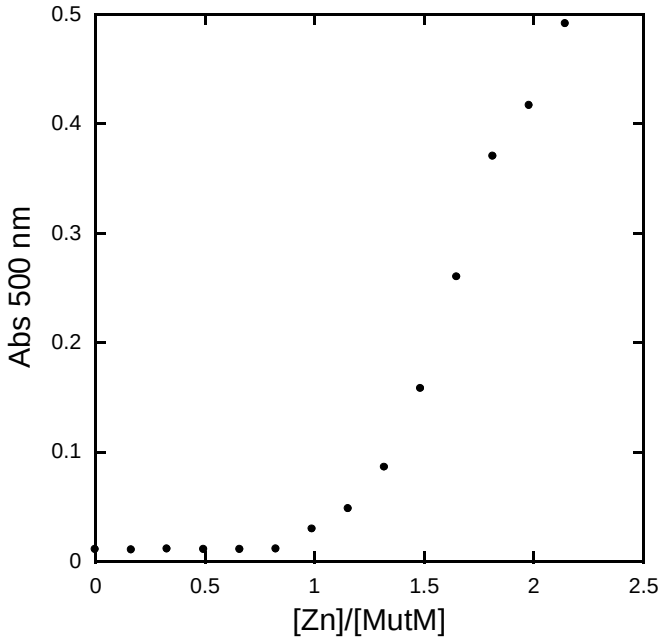

Figure 2.4. Zn(II) titration of apo–MutM. The binding isotherm for titration of Zn(II) into apo–MutM in the presence of PAR indicator, which absorbs at 500 nm when it binds Zn(II). MutM binds the first titrated molar equivalent of Zn(II) before Zn(II) binds to PAR.

conditions. The Zn(II)–PAR dissociation constant is ~10^{-6} M, which is 4 orders of magnitude higher than that of Zn(II) for typical Cys_4 type zinc fingers.

2.3.4 Cadmium binding to MutM. The toxic metal Cd(II) is often used as a surrogate for Zn(II) in metal binding studies of zinc finger proteins as it has similar coordination as Zn(II) and both are d^{10} metals. Cd(II) coordination by cysteines leads to spectroscopic absorbances that reveal information about the coordination complex. Purification of Cd(II)–MutM results in an enzyme with one Cd(II) bound that exhibits a UV absorption due to cysteine thiolate S→Cd(II) ligand-to-metal charge transfer (LMCT), as shown in Figure 2.5. The net absorption spectrum obtained from subtracting the Zn(II)–MutM spectrum from the Cd(II)–MutM spectrum reveals an absorption maximum at 242 nm with a molar absorptivity of 18 $mM^{-1}cm^{-1}$. This is consistent with Cys_4 coordination of Cd(II),[6] and presumably spectroscopically silent Zn(II), as has been shown for other zinc finger proteins.

Cd(II) titration of apo–MutM and Zn(II)–MutM were also performed. The titration into apo–MutM shows an increase in the S^-→Cd(II) LMCT at 242 nm (Figure 2.6A). The binding isotherm indicates that MutM is saturated at ~2.5 molar equivalents of Cd(II) (Figure 2.6C, blue). This suggests an additional binding site for Cd(II) outside the zinc finger. However, the Cd(II) titration of Zn(II)–MutM shows no evidence of S^-→Cd(II) LMCT at 242 nm (Figure 2.6C, red). Additionally, the UV–visible spectrum of Zn(II)–MutM pre-incubated with 20-fold excess Cd(II) shows little increase in absorbance at 242 nm (Figure 2.6B), demonstrating that Zn(II) in the zinc finger cannot be replaced by Cd(II) under these conditions. Unfortunately addition of Cd(II) past 20 equivalents causes precipitation of the protein, so a full titration could not be performed.

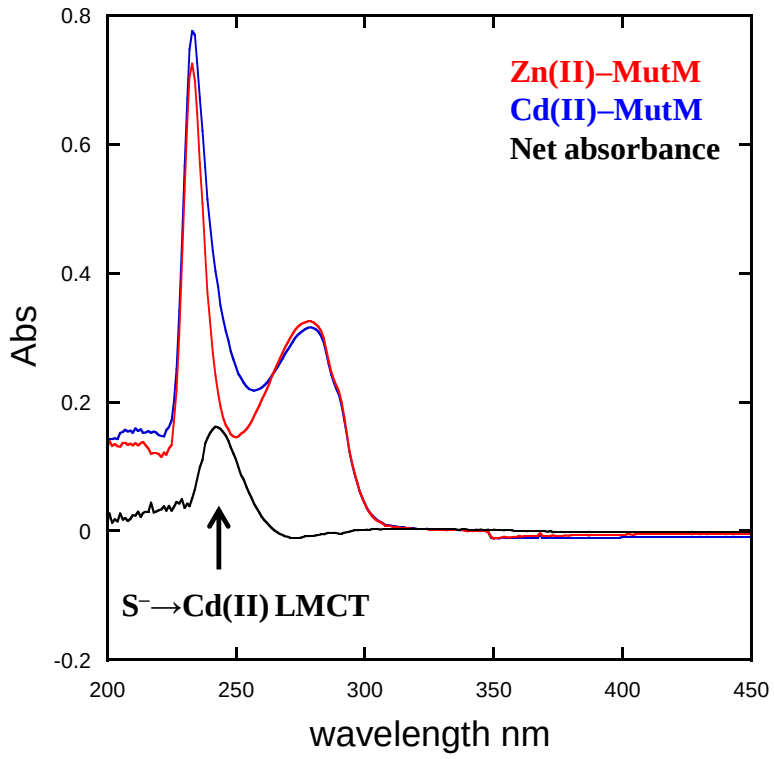

Figure 2.5. UV–visible spectra of Zn(II) and Cd(II)–MutM. The spectrum of as purified Zn(II)–MutM (red) and Cd(II)–MutM (blue) are shown. The peak at 242 nm obtained from subtracting the Zn(II)–MutM spectrum from the Cd(II)–MutM spectrum (black) is due to the cysteine thiolate S→Cd(II) LMCT.

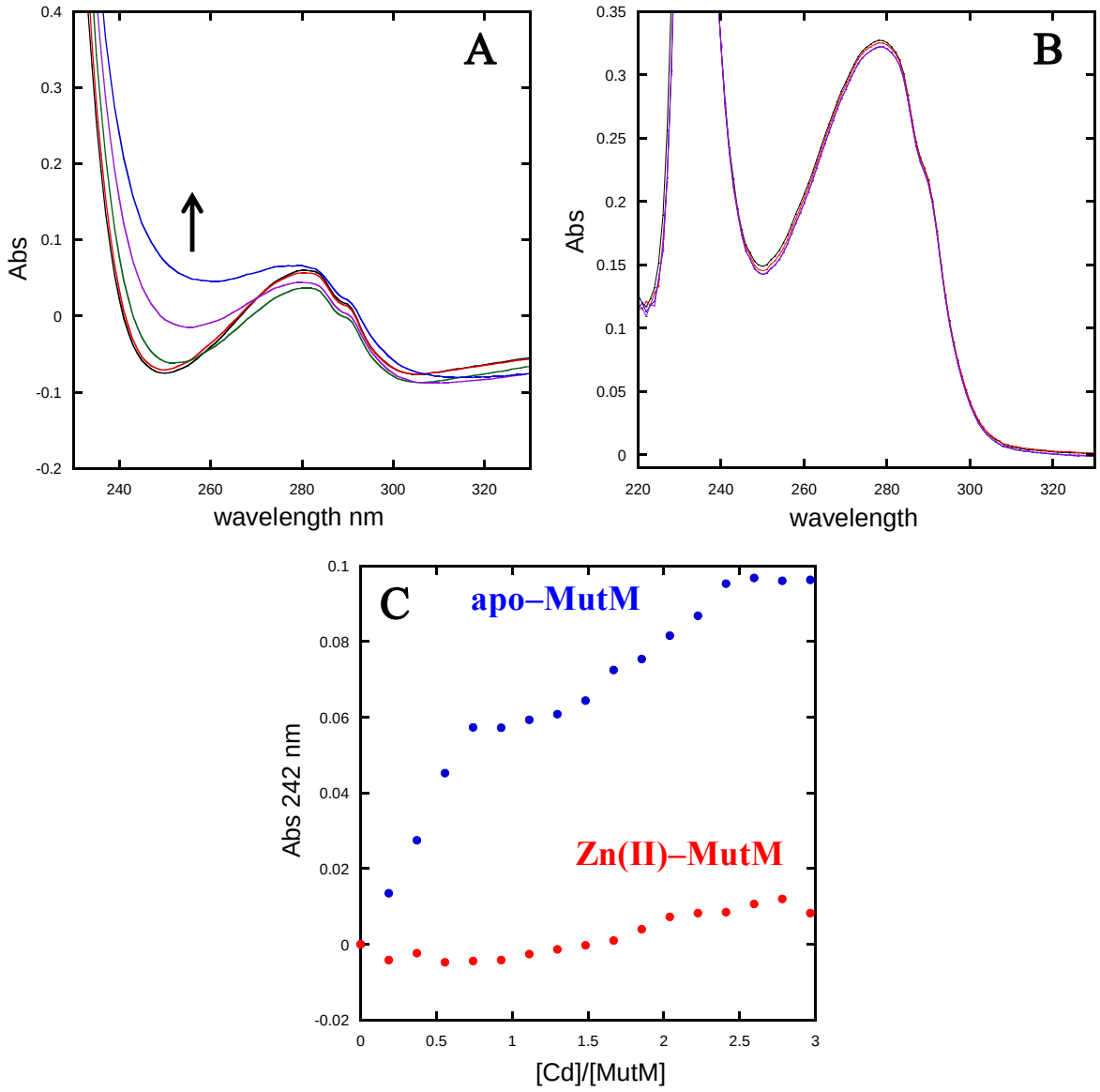

Figure 2.6. UV–visible Cd(II) titration of apo–MutM and Zn(II)–MutM. (A) The titration of apo–MutM shows an increase in the S→Cd(II) LMCT at 242 as Cd(II) is added. (B) The titration of Zn(II)–MutM with Cd(II) up to 20 equivalents.(C) The binding isotherms for Cd(II) titrations into apo–MutM (blue) and Zn(II)–MutM (red).

Since the $S^{-}\rightarrow$Cd(II) LMCT at 242 nm is somewhat obscured by absorbance of the peptide backbone and aromatic residues and Zn(II) is spectroscopically silent, we repeated the titration experiments above with the presence of the Zn(II) indicator PAR. We first titrated PAR with Cd(II) or Zn(II) to create standard curves, which were linear for both metals but with different molar absorptivities (Figure 2.7A, red and blue). Cd(II) titrations of Zn(II)–MutM and Zn(II) titrations of Cd(II)–MutM were then performed with presence of 10-fold excess PAR over protein. The binding isotherm from the Cd(II) titration of Zn(II)–MutM in the presence of PAR (Figure 2.7A, purple) is almost identical to the Cd(II) titration of PAR alone (Figure 2.7A, blue), showing that little Zn(II) is replaced by Cd(II). On the other hand, Cd(II)–MutM titrated with Zn(II) in the presence of PAR (Figure 2.7B, cyan) overlaps with the Zn(II) titration of PAR alone (Figure 2.7B, red) before one equivalent of Zn(II) was added. This indicates that PAR, not MutM, is binding the first molar equivalent of Zn(II). After one equivalent of Zn(II), the slope of the titration curve resembles the PAR standard curve for Cd(II) indicating that Cd(II) is being displaced by Zn(II) and binding to PAR (Figure 2.7B, blue). Overall, MutM binds Zn(II) with higher affinity than Cd(II).

2.3.5 Cobalt binding to MutM. Like Cd(II), Co(II) can also be used as a spectroscopic surrogate for Zn(II) in zinc finger proteins. Co(II) is also considered a carcinogenic metal, so it is also of interest to study its association with MutM for that reason, as well.[12] MutM was expressed with Co(II) in the media and purified as a 1:1 complex. The spectrum of purified Co(II)–MutM protein between 300–900 nm is shown in Figure 2.8A. The absorption peaks between 600–850 nm are the result of $d\rightarrow d$ electronic transitions and are characteristic for Co(II) coordination by four cysteines in a tetrahedral geometry.[8] The absorption peak shown in the UV

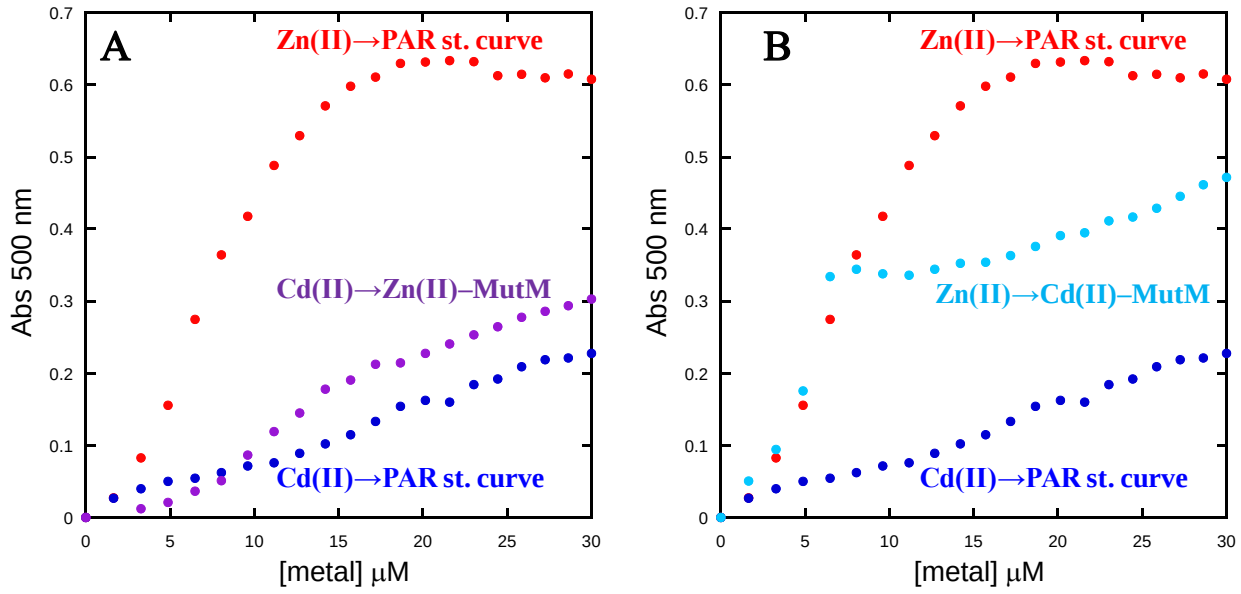

Figure 2.7. Titrations to determine relative affinities of MutM for Zn(II) and Cd(II). Standard curves for PAR titrated with Zn(II) or Cd(II) are in red and blue, respectively. (A) Cd(II) titration of Zn(II)–MutM in the presence of PAR (purple). (B) Zn(II) titration of Cd(II) –MutM in the presence of PAR (cyan).

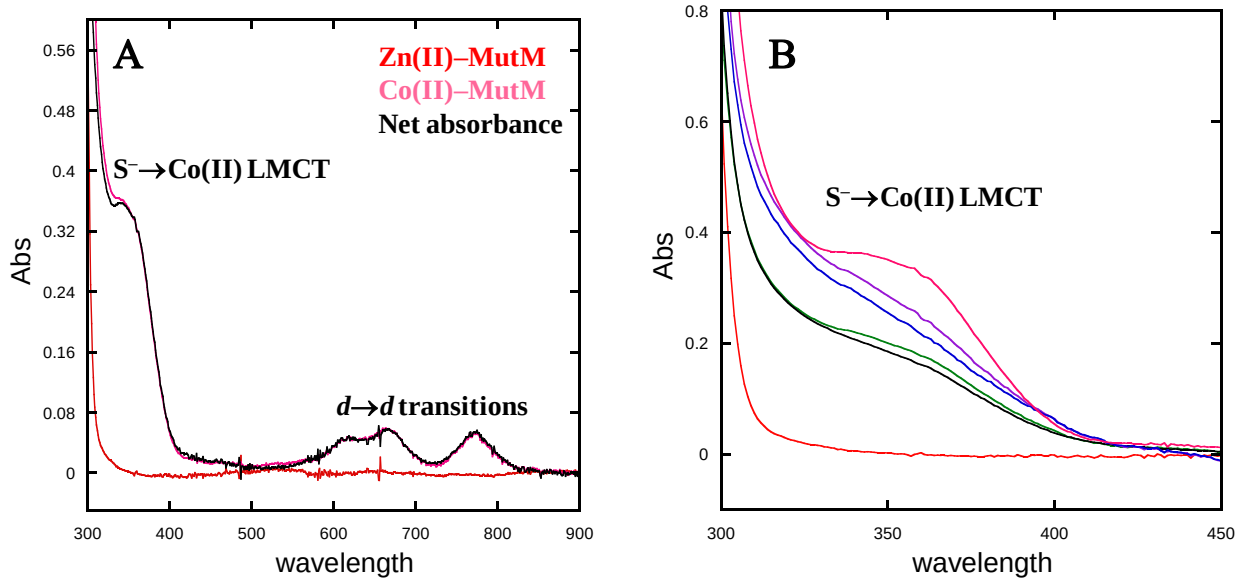

Figure 2.8. UV–visible spectra of Co(II)–MutM. (A) The spectra of as-purified Zn(II)–MutM (red) and Co(II)–MutM (pink) are shown. The net absorbance obtained from subtracting Zn(II)–MutM spectrum form Co(II)–MutM spectrum (black) reveals LMCT transitions (350 nm) and *d*→*d* transitions (600-850 nm). (B) UV–visible spectra of Co(II) titration of apo-MutM. Absorbance at 350 nm due to the LMCT transition increases as Co(II) is added.

range is characteristic to cysteine thiolate $S^- \rightarrow$Co(II) LMCT. The net absorption spectrum, obtained from subtracting the Zn(II)–MutM spectrum from the Co(II)–MutM spectrum, reveals an absorption maximum at 350 nm with a molar absorptivity of 2 $mM^{-1}cm^{-1}$. This is consistent with Cys_4 coordination of Co(II).

Co(II) titration of apo–MutM shows an increase in the $S^- \rightarrow$Co(II) LMCT at 350 nm (Figure 2.8B). Co(II) binding is saturated at 1 molar equivalent of Co(II), showing there is no additional binding site for Co(II) outside the zinc finger. However, the UV–visible spectrum of Zn(II)–MutM pre–incubated with 50-fold excess of Co(II) shows no increase in absorbance at 350 nm (data not shown). This indicates that MutM can bind Co(II) in the metal-free form but it has a significantly lower binding affinity than Zn(II).

2.4 DISCUSSION

2.4.1 Non–native metal binding to MutM. There is no direct evidence that metals inhibit the BER pathway through coordinating with the zinc finger motif of MutM. Here we identified that the 1:1 Cd(II)– and Co(II)–MutM complexes coordinate the metal ion with four Cys residues. As the Cys_4 zinc finger structure is the only metal binding site of MutM where the metal ions can be coordinated with four Cys residues, Cd(II) and Co(II) binding to MutM zinc finger has been verified in this chapter. Furthermore, a tetrahedral geometry of Co(II)–Cys_4 binding can be recognized through UV–visible spectra, consistent with the previous EXAFS studies of Co(II) – MutM.[4] We also tried to construct the Pb(II)–MutM. However, no 1:1 complex could be obtained nor could Pb(II)–Cys coordination could be observed by UV-visible spectroscopy. This may be due to a several orders of magnitude lower binding affinity of Pb(II) to MutM, compared

with Zn(II). This agrees with the previous observation that >1000-fold excess of Pb(II) did not inhibit MutM activity.[3]

It is necessary to mention that a secondary Cd(II) binding site on Cd(II)–MutM is observed when we titrate apo–MutM. According to UV-visible spectrum, this secondary binding site also coordinates with Cd(II) through Cys residues. MutM does possess two cysteine residues outside the zinc finger (Cys_{147} and Cys_{195}) that are positioned with their side-chains within 4.8 Å of each other and could form an additional binding site for metals (details are discussed in Chapter 5). This secondary binding site is not observed in Cd(II) titrations of Zn(II)–MutM or Cd(II)–MutM, however. It is also possible that Cd(II)–MutM binds to extra reducing agent or EDTA during protein construction which provide additional Cd(II)-S LMCT. To clarify this, we need to further investigate the $Cd(II)_2$–MutM species.

2.4.2 Metal competition for MutM. To the best of our knowledge, no relative binding affinities of the non–native metals to MutM have been published. This type of experiment is made more difficult because of the tight binding of Zn(II) to Cys_4 zinc fingers ($K_d \sim 10^{-12}$ M) and apo-protein is hard to obtain. The only Cys_4 type zinc finger that is intensively studied for non–native metal competition is that of XPA, a human DNA binding protein participating in the NER pathway. In this system, Co(II) binding is 3 orders of magnitude weaker than Zn(II) binding using a truncated XPA zinc finger (XPAzf) peptide.[8,13] But, one must also consider that these studies were not conducted with the full-length XPA protein so the actual values could be different.Like XPA, we verify that Co(II) binding to the MutM Cys_4 zinc finger is also significantly weaker than Zn(II) in the full length protein. Therefore, it is unlikely for zinc finger proteins to coordinate Co(II) instead of Zn(II) and it is possible that the inhibition of other DNA

repair proteins by Co(II), such as XPA, is due to alternative mechanisms. With respect to Cd(II), it binds more tightly to the truncated XPAzf with a K_d of ~10^{-13} M, compared to Zn(II), which is ~10^{-10} M. However, no Cd(II) binding affinity to a full length protein containing the Cys_4 zinc finger has been reported.

We investigated the ability of Cd(II) to replace Zn(II) in a full length protein, and, in order to avoid the overlapping absorption of Tyr, Phe and $S^- \rightarrow$Cd(II) charge transfer (240–280 nm), we carried out metal competition titrations of MutM in the presence of the fluorescent chelator PAR. PAR forms complexes with both Zn(II) and Cd(II), which have distinct UV–visible absorptivities. We observed that full length MutM forms relatively stable complex with Zn(II), which is not replaced by excess amount of Cd(II) under the experimental conditions. This is not in agreement with the prediction that Cys_4 zinc fingers generally prefer Cd(II) over Zn(II). This discrepancy can lead to the following conclusions: first, the metal binding properties of a zinc finger depend more on the specific amino acid sequence of the motif rather than the type of zinc finger; second, the full length protein provides better protection for Zn(II) against substitution by non-native metals.

2.4.3 Conclusions and future directions. In this work, we conclude that the Cys_4 zinc finger of MutM can coordinate both Cd(II) or Co(II) in the zinc finger motif as the primary metal binding site. Therefore, if inhibition of MutM by these metal ions is observed, it is most likely due to the structural perturbations at the zinc finger. If the protein is inhibited upon the binding of these metal ions, this could be a mechanism of non–native metal carcinogenesis. We explored the activity of MutM bound to these metal ions in Chapter 3 and further reveal the inhibition mechanism.

Future work should focus on determining whether non-native metals can replace the native Zn(II) under physiological concentrations. For this, metal competition titrations of MutM must be performed to determine the dissociation constants for each metal. Another aspect that should be considered is whether the Cys residues are equivalent in metal coordination. Although Cd(II) and Co(II) binding does not alter the coordination geometry of the truncated MutM Cys_4 zinc finger based on EXAFS, this does not mean that each cysteine has equivalent roles in metal coordination.Detailed studies of some Cys_3His_1zinc fingers revealed an in-equivalence of the Cys residues involved in Zn(II) binding, which lead to the presence of an equilibrium between Cys_3His_1 and Cys_2His_1 coordination modes. It is argued that this transiently non-coordinated thiol may provide a feasible target for metal substitution.[14] Therefore, it is worthwhile to investigate the equivalence of the Cys residues of the MutM zinc finger in terms of metal ion coordination. This can provide further information of the stability of various metal–MutM complexes.

2.5. REFERENCES

(1) Hartwig, A., Asmuss, M., Blessing, H., Hoffmann, S., Jahnke, G., Khandelwal, S., Pelzer, A., and Burkle, A. (2002) Interference by toxic metal ions with zinc-dependent proteins involved in maintaining genomic stability. *Food Chem. Toxicol.40,* 1179–1184.

(2) Salnikow, K., and Zhitkovich, A. (2008) Genetic and epigenetic mechanisms in metal carcinogenesis and cocarcinogenesis: nickel, arsenic, and chromium. *Chem. Res. Toxicol.21*, 28–44.

(3) Asmuss, M., Mullenders, L. H., Eker, A., and Hartwig, A. (2000) Differential effects of toxic metal compounds on the activities of Fpg and XPA, two zinc finger proteins involved in DNA repair. *Carcinogenesis21,* 2097–2104.

(4) Buchko, G. W., Hess, N. J., Bandaru, V., Wallace, S. S., and Kennedy, M. A. (2000) Spectroscopic studies of zinc(II)- and cobalt()-associated escherichia coli formamidopyrimidine-

DNA glycosylase: Extended x-ray absorption fine structure evidence for a metal-binding domain. *Biochemistry39*, 12441–12449.

(5) Buchko, G. W., Hess, N. J., and Kennedy, M. A. (2000) Cadmium mutagenicity and human nucleotide excision repair protein xpa: CD, EXAFS and $^{(1)}H/^{(15)}N$-NMR spectroscopic studies on the zinc(II)- and cadmium(II)-associated minimal DNA-binding domain (M98-F219). *Carcinogenesis21*, 1051–1057.

(6) Busenlehner, L. S., Cosper, N. J., Scott, R. A., Rosen, B. P., Wong, M. D., and Giedroc, D. P. (2001) Spectroscopic properties of the metalloregulatory Cd(II) and Pb(II) sites of s. Aureus pI258 CadC. *Biochemistry40*, 4426–4436.

(7) Chen, X., Chu, M., and Giedroc, D. P. (2000) Spectroscopic characterization of Co(II)-, Ni(II)-, and Cd(II)-substituted wild-type and non-native retroviral-type zinc finger peptides. *J. Biol. Inorg. Chem.5*, 93–101.

(8) Kopera, E., Schwerdtle, T., Hartwig, A., and Bal, W. (2004) Co(II) and Cd(II) substitute for Zn(II) in the zinc finger derived from the DNA repair protein XPA, demonstrating a variety of potential mechanisms of toxicity. *Chem. Res. Toxicol.17*, 1452–1458.

(9) Zamble, D. B., McClure, C. P., Penner-Hahn, J. E., and Walsh, C. T. (2000) The McbB component of microcin B17 synthetase is a zinc metalloprotein. *Biochemistry39*, 16190–16199.

(10) Busenlehner, L. S., and Giedroc, D. P. (2006) Kinetics of metal binding by the toxic metal-sensing transcriptional repressor staphylococcus aureus pI258 CadC. *J. Inorg. Biochem.100*, 1024–1034.

(11) Sabel, C. E., Shepherd, J. L., and Siemann, S. (2009) A direct spectrophotometric method for the simultaneous determination of zinc and cobalt in metalloproteins using 4-(2-pyridylazo)resorcinol. *Anal. Biochem.391*, 74–76.

(12) Hengstler, J. G., Bolm-Audorff, U., Faldum, A., Janssen, K., Reifenrath, M., Gotte, W., Jung, D., Mayer-Popken, O., Fuchs, J., Gebhard, S., Bienfait, H. G., Schlink, K., Dietrich, C., Faust, D., Epe, B., and Oesch, F. (2003) Occupational exposure to heavy metals: DNA damage induction and DNA repair inhibition prove co-exposures to cadmium, cobalt and lead as more dangerous than hitherto expected. *Carcinogenesis24*, 63–73.

(13) Witkiewicz-Kucharczyk, A., and Bal, W. (2006) Damage of zinc fingers in DNA repair proteins, a novel molecular mechanism in carcinogenesis. *Toxicol. Lett.162*, 29–42.

(14) Laity, J. H., Lee, B. M., and Wright, P. E. (2001) Zinc finger proteins: New insights into structural and functional diversity. *Curr. Opin. Struct. Biol.11*, 39–46.

CHAPTER 3

DNA BINDING AND CATALYTIC ACTIVITY OF MUTM DNA GLYCOSYLASE

3.1 INTRODUCTION

Non–native metal ions interfere with proteins that are involved in DNA repair including PARP, p53, XPA and MutM. MutM, a tri-functional 8-oG specific DNA glycosylase in the bacterial BER pathway, was previously shown to be inhibited in a dose–dependent manner by Cd(II), Cu(II) and Hg(II).[1] This previous study was based on electrophoretic mobility shift assays (EMSA) that monitored the dissociation of dsDNA containing an 8-oG modification after MutM base cleavage;[1] however, they did not provide real-time progress of the reaction, nor detailed information about the mechanism of inhibition. Thus, it is unknown whether inhibition is due to metal substitution at the zinc finger or even the specific step in the mechanism that is inhibited. In this chapter, we use a hyperchromicity assay to study the overall kinetics of MutM, develop an 8-oG deaminase coupled assay to monitor the formation of the excised 8-oG base, and conduct fluorescence anisotropy titrations and gel shift assays to investigate the DNA binding of MutM purified with various metal ions.

The continuous hyperchromicity assay (CHA), first developed by Brenslauer and coworkers, provides a real-time, continuous optical signal to quantify product formation and requires minimal sample manipulation.[2] Unlike most of the traditional methods to determine kinetic parameters for BER/NER enzymes, CHA does not require expensive fluorescent or radioactive

DNA–labeling and it does not require quenching of the reaction. The CHA assay, instead, uses the intrinsic hyperchromicity of DNA. Due to aromatic rings of the nucleotide bases, dsDNA absorbs light at 260 nm. The intensity, however, is decreased because of the base stacking interactions. If the two strands dissociate, the bases become un-stacked and therefore the absorbance increases by 30–40%. Here, we use hyperchromicity to track the strand separation of 8-oG modified dsDNA to measure the catalytic activity of MutM. As shown in Figure 3.1, MutM excises the oxidized base at the glycosidic bond and then cuts the backbone at the apurinic site with its 5' AP lyase activity. This destabilizes the strands of dsDNA, causing them to dissociate, thus the absorbance at 260 nm increases because of hyperchromic effect. This assay reports on the rate limiting step leading to strand separation.

Since MutM acts as a tri–functional enzyme in the BER pathway, it is also worthwhile to develop activity assays that monitor the recognition and binding of MutM to damaged DNA, the release of 8-oG (glycosylase activity), in addition to lyase activity. This will allow for more detailed mechanistic information as to what catalytic step or steps are affected by non-native metal substitution. Towards this end, we also developed a coupled enzymatic assay using the recently discovered 8-oG deaminase[3] to detect the excised 8-oG base released from MutM glycosylase activity. In bacteria, the excised 8-oG base is further metabolized by 8-oG deaminase, which converts 8-oG to uric acid and ammonia.[3] Formation of ammonia can be monitored by another coupled enzyme assay shown as in Figure 3.2. This requires the oxidation of NADH to NAD^+, which is detected spectroscopically at 340 nm.[3]

To monitor the initial DNA binding by MutM, fluorescence anisotropy and EMSA were used. Fluorescence anisotropy monitors MutM–DNA binding through the tumbling rate of fluorescein–labeled dsDNA. When MutM is titrated into the DNA, the overall tumbling rate of

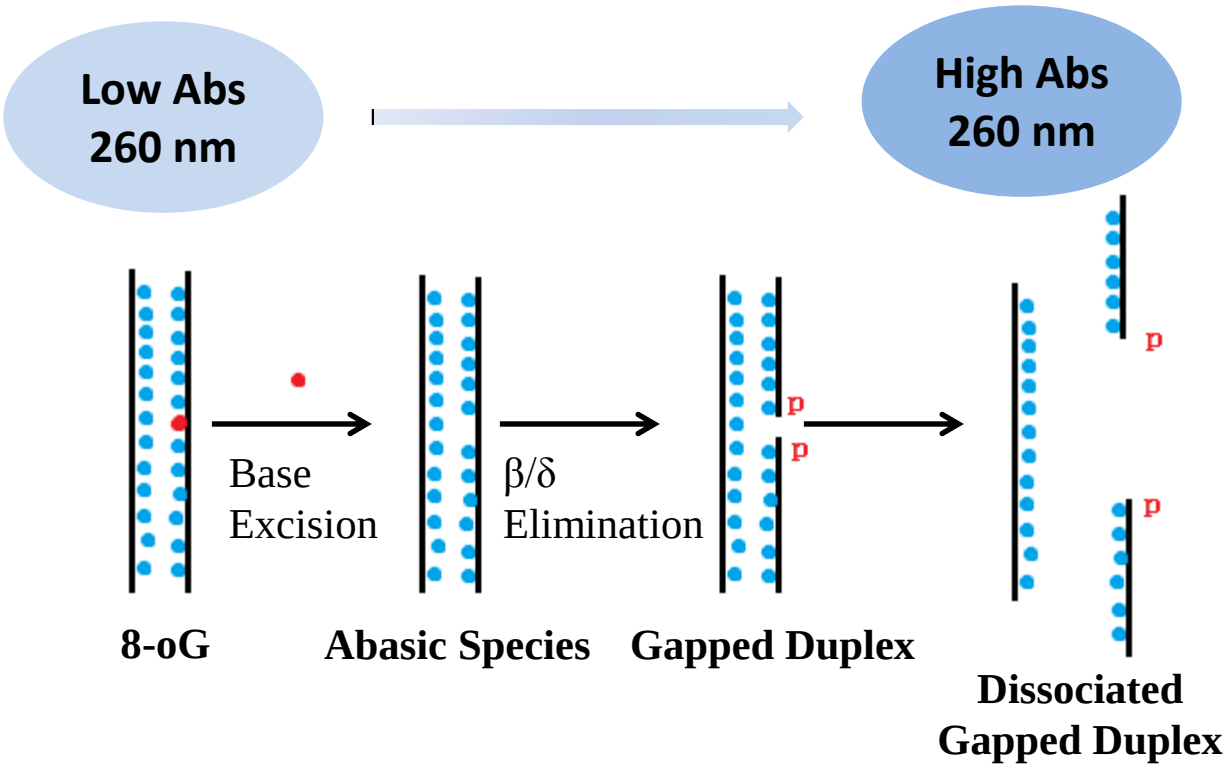

Figure 3.1. Schematic of the hyperchromicity assay. MutM excises the oxidized base out of the dsDNA and cuts the apurinic site, turning the dsDNA with lower UV absorbance at 260 nm into single strands with higher absorbance.[2]

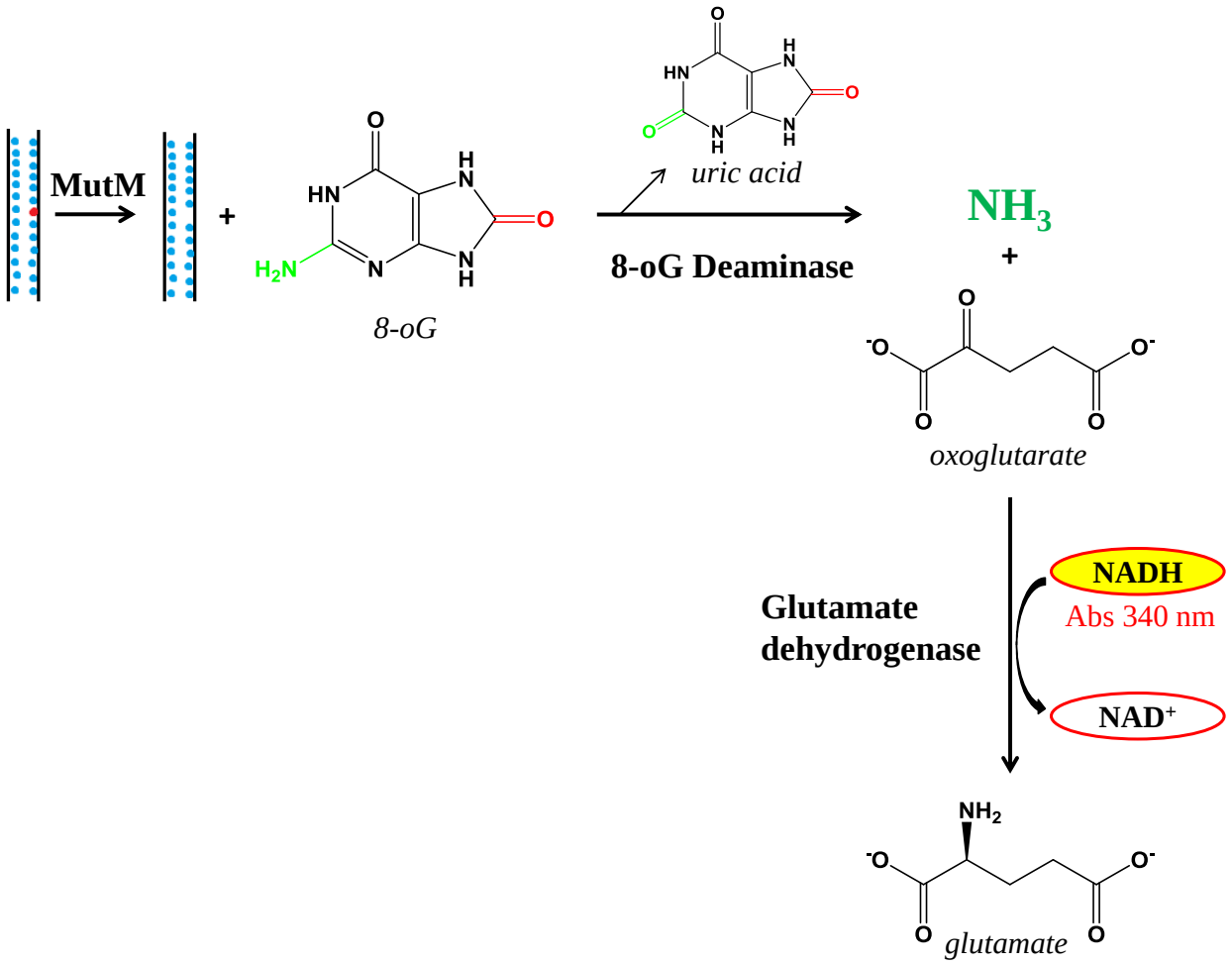

Figure 3.2. The deaminase coupled assay. 8-oG deaminase converts the excised 8-oG to uric acid and ammonia. In the presence of oxoglutarate, ammonia oxidizes NADH to NAD^+ with decrease in absorbance at 340 nm. Structures are created through ChemBioDraw Ultra.

the fluorophore decreases as an increased fraction of dsDNA forms a complex with MutM. This experiment will reveal if non–native metal substitution affects the ability of MutM to bind DNA in the first place, and if this is the mechanism of inhibition.

In the studies presented here, we observed that compared to Zn(II)–MutM, apo–MutM and Cd(II)–MutM lost all enzymatic activity, while Co(II)–MutM retained most of the catalytic activity. Pre-incubation with Cd(II) interferes with, but does not completely, inactivate Zn(II)–MutM under our experimental conditions. We further demonstrate that both DNA binding and base excision are disrupted by Cd(II) coordination to the MutM Zn(II) finger. Implications of these findings will be discussed.

3.2 MATERIALS AND METHODS

3.2.1 Chemicals. All the single stranded oligonucleotides used in this chapter were purchased from Operon, resuspended in TE buffer (10 mM Tris–HCl, pH 8, 1 mM EDTA) and stored at -20 °C. The 15% Mini-Protean TBE Precast gels were purchased from Bio-Rad. L-Glutamic dehydrogenase (GDH), α-ketoglutaric acid (αKG) and β-nicotinamide adenine dinucleotide 2'-phosphate reduced tetrasodium salt hydrate (NADH) were purchased from Sigma. The guanine (G) and 8-hydroxyguanine (8-oG) bases were purchased from Alfa Aesar and Cayman Chemical, respectively.

3.2.2 Continuous hyperchromicity assays. One strand of the dsDNA substrate used in the activity assays was modified with 8-oG (Table 3.1). The non-modified complementary strand contained a cytosine to pair with the 8-oG base. The single stranded, complementary

Table 3.1. Oligonucleotides used in the MutM DNA binding and activity assays.

	Sequence (5' → 3')	Modification	# Bases	T_m(℃)	Purity	Experiments
1	CCTCTCGCCTTCC	8-oG	13	51.7	Salt-free	Activity assays $NaBH_4$-EMSA
2	GGAAGGCGAGAGG	n/a	13	54.8	Salt-free	Activity assays $NaBH_4$-EMSA
3	GGAAGGCGAGAGG	Fluorescein	13	54.8	HPLC	Anisotropy
4	CCTCTCGCCTTCC	n/a	13	54.8	HPLC	Anisotropy
5	GTGGAAGGCGAGAGGG	Fluorescein	16	61.8	HPLC	Anisotropy
6	GTGGAAGGCGAGAGGG	n/a	16	68.8	HPSF	Anisotropy EMSA
7	CCCTCTCGCCTTCCAC	n/a	16	68.8	HPSF	EMSA
8	GGGGCCCGGATCCATGACCATGACCC	n/a	26	75.2	Salt-free	EMSA
9	GGGTCATGGTCATGGATCCGGGCCCC	n/a	26	78.1	Salt-free	EMSA

oligonucleotides were mixed in a 1:1 ratio in buffer N (100 mM NaH_2PO_4, pH 8, 150 mM NaCl), heated to 95 °C for 5 min, and cooled to room temperature. The annealed, dsDNA was stored at −20 °C. The relative extinction coefficient between the dsDNA (substrate) and ssDNA (products) was determined.[2] Product formation was mimicked by combining a proportional decrease the substrate 13-mer duplex with an increasing mixture of the theoretical products (excised 8-oG, 5'-CCTCTC-3', 5'-CCTTCC-3', and the non-modified 13-mer oligonucleotide), such that 0, 20, 40, 60, 80 and 100% product are present. The relative extinction coefficient $\varepsilon_{100\%}$ corresponding to 100% product formation is 27.1$mM^{-1}cm^{-1}$ (Figure 3.3),which is consistent with the reported value of 25.2 $mM^{-1}cm^{-1}$ for a slightly different DNA substrate.[2]

Kinetic measurements were performed on Varian Cary 100 UV–visible spectrophotometer with dual cell peltier temperature regulation. The duplex substrate was diluted with buffer F (10 mM NaH_2PO_4, pH 7.5, 100 mM NaCl) to obtain a 1 mL sample with 100–400 nM dsDNA. This was added to a 10 mm semi-micro black wall quartz cuvette and equilibrated at 25 °C for 5 min. The reaction was initiated with MutM (50–500 nM), mixed (dead time 20s), and then the reaction was followed by spectroscopically at 260 nm. Product formation was estimated by using the relative extinction coefficient of the products, determined above.[2]

3.2.3 8-oG deaminase coupled assays. The plasmid containing 8-oG deaminase was a generous gift from Dr. Frank Raushel (Texas A&M University) and the enzyme was purified, as described. The 8-oG deaminase preparation was tested for activity according to R. S. Hall *et al*.[3] MutM kinetic measurements were performed on a Varian Cary 100 UV–visible spectrophotometer with dual cell peltier temperature regulation. The 1 mL reaction contained 8-oG modified duplex substrate (0.2–2 μM) was mixed with GDH (0.5%), αKG (5 mM), and

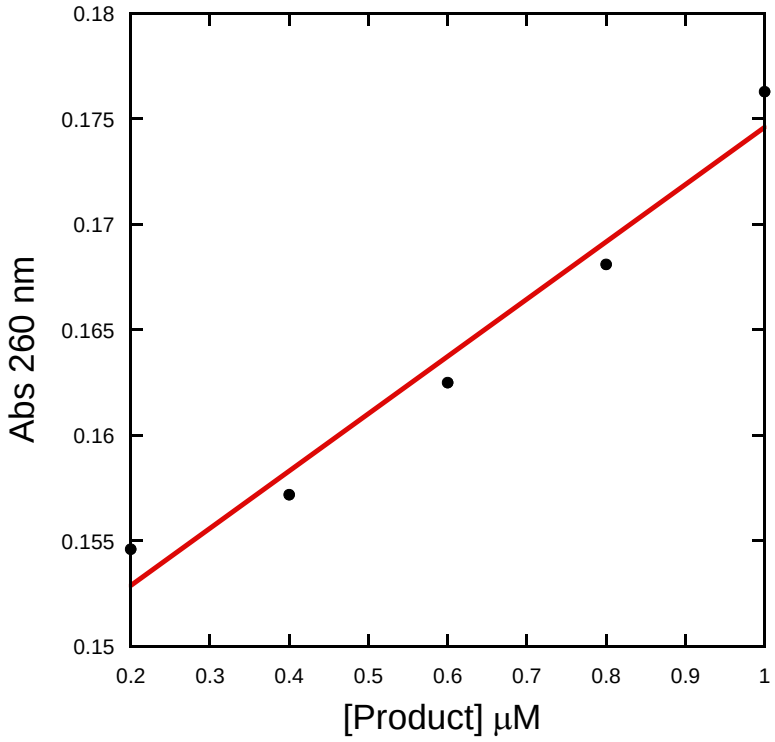

Figure 3.3. The relative extinction coefficient of hyperchromicity assay products. This assumes 100% of the product is formed. The linear fit yielded an extinction coefficient of 27.1 $mM^{-1}cm^{-1}$.

NADH (200 nM) in buffer G (20 mM HEPES, pH 7.5, 100 mM KCl). The sample was equilibrated at 25 °C for 5 min. The reaction was initiated addition of MutM into the cuvette (dead time 20s with manual mixing), followed by continuous monitoring the absorbance at 340 nm. Product formation was calculated using the extinction coefficient 6220 $M^{-1}cm^{-1}$ of NADH at 340 nm.

3.2.4 Fluorescence anisotropy titrations. Because of the intrinsic activity of MutM, dsDNA with the 8-oG mutation could not be used for DNA binding titrations. Instead, non-modified DNA was used, as is common in the literature.[4] The oligonucleotides were modified with fluorescein at the 5' end (Table 3.1). The experiments were performed in both non-continuous and continuous titrations. For non-continuous titrations, individual samples were made in a Greiner bio-one black μ clear 96-well (half area) plate. Double-stranded, non-modified DNA (50–100 nM) in buffer E (50 mM HEPES, pH 8, 100 mM KCl, 1 mM EDTA, 0.5 mM TCEP, 1 mM $MgCl_2$) was mixed with increasing concentrations of MutM, ranging over 2 orders of magnitude lower and higher than the dsDNA concentration. Samples were incubated in the dark for 20 min at room temperature and the plate was read by the BioTek Synergy 2 Plate Reader with excitation and emission wavelengths for fluorescein at 485 nm and 520 nm, respectively.

The florescence anisotropy experiments were also conducted as continuous titrations.[5] The oligonucleotides were diluted in a 10 mm clear wall quartz cuvette with buffer E to obtain a 2 mL sample with 2–5 nM dsDNA. The initial fluorescence anisotropy was recorded prior to the addition of MutM. MutM was titrated into the DNA, incubated for 10 min with gentle stirring at ambient temperature, and then the fluorescence polarization was recorded by the ISS PC1 photon

counting Spectrofluorimeter with excitation and emission wavelength at 485 nm and 520 nm, respectively. Anisotropy was determined by

$$r = \frac{2P}{3 - P}$$

where r is fluorescence anisotropy and P is the polarity of emission light. The anisotropy was plotted against MutM concentration and the binding isotherm is fit to

$$r = \frac{P_T + DNA_T + K_d - \sqrt{(P_T + DNA_T + K_d)^2 - 4P_T DNA_T}}{2DNA_T} \cdot (r_b - r_f) + r_f$$

where P_T and DNA_T are concentrations of MutM and the dsDNA, respectively, K_d is the dissociation constant of MutM–DNA binding, r_b is the anisotropy in the presence of saturated MutM and r_f is the anisotropy of the free dsDNA.

3.2.5 Electrophoreticmobility shift assays. Since we tested non–specific and specific DNA binding of MutM through EMSA, both 8-oG modified and non-modified DNA duplex were used in the assays (Table 3.1). Double stranded DNA (10-20 μM) was incubated with metallated MutM preparations (5–50 μM) in buffer E at room temperature for 20 min. Then, 3 ×loading dye (7.5% ficoll, 0.05% bromophenol blue in 1 ×TBE buffer) was added.[6] To test for specific DNA binding and the ability of MutM to act on the 8-oG base excision, dsDNA with 8-oG modified was incubated with metallated MutM preparations in buffer E with the addition of 50 mM $NaBH_4$, which traps the Schiff base intermediate formed between Pro1 of MutM and the pentose of DNA.[7] Urea (8M) was added to the loading dye to interfere with non–specific DNA binding. If MutM is active, there will be a covalently bound DNA–MutM complex that cannot be dissociated with urea. All the EMSA samples were run on a pre-equilibrated 10% TBE precast gel for 45 min at 200 V at 4 ℃.[8] The DNA and protein bands were stained with SYBR Green

EMSA nucleic acid gel stain and SYPRO Ruby EMSA protein gel stain, purchased from Life Technologies and detected by the MultiDoc-It Digital Imaging System.

3.3. RESULTS

3.3.1 Characterization of MutM activity. Changes in hyperchromicity are widely used to monitor dsDNA dissociation. The hyperchromic effect, or the increased absorbance of ssDNA compared to the same concentration of dsDNA, was used to characterize overall activity of MutM. Here we use the continuous hyperchromicity assay (CHA) to monitor the catalytic activity of MutM purified with various metals and reveal the inhibition of MutM by non-native metal binding to the zinc finger.[2] For Zn(II)–MutM, the initial velocity of the reaction is dependent on the MutM concentration, as well as temperature (Figure 3.4 A,B). The Michaelis-Menton plot of initial velocity as a function of [MutM] yields a K_m of 52 ($\pm$4.3) nM (Figure 3.4 C), which is comparable to the reported K_m of 45 nM for Zn(II)−MutM.[2] The activities of apo–, Cd(II)–, and Co(II)–MutM preparations were then measured. As expected, apo–MutM has no detectable activity. MutM purified with Cd(II) does not show measurable activity, while MutM purified with Co(II) has similar initial velocity as Zn(II)–MutM (Figure 3.5). In Chapter 2, we determined that both Co(II) and Cd(II) coordinate to Cys residues in the zinc finger motif. Interestingly, we observe that Cd(II) inactivates MutM, however, Co(II) does not. This indicates that MutM displays some flexibility in its metal preference.

The CHA studies above used purified preparations of MutM with non–native metals. This does not address whether these metals will inhibit the Zn(II) form of the enzyme when added to the solution. To investigate the effects of non–native metals on Zn(II)–MutM activity, Zn(II)–

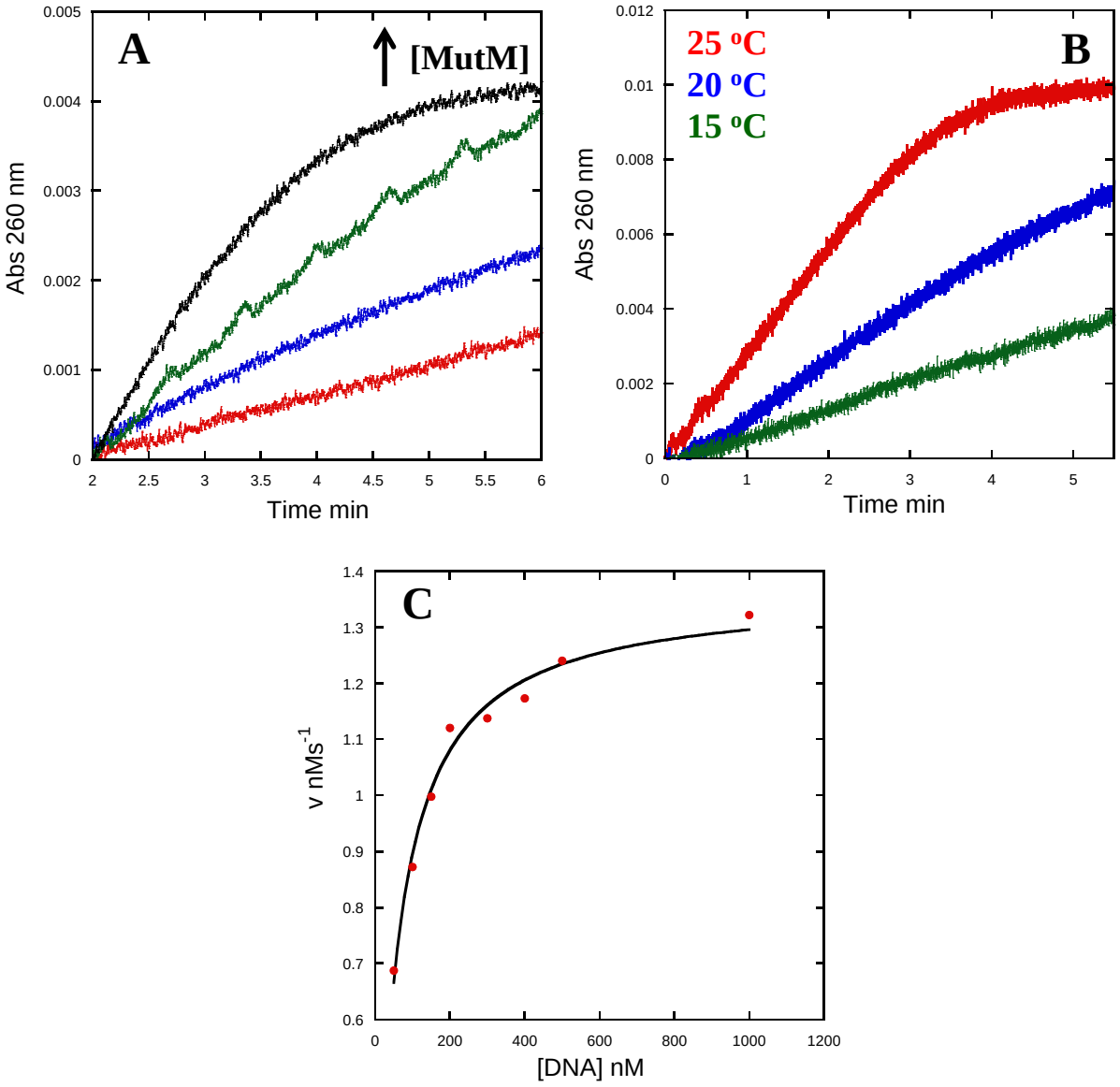

Figure 3.4. Initial characterization of Zn(II)–MutM activity from hyperchromicity assays. (A) Shown are representative progress curves showing the dependence of Zn(II)–MutM activity on the concentration of MutM from 75nM to 500nM, with 400 nM 8-oG modified DNA. (B) The temperature dependence of Zn(II)–MutM catalyzed dsDNA dissociation (15-25 ℃) is shown. (C) The Michaelis-Menton curve of MutM catalyzed dsDNA dissociation is shown. A fit to the standard Michaelis-Menton equation yielded a K_m of 52 ±4.3 nM.

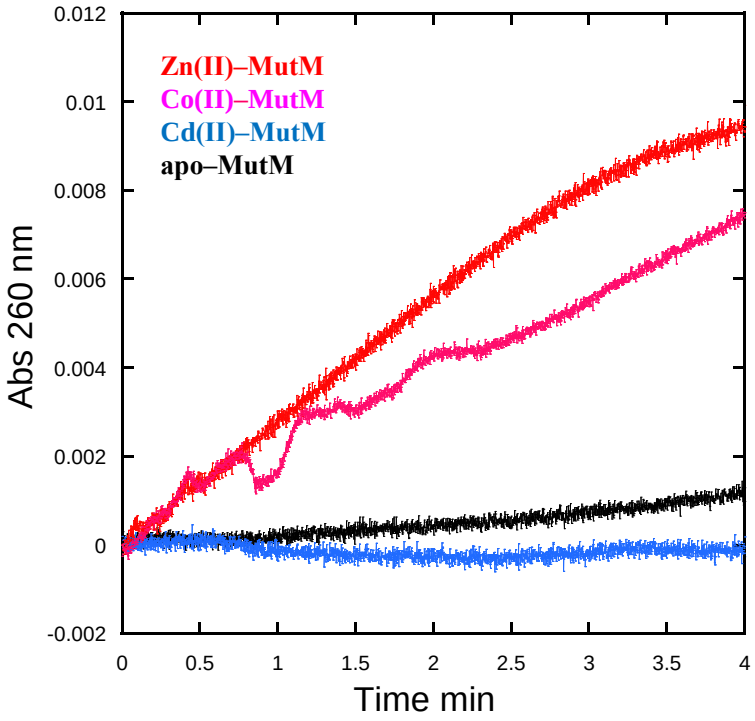

Figure 3.5. Metallated MutM reaction curves from hyperchromicity assays. Shown are representative progress curves for 200 nM as-purified MutM with Zn(II), Co(II), and Cd(II) bound in red, pink, and blue, respectively. Apo–MutM is shown for reference. The concentration of the 8-oG modified DNA is 400 nM.

MutM was pre–incubated with increasing concentrations of Co(II), Cd(II) or Pb(II) for 3 hr at room temperature before the activity was measured. Only Cd(II) shows a dose–dependent inhibition of Zn(II)–MutM activity (Figure 3.6A). However, up to 10-fold excess of Cd(II) over the Zn(II) concentration does not completely inactivate the enzyme. When compared with the activities of MutM purified with Cd(II), this suggests that Zn(II) is not fully replaced by Cd(II) under these conditions. Zn(II)–MutM stability is further confirmed by EDTA chelating experiments in which Zn(II)–MutM is pre–incubated with 10-, 100- and 1000-fold molar excess of EDTA for 3 hr before activity measurements (Figure 3.6B). The progress curve shows slight inhibition with 1000-fold excess EDTA. These experiments indicate that Zn(II) forms a thermodynamically stable complex with MutM through the zinc finger structure.

In order to determine if glycosidic bond cleavage is being affected by Cd(II) coordination, we developed the 8-oG deaminase coupled assay to monitor the formation of the excised base. Since Co(II) does not inhibit MutM activity as determined by CHA, we did not perform this coupled assay with Co(II)–MutM. The 8-oG deaminase substrate, 8-oG,[3] is provided by the base cleavage reaction of MutM with 8-oG modified dsDNA. The rate of the decrease in absorbance at 340 nm, due to the consumption of NADH, is dependent on the concentration of Zn(II)–MutM (Figure 3.7A). Damaged base excision activities of apo–, Cd(II)–, and Zn(II)–MutM preparations were compared. With the same enzyme concentration (1 μM), an initial rate of 4.02 μM min^{-1} is observed for Zn(II)–MutM(Figure 3.7B). In comparison, rate of apo–MutM initiated reaction is 0.45 μM min^{-1} and of Cd(II)–MutM is 0.37 μM min^{-1}. This assay confirms that the first catalytic step, 8-oG glycosylase activity, is inhibited by Cd(II) when coordinated in the zinc finger. Thus we believe the inhibition observed in the CHA assay is actually reporting on the fact that Cd(II) inhibits base excision, and not the AP lyase activity.

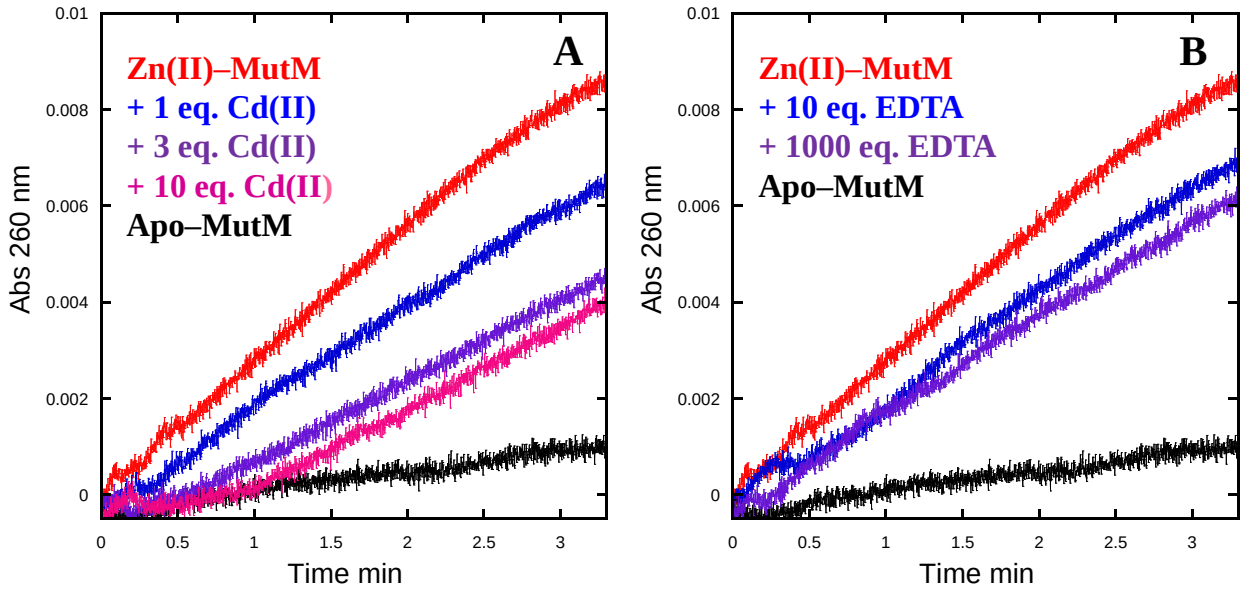

Figure 3.6. MutM inhibition by Cd(II) and EDTA. (A) Shown are representative progress curves comparing the activity of 200 nM Zn(II)–MutM in the presence of 1, 3 and 10 molar equivalents of Cd(II) over [MutM] in blue, purple and pink, respectively, with 400 nM 8-oG modified dsDNA. The reaction curve for apo–MutM (black) is shown for reference. (B) Shown are representative progress curves comparing the activity of 200 nM Zn(II)–MutM in the presence 10 and 1000 molar equivalents of the chelator EDTA over [MutM], with 400 nM 8-oG modified dsDNA. The reaction curve for apo–MutM (black) is shown for reference.

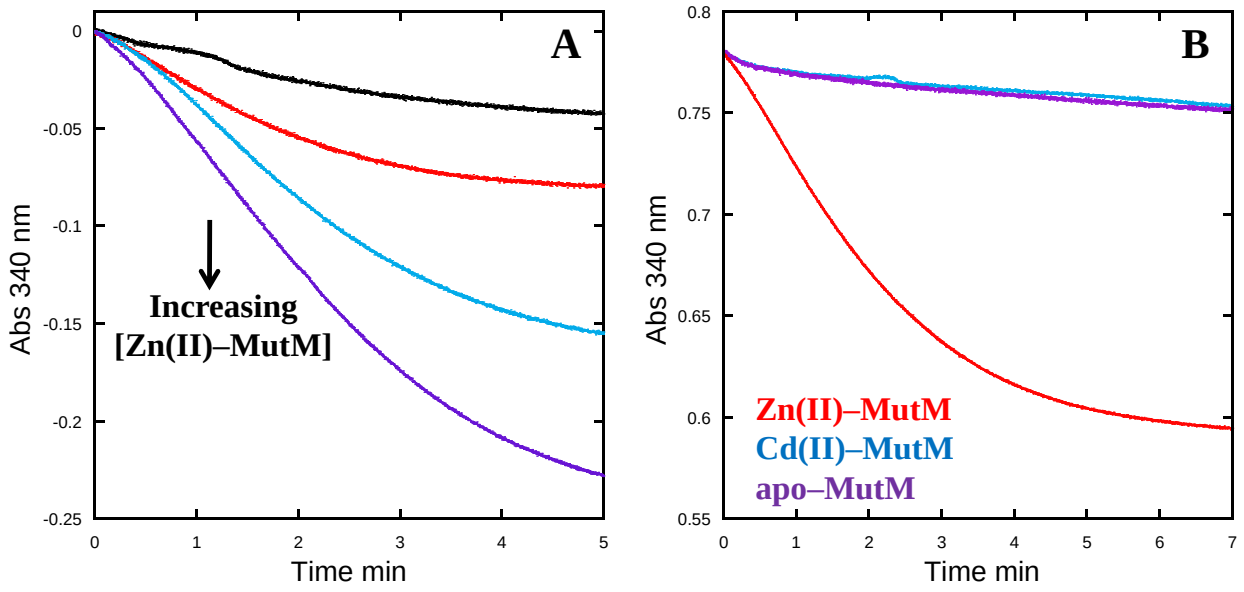

Figure 3.7. The 8-oG glycosylase reaction kinetics of Zn(II)– and Cd(II)–MutM. The 8-oG deaminase coupled assay was performed using as purified preparations of MutM and representative progress curves are shown. (A) An increase in Zn(II)–MutM concentration from 500 nM to 2000 nM, with 2 μM 8-oG modified dsDNA. (B) Cd(II)–MutM does not have measurable activity (blue) compared to Zn(II)–MutM (red). The residual activity is similar to apo–MutM (purple). A concentration of 2 μM 8-oG modified dsDNA was used in the experiment.

3.3.2 MutM DNA binding affinity. Non-native metal binding to MutM can also potentially interfere with DNA binding/base recognition since the zinc finger structure participates in the hydrogen bond network between MutM and the damaged dsDNA substrate.[9] This must also be considered as a step that can be inhibited by non–native metals. Both the non-specific and specific DNA binding affinity of MutM is tested here. Since MutM can discriminate between normal and damaged DNA, non−specific DNA binding is expected for Zn(II)−MutM. To examine this type of binding, non–damaged dsDNA of the same sequence is used. The DNA binding properties of Zn(II)–, Cd(II)–, Co(II)– and apo–MutM were investigated using fluorescence anisotropy with two different lengths of dsDNA where one strand is labeled with a fluorescein fluorophore (Table 3.1). The binding isotherm of the 13-mer dsDNA titrated with Zn(II)–MutM reveals a dissociation constant (K_d)of 749 ± 61 nM, which is within the reported range for similar DNAs[10,11] (Figure 3.8). Co(II)–MutM exhibits a similar DNA binding affinity (K_d = 778 nM ± 82), as expected. The Cd(II)–MutM titration of the 13-mer dsDNA shows that the K_d increases to ~1 ± 0.1 μM for this preparation. Parallel experiments with the 16-mer dsDNA show consistent binding affinity of metallated MutM preparations (Table 3.2). Therefore, the fluorescence anisotropy titration experiments indicate that the non–specific DNA binding of MutM is weakened if Cd(II) is coordinated in the zinc finger, but not if Co(II) is bound. Compared to apo–MutM, which has a negligible affinity for DNA (Figure 3.8, green), Cd(II)–MutM still retains some non-specific binding. We conclude from these studies that Cd(II) does not cause the protein to misfold, but may disrupt key interactions with DNA. Further structural studies in Chapter 4 will address this issue.

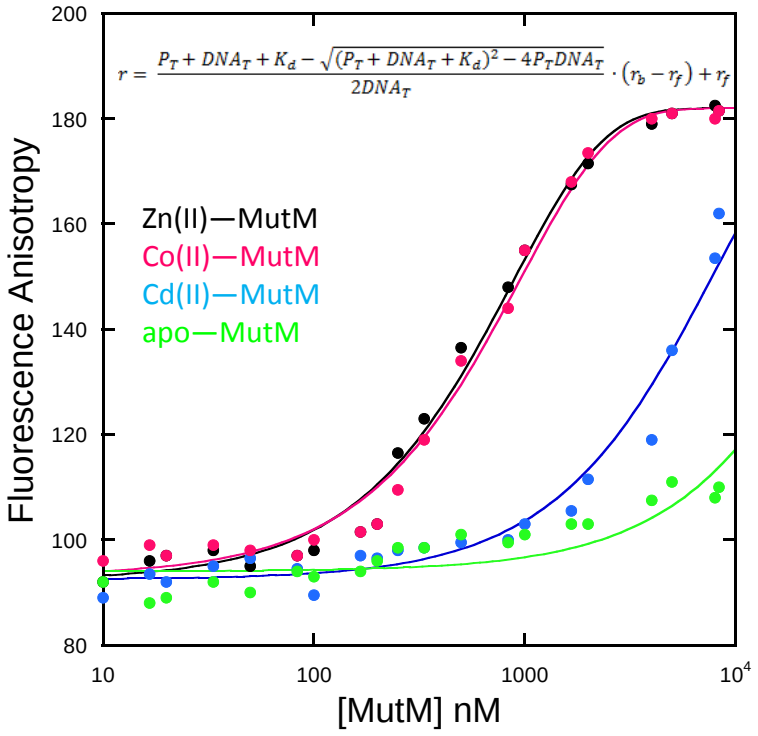

Figure 3.8. Fluorescence anisotropy titrations of Zn(II)–, Co(II)–, Cd(II)–, and apo–MutM. Fluorescein-labeled 13-mer dsDNA that did not contain damaged base was titrated with Zn(II), Co(II), and Cd(II) MutM preparations as shown in black, pink, and blue respectively. Apo−MutM was also titrated as a control (black). The curves were fit to the equation shown and the K_d values are reported in Table 3.2.

Table 3.2. Measured dissociation constants for fluorescence anisotropy titrations.

dsDNA	Zn(II)–MutM	Co(II)–MutM	Cd(II)–MutM	Apo–MutM
13-mer (3,4)	749 ± 61 nM	778 ± 82 nM	1190 ± 87 nM	N/D
16-mer (5,6)	712 ± 86 nM	750 ± 98 nM	1405 ± 110 nM	N/D

Testing the specific DNA binding affinity of MutM is more complicated. MutM does not form a covalent complex with DNA until it recognizes the 8-oG damaged base and flips it out from the dsDNA helix into the active site. During this process, a Schiff base intermediate is formed between the side chain of Pro1 and C1' of the pentose sugar(Figure 3.9). The next step would be glycosylase bond cleavage; however, sodium borohydride ($NaBH_4$) is used to trap this covalent intermediate so that the specific DNA binding can be detected on a gel shift assay (Figure 3.10).[12,13] The EMSA experiments were performed with the 8-oG modified DNA in the presence of $NaBH_4$ with increasing amounts of metallated MutM. A denaturant is added to the sequence–specific binding reactions to dissociate the non-specific binding. With increasing MutM concentration, the gels shows shifted bands corresponding to the Zn(II)–MutM–dsDNA complex. Co(II)–MutM also forms covalent dsDNA complexes comparable to that of Zn(II)–MutM (Figure 3.10A); however, a Cd(II)–MutM–dsDNA covalent complex is hardly visible (Figure 3.10B). This confirms that Cd(II)–MutM cannot specifically bind to of 8-oG damaged DNA and form the first step in glycosylase activity, nucleophilic attack of C1' to form a covalent enzyme–DNA Schiff base intermediate.

Overall, the DNA binding properties (both non–specific and specific) of Co(II)–MutM are similar to that of Zn(II)–MutM. Cd(II)–MutM exhibits weaker non–specific binding with DNA than Zn(II)–MutM, but can still bind DNA with measurable affinity. However, no specific binding between Cd(II)–MutM and the 8-oG damaged dsDNA is observed.

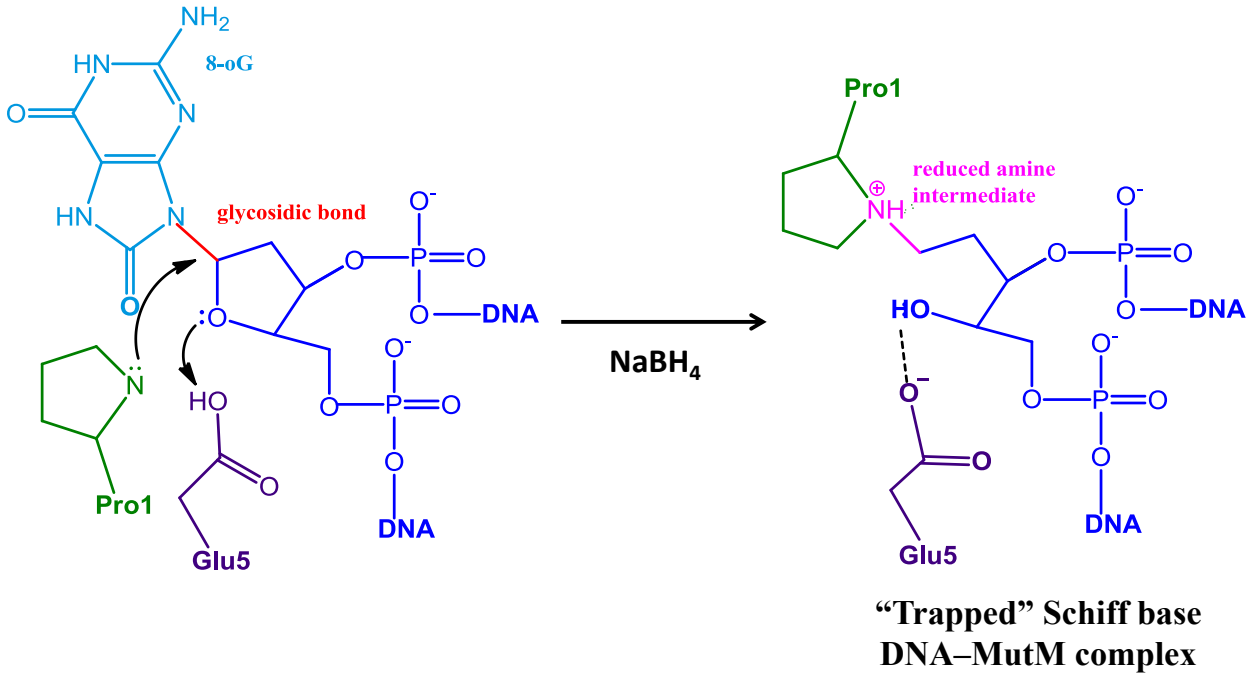

Figure 3.9. Schiff base intermediate formation. During the base excision, the side chain of Pro1 attacks the C1' of the DNA pentose as a nucleophile and a Schiff base imine intermediate is formed. This covalent intermediate can be trapped by $NaBH_4$ via reduction to an amine.

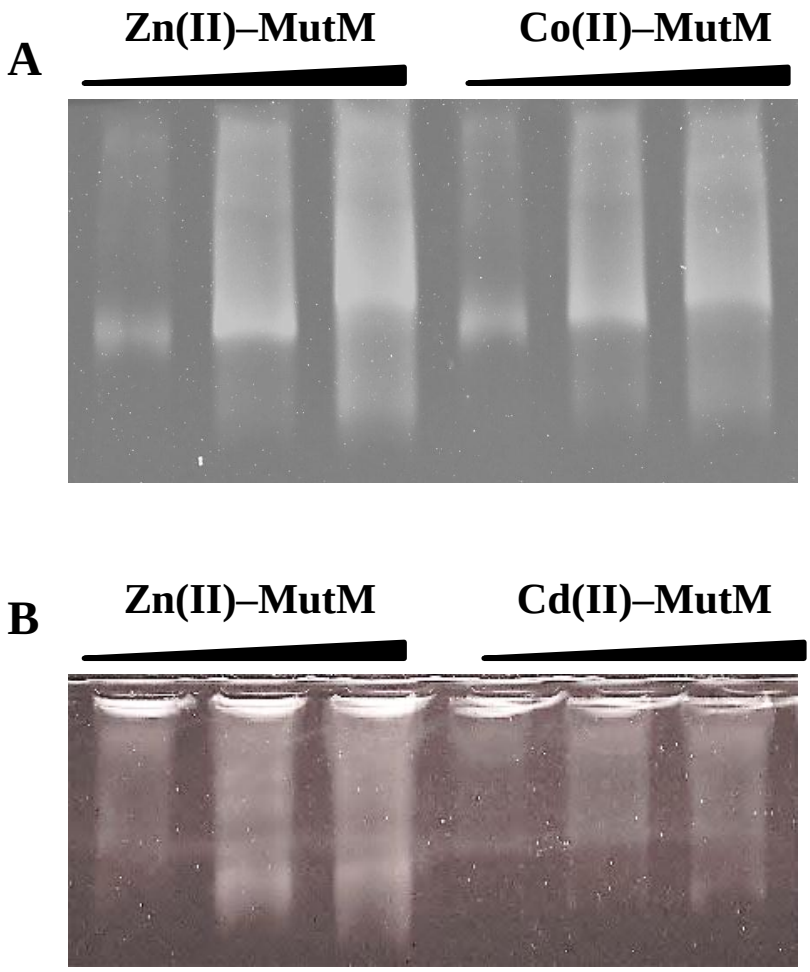

Figure 3.10. EMSA gels monitoring formation of a covalent MutM–DNA complex. The top strand of this dsDNA (20 μM) is modified with 8-oG. The MutM–DNA covalent complex is trapped by $NaBH_4$ and non–specific binding is disrupted by urea. The gels were stained with SYBR Green. (A) Reactions with increasing Zn(II)–MutM (lanes 1–3) and Co(II)–MutM (lanes 4–6). (B) Reactions with increasing Zn(II)–MutM (lanes 1–3) and Cd(II)–MutM (lanes 4–6). The concentrations of MutM preparations are 20 μM, 30 μM, and 40 μM.

3.4 DISCUSSION

3.4.1 MutM inhibition by Cd(II). Our investigation of MutM activity by the hyperchromicity assay confirms the loss of overall activity for purified Cd(II)–MutM, which supports the idea that Cd(II) inhibits MutM activity by occupying the zinc finger metal binding site as discussed in Chapter 2. In terms of the ability of Cd(II) to replace Zn(II) from the zinc finger, our data shows dose–dependent inhibition of Zn(II)–MutM activity by Cd(II), which is in agreement with published EMSA results.[14] However, Cd(II) does not completely displace Zn(II) from the zinc finger based on the fact that the Zn(II)–MutM pre–incubated with 10–20 fold excess Cd(II) retains about 50% catalytic activity, while purified Cd(II)–MutM exhibits no activity. Therefore, Zn(II) coordination is thermodynamically very stable. These results could also explain what was observed in the previous EMSA experiments that simultaneous treatment of MutM with Zn(II) and Cd(II) prevented inhibition, while post–treatment with Zn(II) did not prevent Cd(II) inhibition.[14]

While it is clear from the hyperchromicity assay that the overall activity of MutM is inhibited by Cd(II), we wanted further insight into which catalytic step was most affected. The deaminase coupled activity assay was used to test the damaged base excision activity of Cd(II)– and Zn(II)–MutM. We observe a 10-fold lower reaction rate catalyzed by Cd(II)–MutM, compared to that catalyzed by Zn(II)–MutM.However, it was still not clear whether Cd(II)–MutM simply lost the glycosylase activity or it failed to recognize the damaged DNA. It is important to point out that further clarification of the mechanism of inhibition has not been reported in the literature. We are the first to delve into the mechanism and we determine that

Cd(II)–MutM does not form a covalent bond with the 8-oG modified dsDNA. Presumably there is no nucleophilic attack by Pro1 and, consequently, no excision of the damaged base.

A previous study demonstrated that any single zinc finger cysteine mutated to a non-ligating residue (Cys→Gly) mainly interfered with base excision rather than AP lyase activity of MutM.[15] Therefore, a properly structured zinc finger is essential for MutM glycosylase activity towards 8-oG damaged DNA bases. This implies that Cd(II) may distort the zinc finger structure and that this contributes to enzymatic inactivation. It was also illustrated that the single Cys→Gly mutations in the zinc finger may change the orientation of another key zinc finger amino acid residue, Arg258.[15] Based on the crystallographic structure of MutM co-crystallized with damaged DNA, Arg258 forms a hydrogen bond with the damaged base.[9] A change its orientation led to diminished MutM–DNA binding capacity. According to our experimental results, Cd(II) coordination with the zinc finger may also induce such a structural change because of the diminished specific DNA binding. This could be explained through distortion of the finger since Cd(II) has a larger ionic radius compared to Zn(II). Further, the fluorescence anisotropy titrations and EMSA analysis of Cd(II)–MutM with the non–damaged DNA confirms that Cd(II)–MutM still possesses the required non–specific DNA binding, but with lower affinity than Zn(II)–MutM. This means that the damaged base recognition and excision is the main step disturbed by Cd(II) coordination to the MutM zinc finger.

3.4.2 MutM is not inhibited by Co(II) and Pb(II). According to the activity assays, Co(II) and Pb(II) do not significantly inhibit Zn(II)–MutM if added to the reaction mixture. In fact, Pb(II) does not interfere with MutM activity even with 1000-fold excess Pb(II) over MutM (data not shown). This could be due to the large ionic radius (1.33 Å) or the fact that Pb(II) prefers

trigonal (Cys_3) coordination due to the 6*s* lone pair electrons.[1] Since Co(II) is less preferred by the Cys_4 zinc finger, at first, it was not clear if Co(II) could not replace Zn(II) under the experimental conditions or if the substitution causes no loss of activity. Here, we directly show that Co(II)–MutM functions almost identically as Zn(II)–MutM in both activity assays and DNA binding assays. Moreover, the sodium borohydride trapping experiments confirm that Co(II)–MutM recognizes and covalently binds to 8-oG damaged DNA just as well as Zn(II)–MutM. Overall, these observations are consistent with the previous showed that Co(II) and Pb(II) do not interfere with the rate of dsDNA dissociation catalyzed by MutM.[14]

3.4.3 Conclusions and future directions. We demonstrate that the overall MutM enzymatic activity is abrogatedwith Cd(II), but not with Co(II). Investigation of individual catalytic steps of the reaction reveals that the damaged base recognition and excision is most disturbed by Cd(II) coordination to the zinc finger. We could infer that Cd(II) might affect other human zinc finger DNA repair proteins in similar way and this may contribute, as a whole, to Cd(II)-induced carcinogenesis. On the other hand, we did not find evidence that Co(II) coordination to the zinc finger inhibits DNA repair proteins, consistent with a variety of zinc finger proteins;[16,17] thus, we believe this is an unlikely mechanism for Co(II) carcinogenesis. To further reveal the mechanism of Cd(II) inhibition and determine whether this is a common inhibition mechanism of the zinc finger DNA repair proteins, an insight into the structural change of the protein with Cd(II) binding is necessary. Besides, since Cd(II) replacement of Zn(II) does not alter the geometry of the zinc finger, other metal ions that replace Zn(II) with altered geometry, like Hg(II) and Ni(II),[18] could be investigated to help us generate an inhibition pattern of the zinc finger protein by various metals.

3.5 REFERENCES

(1) Hartwig, A., Asmuss, M., Blessing, H., Hoffmann, S., Jahnke, G., Khandelwal, S., Pelzer, A., and Burkle, A. (2002) Interference by toxic metal ions with zinc-dependent proteins involved in maintaining genomic stability. *Food. Chem. Toxicol.40*, 1179–1184.

(2) Minetti, C. A., Remeta, D. P., and Breslauer, K. J. (2008) A continuous hyperchromicity assay to characterize the kinetics and thermodynamics of DNA lesion recognition and base excision. *Pro.c Natl. Acad. Sci. U S A105*, 70–75.

(3) Hall, R. S., Fedorov, A. A., Marti-Arbona, R., Fedorov, E. V., Kolb, P., Sauder, J. M., Burley, S. K., Shoichet, B. K., Almo, S. C., and Raushel, F. M. (2010) The hunt for 8-oxoguanine deaminase. *J. Am. Chem. Soc.132*, 1762–1763.

(4) Nam, K., Verdine, G. L., and Karplus, M. (2009) Analysis of an anomalous mutant of MutM DNA glycosylase leads to new insights into the catalytic mechanism. *J. Am. Chem. Soc.131*, 18208–18209.

(5) Busenlehner, L. S., Cosper, N. J., Scott, R. A., Rosen, B. P., Wong, M. D., and Giedroc, D. P. (2001) Spectroscopic properties of the metalloregulatory Cd(II) and Pb(II) sites of s. Aureus pI258 CadC. *Biochemistry40*, 4426–4436.

(6) Kim, R., Yokota, H., and Kim, S. H. (2000) Electrophoresis of proteins and protein-protein complexes in a native agarose gel. *Anal. Biochem.282*, 147–149.

(7) Qi, Y., Spong, M. C., Nam, K., Banerjee, A., Jiralerspong, S., Karplus, M., and Verdine, G. L. (2009) Encounter and extrusion of an intrahelical lesion by a DNA repair enzyme. *Nature462*, 762–766.

(8) Lane, D., Prentki, P., and Chandler, M. (1992) Use of gel retardation to analyze protein-nucleic acid interactions. *Microbiol. Rev.56*, 509–528.

(9) Jiricny, J. (2010) DNA repair: How MutM finds the needle in a haystack. *Curr. Biol.20*, R145-147.

(10) Blainey, P. C., van Oijen, A. M., Banerjee, A., Verdine, G. L., and Xie, X. S. (2006) A base-excision DNA-repair protein finds intrahelical lesion bases by fast sliding in contact with DNA. *Proc. Natl. Acad. Sci. U. S. A.103*, 5752–5757.

(11) Nash, H. M., Bruner, S. D., Scharer, O. D., Kawate, T., Addona, T. A., Spooner, E., Lane, W. S., and Verdine, G. L. (1996) Cloning of a yeast 8-oxoguanine DNA glycosylase reveals the existence of a base-excision DNA-repair protein superfamily. *Curr. Biol.6*, 968–980.

(12) Li, G. M. (2010) Novel molecular insights into the mechanism of GO removal by MutM. *Cell Res.20*, 116–118.

(13) Gilboa, R., Zharkov, D. O., Golan, G., Fernandes, A. S., Gerchman, S. E., Matz, E., Kycia, J. H., Grollman, A. P., and Shoham, G. (2002) Structure of formamidopyrimidine-DNA glycosylase covalently complexed to DNA. *J. Biol. Chem.277*, 19811–19816.

(14) Asmuss, M., Mullenders, L. H., Eker, A., and Hartwig, A. (2000) Differential effects of toxic metal compounds on the activities of Fpg and XPA, two zinc finger proteins involved in DNA repair. *Carcinogenesis21*, 2097–2104.

(15) Castaing, B., Geiger, A., Seliger, H., Nehls, P., Laval, J., Zelwer, C., and Boiteux, S. (1993) Cleavage and binding of a DNA fragment containing a single 8-oxoguanine by wild type and mutant Fpg proteins. *Nucleic Acids Res.21*, 2899–2905.

(16) Frankel, A. D., Berg, J. M., and Pabo, C. O. (1987) Metal-dependent folding of a single zinc finger from transcription factor IIIV. *Proc. Natl. Acad. Sci. U. S. A.84*, 4841–4845.

(17) Predki, P. F., and Sarkar, B. (1994) Metal replacement in "Zinc finger" and its effect on DNA binding. *Environ. Health. Perspect.102 Suppl 3*, 195–198.

(18) Witkiewicz-Kucharczyk, A., and Bal, W. (2006) Damage of zinc fingers in DNA repair proteins, a novel molecular mechanism in carcinogenesis. *Toxicol. Lett.162*, 29–42.

CHAPTER 4

STRUCTURE OF THE MUTM DNA GLYCOSYLASE

4.1 INTRODUCTION

MutM, an *E. coli* DNA glycosylase, is inhibited by non-native metals including Cd(II), Cu(II) and Hg(II).[1] In Chapter 2, we determined that Cd(II) and Co(II)–MutM coordinate MutM through the zinc finger motif. In Chapter 3, we also demonstrated that, compared to Zn(II)–MutM, Cd(II)–MutM has no glycosylase activity, while Co(II)–MutM retains most of its activity. Further, the Cd(II) can only bind DNA non-specifically and cannot undergo the first catalytic step in its mechanism, 8-oG base cleavage. In this chapter, we provide insight into the overall structure of MutM coordinated with various metals though backbone amide Hydrogen–Deuterium exchange mass spectrometry (HDX–MS) to reveal conformational changes and how they affect DNA binding and catalytic activity of MutM.

MutM is a 269 amino acid long protein with two domains linked by a hinge region. The N-terminal domain (Figure 4.1, grey) is a β-sandwich that consists of nine antiparallel β-strands (β1–β9) with two α-helices on each side of the β-sandwich (αA and αB). The C-terminal domain (Figure 4.1, yellow, orange and red) is composed of four helices (αC–αF) and two β-strands (β10 and β11) that form a zinc finger motif (Figure 4.1, red). The essential regions for DNA binding and enzymatic activities are located in the pocket between the two domains. A characteristic DNA binding motif, H2TH composed of the αD–αE helices (Figure 4.1, orange) is located in this

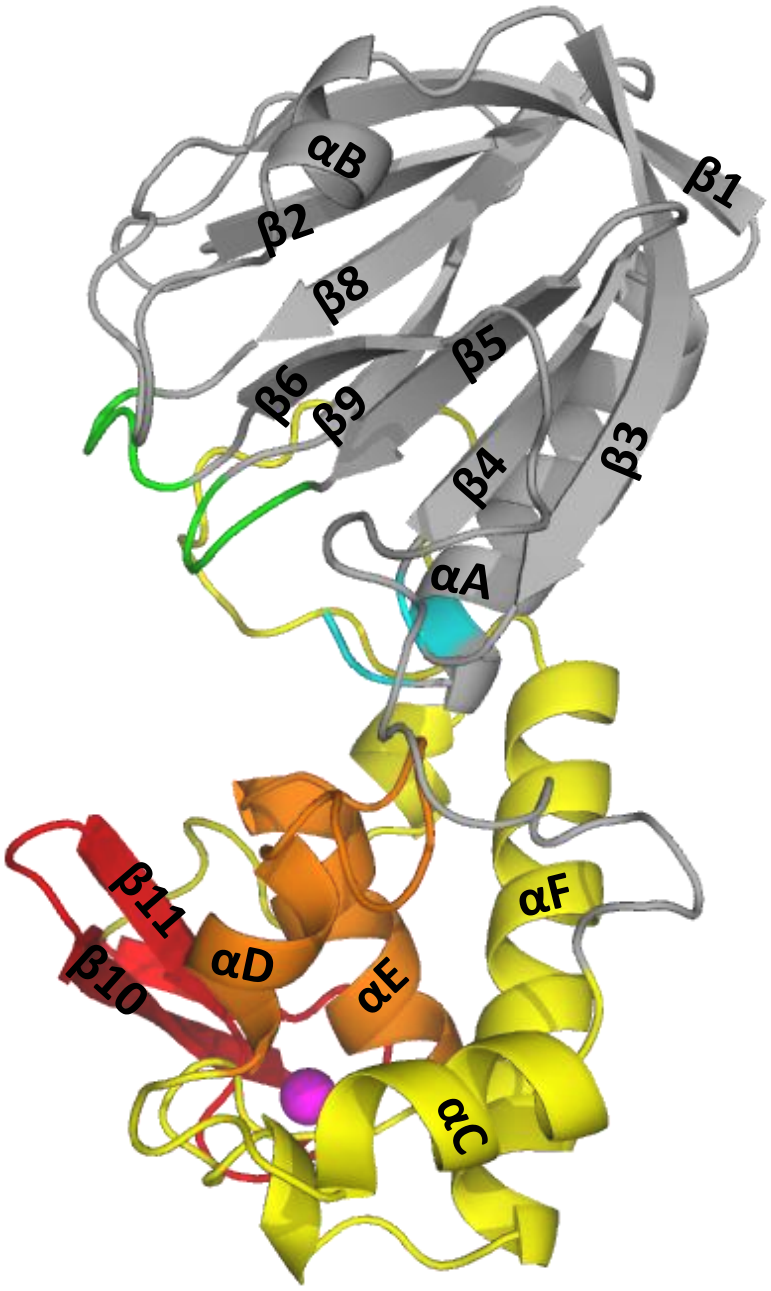

Figure 4.1. The overall structure of MutM. The N-terminal domain (grey) consists of a two layered β-sandwich and two α-helices. The C-terminal domain consists of four α-helices (yellow and orange) and a β-hairpin of the zinc finger motif (red). DNA binding and catalytic sites are in the cleft between the two domains. Figure made using PDB 1K82.

region. H2TH motif participates in non-specific DNA binding. Recognition of 8-oG is accomplished by the zinc finger motif, together with two loops between β5–β6 and β8–β9 (Figure 4.1, green), which are also located in the pocket. Other essential residues of the catalytic site are at the bottom of the pocket (Figure 4.1, cyan).[2]Figure 4.2 shows the MutM active site binding to damaged DNA wherethe 8-oG base is flipped out from the double helix and accommodated by the side chains of key amino acid residues around the active site.[3] Non–native metal binding could cause distortion of the zinc finger and potentially other motifs that interact with DNA, leading to loss of activity.

Here, we use protein backbone amide HDX–MS to localize the conformational changes within MutM due to non-native metal binding at the zinc finger. At neutral pH and standard temperature, the rate of deuterium incorporation into the protein backbone relies on the solvent accessibility of amide hydrogens and the flexibility or dynamics of the local structure.[4] Therefore, HDX–MS has been used to study protein structures, protein–protein and protein–DNA interactions, as well as ligand binding effects. It is sensitive enough to reveal subtle protein conformational changes and provides not only structural, but also dynamic information of the protein.[4] In this work, the structures of Cd(II)– and Co(II)–MutM are compared to that of Zn(II)–MutM using this technique. We observed conformational changes at the zinc finger motif, H2TH, and active site of Cd(II)–MutM, which contribute to the loss of activity. Co(II) coordination to zinc finger causes a significantly smaller change in MutM structure and dynamics, compared to Cd(II), which is consistent with our previous observation that Co(II)–MutM retains most of the activity. With these observations, we present a possible mechanism of Cd(II) inhibition of MutM in this chapter.

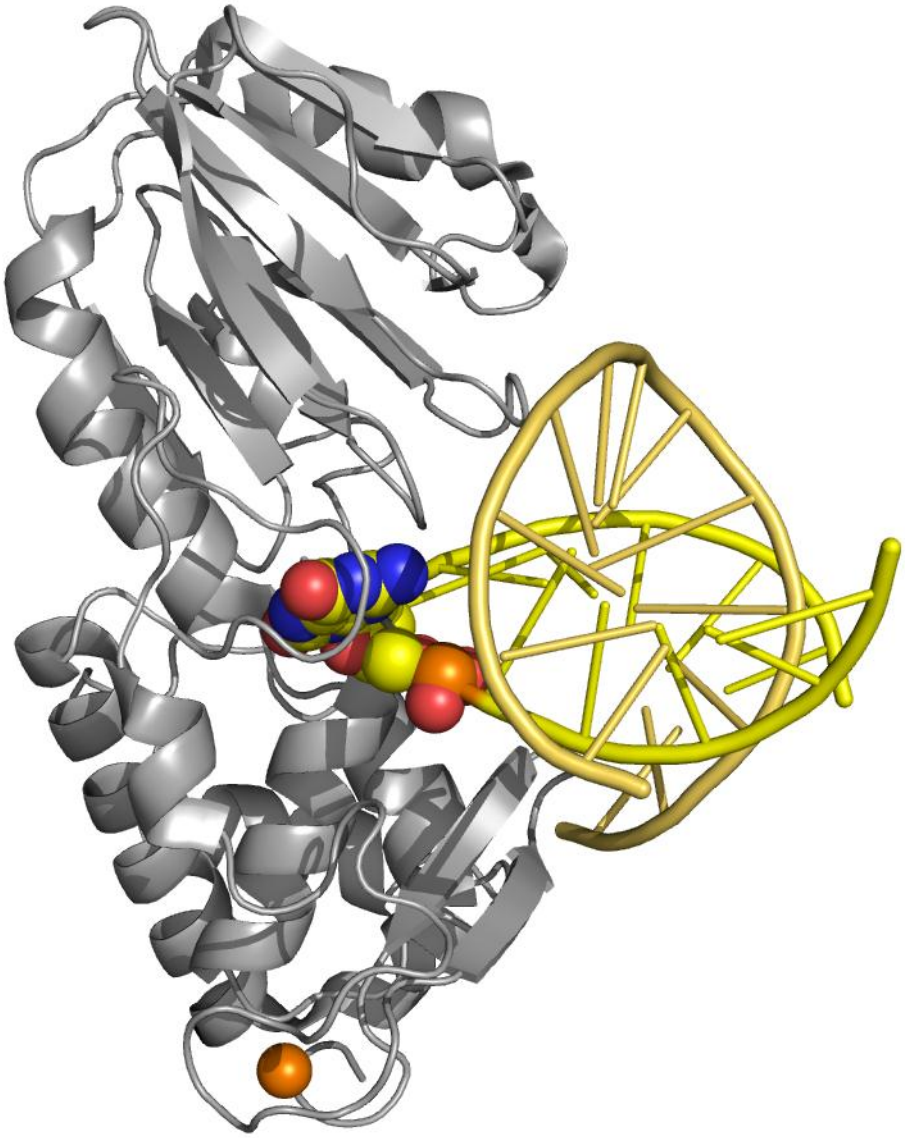

Figure 4.2. Structure of MutM with 8-oG base extruded from the DNA. This structure was created from PDB 1R2Y. The DNA helix is in yellow and the 8-oG is represented in space-filling mode. The Zn(II) in the zinc finger is an orange sphere. Note, the orientation of this figure is rotated 180 °from Figure 4.1.

4.2 MATERIALS AND METHODS

4.2.1 Chemicals. Potassium phosphate was purchased from Fisher Scientific and the buffers were made with HPLC grade water and acetonitrile, which were purchased from EMD. Deuterium oxide (D_2O, 99.99% at. D) was purchased from Acros Organics and porcine gastric mucosa pepsin from from Sigma.

4.2.2 Hydrogen/Deuterium exchange (HDX). MutM with various metals was prepared as described in Chapter 2. The peptides that result from a pepsin digestion of MutM were presented in Chapter 2 (Figure 2.2). The full peptide map has approximately 80% sequence coverage. The MutM stock (100 μM) was made in Buffer A (50 mM HEPES, pH 8.0, 50 mM NaCl, 1 mM TCEP). Pepsin (2 mg/mL) was made fresh in Buffer I (10 mM potassium phosphate, pH 7.2) or Buffer Q (10 mM potassium phosphate, pH 2.4) and kept on ice. Deuterium exchange was initiated by addition of 40 μL D_2O into 10 μL of MutM stock at 25 °C in a thin-wall PCR tube. The deuterium–protein samples were incubated at 25 ℃ in a water bath and exchange was quenched at specific time points (15 s – 2 h) by 50 μL Buffer Q. The sample was immediately transferred to an ice bath. Pepsin was added (0.1 μg/μg protein) and the digestion proceeded for 5 min. Digested MutM peptides were separated by liquid chromatography on a 50 mm × 2 mm Phenomenex C_{18} reverse–phase column (5 micron) submerged in an ice water bath and mass spectra were collected using SmartFrag™ settings by the Bruker HCTultra PTM mass spectrometer in positive ion mode from 300-1500 *m*/*z*.[5]

The mass spectrometry data was processed both manually, as described,[5] and through HDExaminer (Sierra Analytics). The amount of deuterium incorporated at each time point was calculated using

$$D = \frac{N(m_t - m_{0\%})}{m_{100\%} - m_{0\%}}$$

where *N* is the total number of exchangeable peptide amide protons less one for the N-terminal amide proton and/or any proline residues. The centroid values $m_{0\%}$, m_t and $m_{100\%}$ are of the peptide in the non–deuterated, the partially deuterated at time *t*, and the fully–deuterated control samples, respectively. The non–deuterated sample was made by addition of 40 µL H_2O instead of D_2O into 10 µL of MutM stock and the fully–deuterated sample was made by incubating the exchange reaction at 65 ℃ for 6 h. The amount of deuterium incorporated in each peptide was plotted as a function of time in minutes. The resulting progress curve for each peptide was fit using KaleidaGraph (Synergy Software) to single or double exponential equations,

$$y = N - (D_1 * e^{-k_1 * t})$$

$$y = N - (D_1 * e^{-k_1 * t}) - (D_2 * e^{-k_2 * t})$$

where*N* is the total number of exchangeable amide protons,D_1 and D_2 are the numbers of deuterons incorporated at exchange rates ofk_1 and k_2, respectively, as a function of time, *t*, in minutes.

4.2.3 Model of Zn(II) MutM structure. A structural model of Zn(II)–MutM without DNA was created using the trapped DNA–MutM complex structure (PDB code 1K82) using Swiss-Model, ModWeb and M4T[6] online programs using standard alignments and default settings. Eight models were created for each and averaged.

4.3 RESULTS

4.3.1 Structural model of DNA-free Zn(II)–MutM. Currently, there is no structure of *E. coli* MutM in the absence of DNA, but one does exist for a related bacterium,*T.thermophilus*.[2] The ClustalX[6] sequence alignment of *E. coli* and *T.thermophilus* MutM is shown in Figure 4.3. The sequence identity is 38% but the sequence homology is 68%. We required a DNA-free MutM model to localize the peptides that are altered in HDX-MS experiments because the proteinwe used did not containDNA. Since there is a conformational change in MutM with and without DNA, we felt this was necessary to interpret our data.We made MutM structural modelsfrom 3 programs (Swiss-Model, ModWeb, and M4T)[6] using DNA-trapped MutM as the basis structure. The overlay of the three models shows that the agreement between the models is good(Figure 4.4A). The model made by Swiss-Model has the lowest minimized energy so it is used in the following discussions. Wethen overlaid of this MutM model with the crystal structure of the DNA-free *T.thermophilus* MutM to determine if the structures are similar (Figure 4.4B). The overall folding of the model and the structure matches, including the active site and the H2TH motif. The most important difference is that orientation of zinc finger and the loop between β8–β9 is slightly changed in the *E. coli* MutM model so that the mouth of DNA binding pocket is relatively closed. Therefore, we are able to use the predicted model to localize the peptides,but to discuss the orientation and possible interactions of specific amino acid residues, we will refer to the *T.thermophilus* structure.

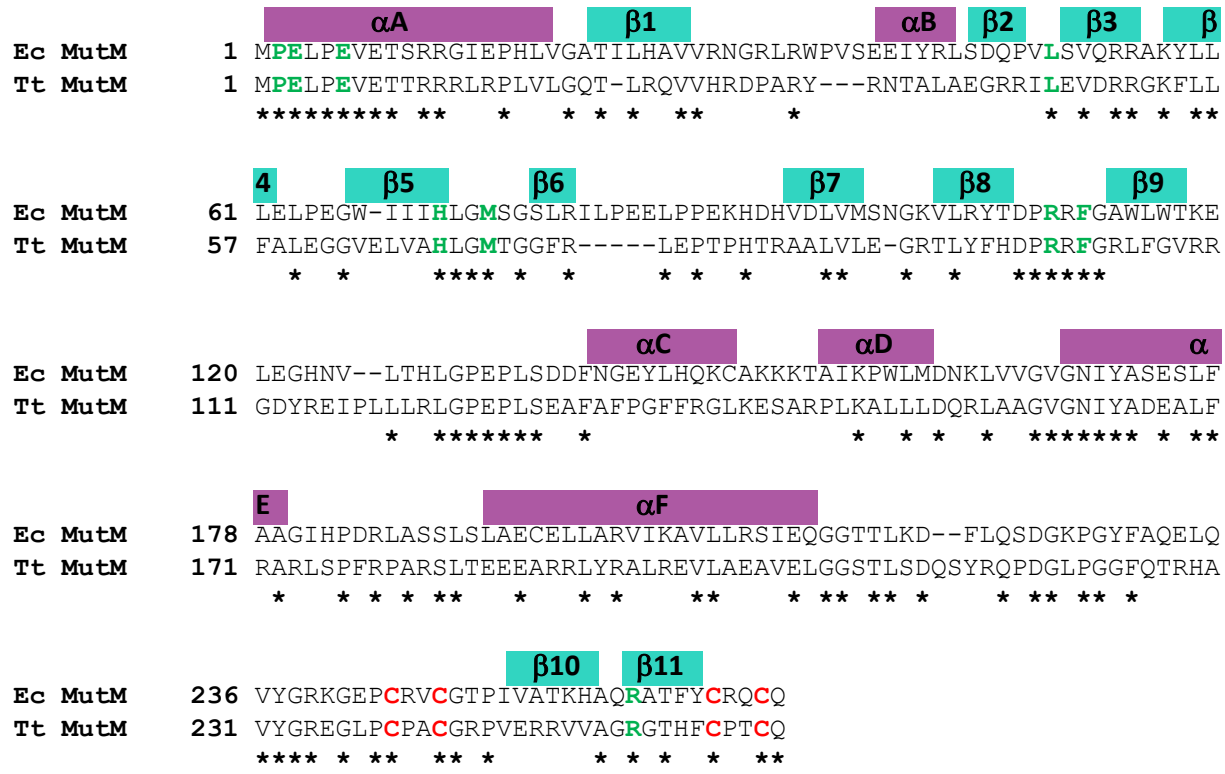

Figure 4.3. Aligned sequences of *T. thermophilus* MutM and *E. coli* MutM. The asterisks indicate the conserved amino acid residues. Conserved amino acid residues that are essential for 8-oG recognition and excision are highlighted in green and Cys residues that coordinate to Zn(II) in red. Alignment of the secondary structures are shown in purple (α-helices) and cyan (β-strands) squares based on the structure of the *T. thermophilus* MutM (PDB 1EE8).

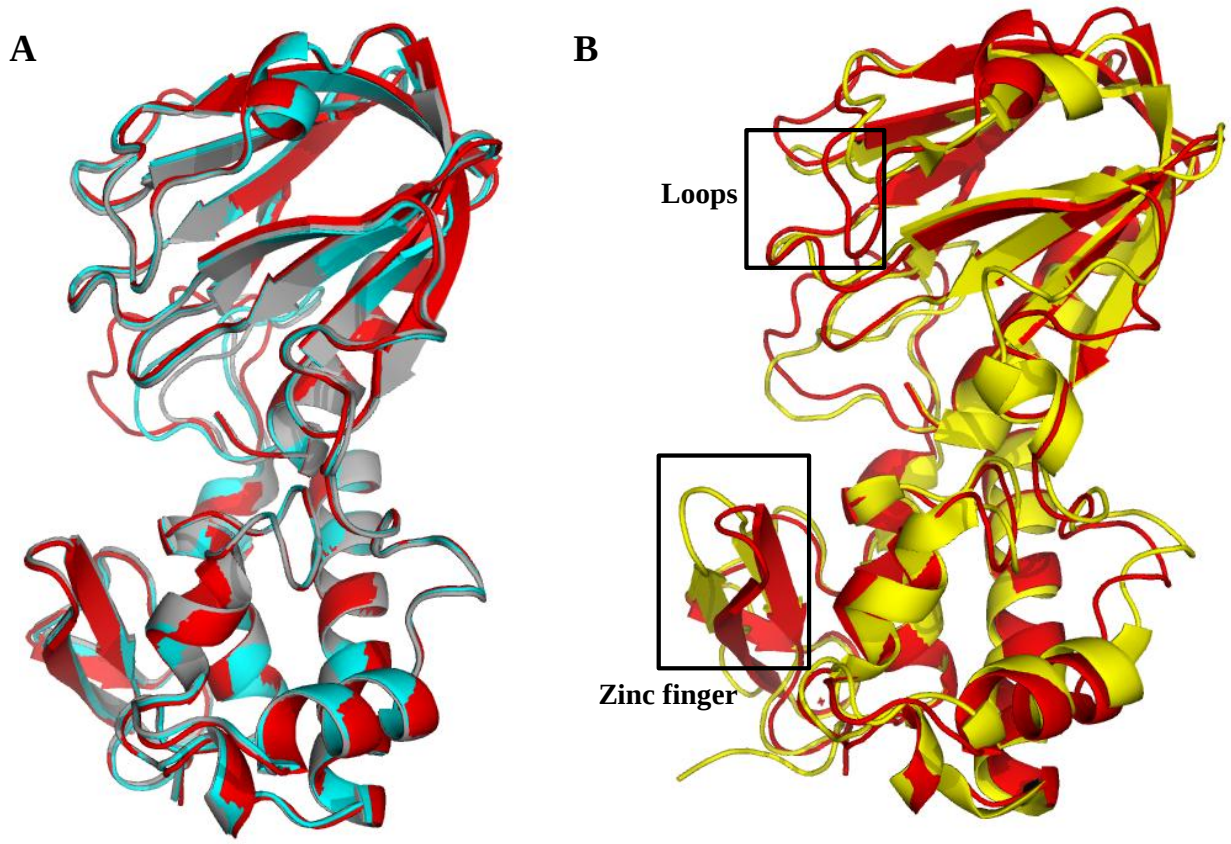

Figure 4.4. Overlay of the MutM structural models. (A) The models created from Swiss-Model (red), ModWeb (cyan), and M4T (grey) are aligned and overlaid in PyMol. (B) Overlay of the *E. coli* MutM model made with Swiss-Model (red) and the DNA-free *T.* thermophilus MutM crystallographic structure (yellow). Differences in zinc finger and β8-β9 loop orientations are shown in black squares.

4.3.2 Solvent accessibility of Cd(II)–MutM. The deuterium exchange rate of backbone amide protons is primarily dependent on the relative solvent accessibility of the amide hydrogen to D_2O (*i.e.*, buried or hydrogen-bonded), but also the backbone flexibility (*i.e.*, dynamics).[4] To localize conformational changes, if any, caused by non-native metal substitution of Zn(II) in the finger motif of MutM, we use the first 30 sec of a HDX time course as a rough estimate of the relative solvent accessibility of backbone amides. Peptides with amides that are protected or exposed by non-native metal binding in the Zn(II) finger are identified after pepsin digestion and quantified by MS through a decrease/increase in the amount of deuterium incorporated. These values were compared to those for Zn(II)–MutM.

The difference plot of the percent deuterium incorporation in Cd(II)–MutM backbone amides relative to Zn(II)–MutM is shown in Figure 4.5A. The corresponding peptides are indicated on the structural model of Zn(II)–MutM (Figure 4.5B). About 2/3 of these peptides are part of, or within, interaction distance of the zinc finger motif, which is clearly altered by Cd(II) binding. Cd(II) leads to solvent protection within peptide 263–269, which contains Cys264 and Cys267 from the zinc finger motif. Minor deuterium exchange protection is observed for peptides N-terminal to the zinc finger (231–234, 235–253 and 254–262),which contain Cys244 and Cys247, as well asresidues involved in DNA binding. For example, Lys255–Arg258 form a β-hairpin loop that participates in DNA binding through Arg258, which interacts specifically with the C2' oxo group of cytosine in the 8-oG:C pair.[7] Two peptides from the H2TH DNA binding motif (αE), peptides 164–171 and 172–176, were also protected from D_2O when Cd(II) is bound. In fact, peptide 164-171 has the largest change in protection compared to that of Zn(II), so it is clear that Cd(II) affects the primary DNA binding region outside the Zn(II) finger motif, too. Some peptides also became more solvent protected with Cd(II) bound but are relatively

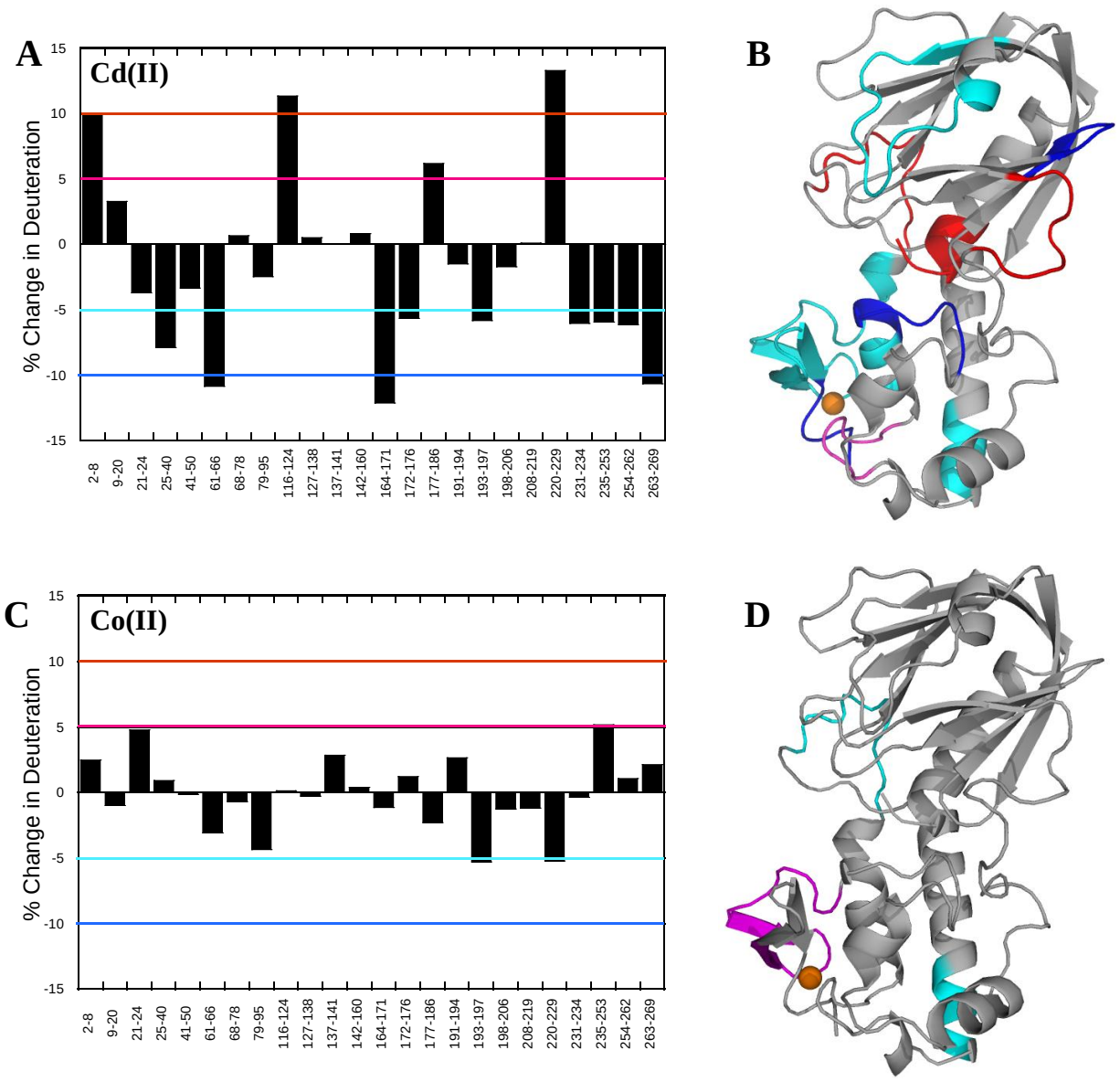

Figure 4.5. Change in D_2O accessibility upon Cd(II) or Co(II) binding. Difference in the percentage of deuterium exchange (y-axes) after 30 s incubation in D_2O for each pepsin–digested peptide (x-axes) was calculated by $(D_{Cd}-D_{Zn})/N$ for (A) Cd(II)–MutM and (C) Co(II)–MutM . The cyan and blue lines signify a greater than 5 and 10% decrease in deuterium incorporation, respectively. The magenta and red lines signify a greater than 5 and 10% increase in deuterium incorporation, respectively. The color coded peptides for (B) Cd(II)–MutM and (D) Co(II)–MutM are plotted on the *E. coli* MutM model.

distant from the zinc finger structure (25–40, 61–66, and 193–197). Peptides 25–40 and 61–66 reside in the N-terminal domain and are not in the DNA binding pocket.Peptide 193–197 is at the beginning of αF containing Cys195, one of the two Cys residues outside the zinc finger. To summarize these results, most areas protected by Cd(II) were within the immediate vicinity of the zinc finger motif, as expected.

There were three regions of Cd(II)–MutM that displayed an increase in deuterium incorporation compared to Zn(II), which indicates that a conformational change exposed previously inaccessible peptides upon Cd(II) substitution. The greatest increase was observed for peptides in the DNA binding pocket and active site (2–8, 116–124 and 220–229). Peptide 2–8 is located at the bottom of the DNA binding pocket and contains residues essential for catalytic activity.[2] Peptides 116–124 and 220–229 are within the "hinge" of the DNA binding pocket, connecting the N-terminal and C-terminal domains, the zinc finger structure and αF, respectively. Generally, these regions with increased solvent accessibility upon Cd(II) substitution surround the catalytic site of MutM, indicating loss of hydrogen bonding.

4.3.3 Solvent accessibility of Co(II)–MutM. Since as purified Co(II)–MutM retains most of its activity compared to Zn(II)–MutM, we investigated whether Co(II) altered the protein conformation through HDX–MS. This allowed us to compare the conformational change of MutM due to binding a toxic metal like Cd(II) and a non-toxic metal like Co(II). A difference plot of the percent deuterium incorporated at 30 sec in Co(II)–MutM relative to Zn(II)–MutM is shown in Figure 4.5C. The corresponding peptides are indicated on the structural model of Zn(II)–MutM (Figure 4.5D). Changes in solvent accessibility of backbone amides caused by Co(II) substitution are relatively small. Protection values from D_2O of >5% are observed for peptides 193–197 and 220–229. A similar percentage of protection for peptide 193–197 is also

observed for Cd(II)–MutM. Yet, for peptide 220–229, part of the hinge region of the DNA binding pocket, the slight protection with Co(II) is opposite to that for Cd(II)–MutM where this was the largest increase in deuterium incorporation. The only Co(II)–MutM peptide that has an increased deuterium exchange greater than 5% is peptide 235–253. This peptide is the N-terminal part of the zinc finger motif and contains Cys244 and Cys247. Overall, Co(II) binding causes relatively small changes in solvent accessibility, most of which are opposite to that caused by Cd(II) binding. This implies that the structure of the Co(II)-bound enzyme is the most similar to Zn(II)–MutM, which could partly explain why Co(II)–MutM retains catalytic activity.

4.3.4 Backbone Dynamics. Besides solvent accessibility, the deuterium exchange rate is also dependent on the backbone flexibility of the peptide. This makes HDX an excellent tool to study the dynamics of the protein, which is especially important to understand the catalytic movements of an enzyme.[4] We compare the deuterium exchange rates of Cd(II)– and Co(II)–MutM with that of Zn(II)–MutM for each peptide to localize regions affected by non-native metal binding. Identification of these regions, which are most likely required for catalytic activity, can help to explain the mechanism of Cd(II) inhibition of MutM.

Generally, no dramatic change in MutM dynamics is observed upon Cd(II) binding. Two peptides that have altered backbone exchange rates (decreased more than 5-fold) include 61-66 and 191-194 (Figure 4.6A, B). Peptide 61–66 is the loop between β4 and β5 on the N-terminal domain (Figure 4.7, blue) and peptide 191–194 (Figure 4.7, cyan) is at the beginning of αF on the C-terminal domain. These are some distance from the zinc finger motifindicating that metal substitution transmits conformational changes to other areas through changes in hydrogen bonding as evidenced by the changes in solvent accessibility of surrounding peptides (Figure

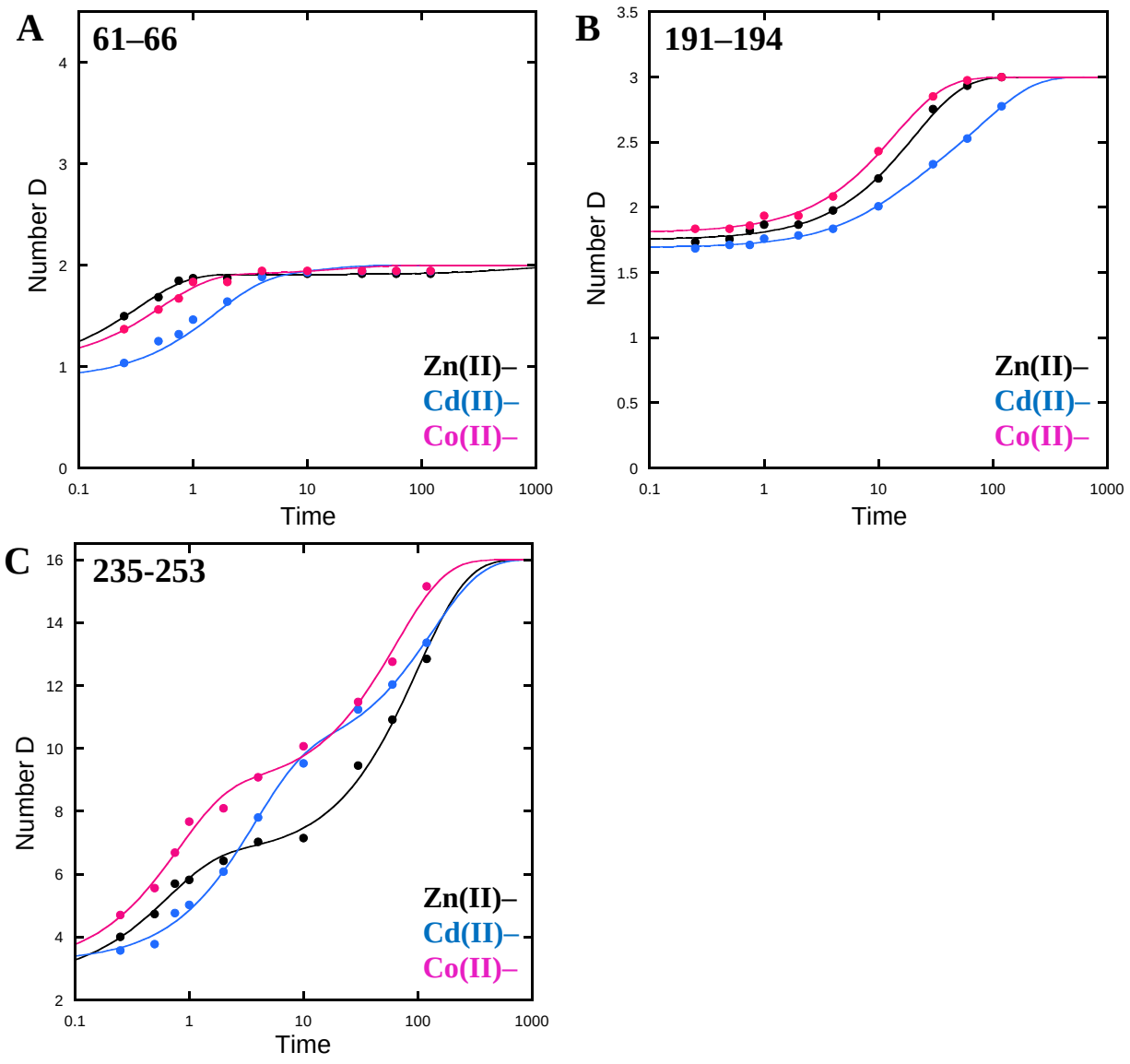

Figure 4.6. HDX–MS rate profile for the peptides shown in Figure 4.7. Shown are kinetic traces for the number of deuterons incorporated into peptides from Cd(II)–MutM (blue), Co(II)–MutM (pink), and Zn(II)–MutM (black) as a function of incubation time in D_2O. The data are an average of more than 3 HDX sets and were fit to single and double exponential equations to obtain the rate constants for exchange and the corresponding number of deuterons on each phase. (A) Peptide 61-66. (B) Peptide 191-194. (C) Peptide 235-253.

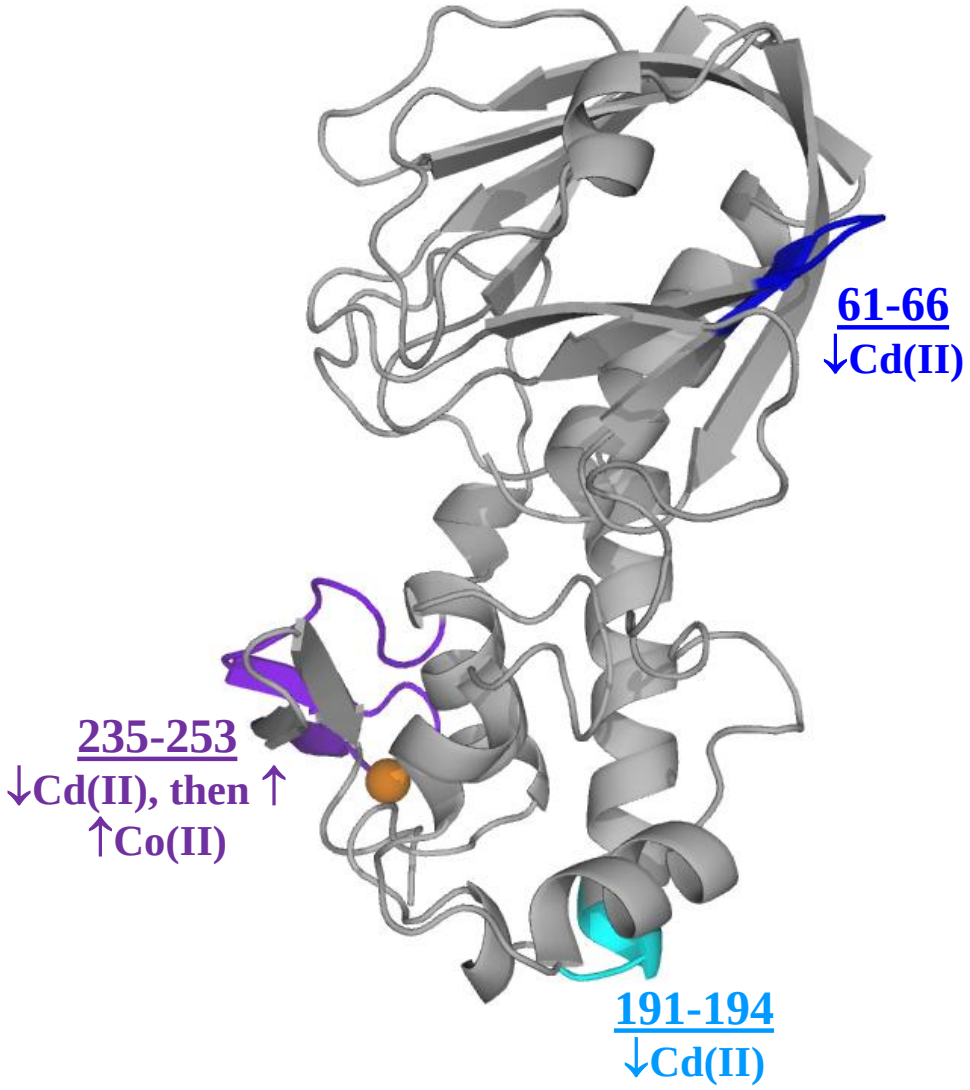

Figure 4.7. Regions of altered backbone dynamics upon Cd(II) or Co(II) binding. Peptide 61–66 (blue) and 191–194 (cyan) show decreased rates of deuterium incorporation when Cd(II) is bound. Peptide 235–253 (purple) shows a slightly decreased rate of deuterium incorporation at early time points but an increased rate at later time points for Cd(II). For Co(II)–MutM, deuterium exchange rate of peptide 235–253 is increased. Peptides are mapped onto the *E. coli* MutM model.

4.5B). The most noticeable difference in exchange kinetics occurs for the zinc finger peptide 235–253 (Figure 4.7, purple), which coordinates Cd(II) through Cys244 and Cys247. This peptide shows decreased dynamics before 2 min, consistent with increased solvent accessibility, but increased dynamics at the later time points most likely due to slower time regime molecular motions (Figure 4.6C).

In terms of changes in dynamics with Co(II) coordination, peptide 235–253 is also the only peptide that shows an observable increase in backbone dynamics, compared to Zn(II)–MutM (Figure 4.6C). As expected, very similar backbone exchange rates to Zn(II)–MutM are observed for most of the peptides derived from Co(II)–MutM, since Co(II) still retains catalytic activity. In total, backbone dynamic changes caused by Cd(II) binding could be potentially related to the functional change of Cd(II)–MutM.

4.4 DISCUSSION

To clarify the mechanism of non–native metal inhibition of a specific zinc finger protein, it is necessary to localize the overall or localized structural changes of the protein upon non–native metal binding. The previous study of metal–zinc finger based on EXAFS pointed out that Co(II) and Cd(II) are isostructural substitutes of Zn(II) in Cys_4 type zinc finger, with 0.2 Å longer metal–S bond for Cd(II).[8] However, they did not reveal how this subtle change in bond length affects the structure of the protein to disrupt its catalytic activity. The HDX–MS technique is a sensitive tool to reveal subtle conformational changes of the full length protein in solution. With the catalytic mechanism of MutM known, we are able to correlate the binding to non-native metal ions to the structural/dynamic changes and, therefore, function of MutM.

In this work, we investigated the secondary structure and backbone flexibility of full length MutM through HDX–MS. The deuterium exchange properties of Cd(II)– and Co(II)–MutM were compared with that of Zn(II)–MutM. We observed little difference in deuterium incorporation between Co(II)– and Zn(II)–MutM, but for Cd(II)–MutM we observed structural perturbation to the zinc finger, the H2TH DNA binding region, and the catalytic pocket. These changes help to explain why MutM is inhibited by Cd(II), but not by Co(II).

4.4.1 Zinc finger region is protected and constrained by Cd(II) binding. The effective ionic radii of Zn(II), Co(II) and Cd(II) are 0.74, 0.65 and 0.94 Å, respectively. This larger radius for Cd(II) leads to a 0.2 Å longer Cd(II)–S bond compared to Zn(II) as observed from the Cys_4 zinc finger EXAFS spectra reported by Buchko and coworkers.[8] In MutM, the β-hairpin loop of the zinc finger extends into the inter–domain DNA binding cleft. Proper arrangement of the H2TH DNA binding motif relative to the zinc finger is maintained by a hydrogen bond network (Figure 4.8A).[7]The longer Cd(II)–S bondslikelydistort the finger and alters thisbonding network. The decrease in D_2O accessibility indicates that either new hydrogen bonds are formed that protect backbone amides from exchange or that solvent is excluded due to increased hydrophobic interactions, which are important for domain stabilization in the DNA-free state. This protection could change the orientation of Arg258, a conserved amino acid residue on the β-hairpin loop of the zinc finger, which is part of peptide 254-262. The side chain of Arg258 hydrogen bonds with the C2' oxo group of cytosine in the 8-oG:C pair. The Arg258 side chain works in concert with the conserved Arg108residue on the loop between β8–β9 on the opposite side of the DNA pocket, to disrupt the hydrogen bonds between the 8-oG:C bases (Figure 4.2).[7] Any change in Arg258 orientation, hydrogen bonding or dynamics could disrupt "communication" between the

two Arg residues that are likely bridged by a water molecule in the absence of DNA. Thus, HDX−MS is able to detect the small change in the structure of the zinc finger upon Cd(II) binding that appears to stabilize the domain,

As mentioned above, the H2TH motif is within interaction distance of the zinc finger and is also protected from deuterium exchange. Since this region interacts with the DNA backbone but does not impart specificity,[7] this could potentially explain the decreased affinity for non-specific DNA binding of Cd(II)–MutM compared to Zn(II)–MutM (Chapter 3). Overlay of the DNA bound MutM and free MutM is shown in Figure 4.8B. An orientation change of the zinc finger is observed for the DNA-bound structure (red) compared to the DNA-free MutM (gray). This difference is due to the MutM–DNA interactions serves to bring the zinc finger and the H2TH DNA binding motif closer to each other if DNA is present. As discussed previously, Cd(II) coordination protects amides in the zinc finger and H2TH DNA binding region from deuterium exchange. This may shift the dynamic equilibrium of MutM towards a conformation that has less affinity for DNA. This is consistent with the weak non-specific DNA binding and the lack of 8-oG recognition observed in Chapter 3. It is clear from the HDX results with fully active Co(II)–MutM that the same zinc finger region (peptide 235-253) is slightly more solvent accessible than Zn(II)–MutM so some structural flexibility in this region is required for activity.

4.4.2 Cd(II) binding opens DNA binding pocket. Besides the zinc finger motif and regions that are within direct contact with zinc finger, we observed increased deuterium access to amides at the bottom of the DNA binding pocket and hinges of the binding cleft. This suggests that Cd(II) binding transmits a conformational change to regions remote from the zinc finger and that are most likely responsible for the loss of catalytic activity. The most important solvent exposed

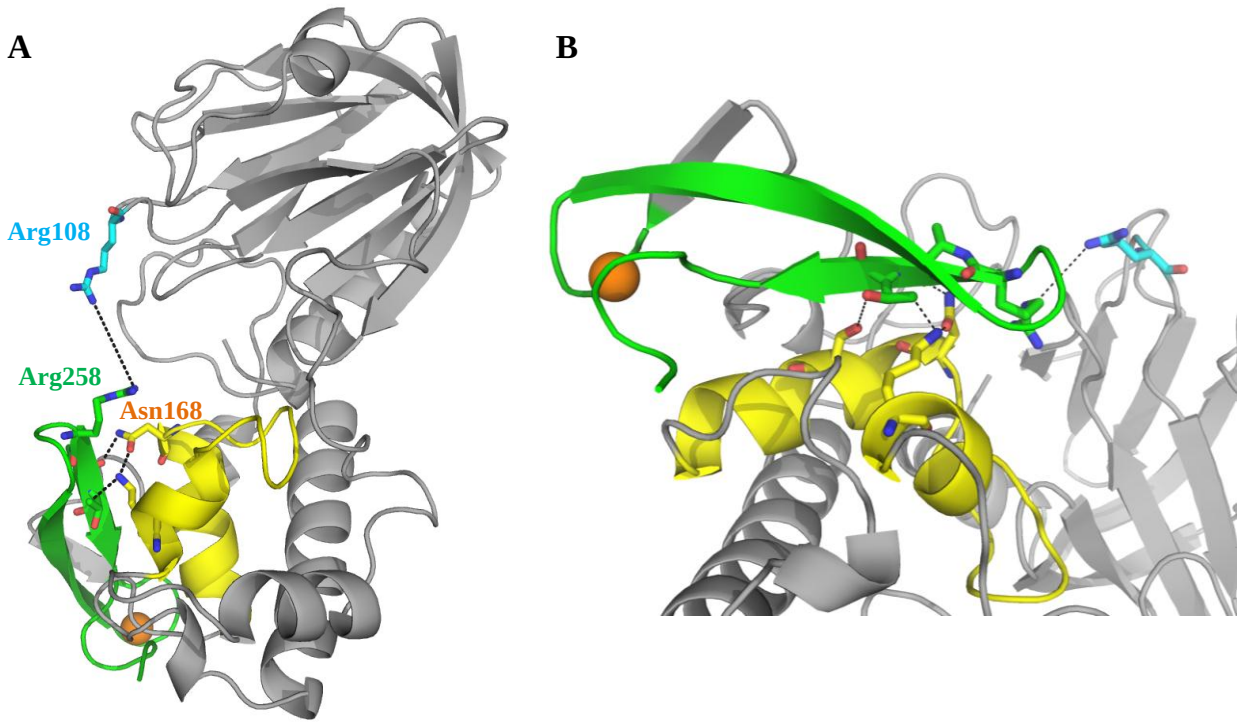

Figure 4.8. Hydrogen bonding network between the zinc finger and H2TH motifs. Side chains that maintain the arrangement between the zinc finger (green) and H2TH (yellow) motifs are shown in sticks. Arg108 (cyan) is also shown and the distance to Arg258 is ~8Å, which spans the DNA binding pocket. (A) Full-view of MutM. (B) Rotated and zoomed in view.

region is the conserved N-terminal active site (peptide 2-8). The C1′ cation of the deoxyribose in 8-oG left by base excision is stabilized by a hydrogen-bonding network, including a bound water and the carboxylate of Glu5 and forms a Schiff base with the α-imino group of Pro1 as a reaction intermediate. Side chains of these residues, together with surrounding water molecules, form a delicate architecture with the 8-oG damaged base that serves to "flip" the base out from the double helix and into the active site, exposing the glycosidic bond for cleavage (Figure 4.9).[7] A relaxed secondary structure could alter the relative orientation of these residues and possibly contribute to the loss of glycosylase activity by Cd(II)–MutM. Alternatively, conformational change within this pocketmay alter the hydrogen bond networks and/or surface charge of the inter-domain cleft. Regardless, HDX–MS clearly shows there is communication between the zinc finger and the active site that is essential for MutM activity.

The other solvent accessible peptides are located on the two hinges between N-terminal and C-terminal domain. These regions serve as the "walls" of the active site at the bottom of the cleft, helping to accommodate the leaving 8-oG base product. Additionally, DNA binding and damaged base excision requires the gripping motion of the hinges to bring the two domains closer.[9] If the hinge region is destabilized as is observed by increased deuterium exchange for Cd(II)–MutM, this could compromise MutM catalytic activity. Again, comparison of the DNA-bound MutM and DNA-free MutMstructures shows more structured hinges for the free MutM. Thus, the destabilization of these hingescaused by Cd(II) coordination may diminish the normal interactions between MutM and DNA that are necessary for 8-oG recognition and base extrusion. In comparison, the hinge region of Co(II)–MutM does not display changes in dynamics or solvent accessibility compared to Zn(II)–MutM. This supports the idea that a bigger metal ion

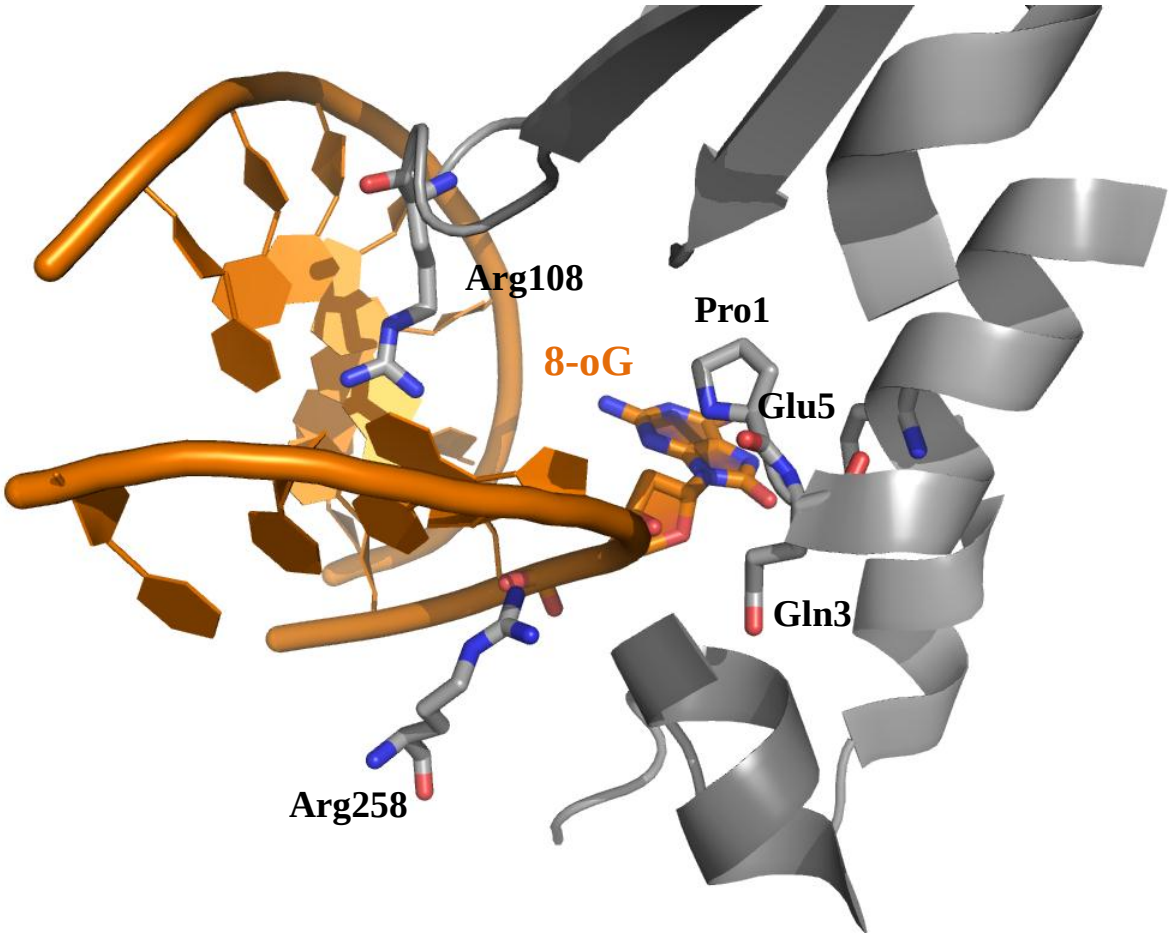

Figure 4.9. MutM–DNA interactions. Arg258 and Arg108 work in concert to separate the 8-oG:C base pair. Pro1 and Glu5 help to extrude the 8-oG base from the double helix.

coordinated at the zinc finger leads to opening of the pocket and/or increased backbone dynamics that would inhibit the glycosylase activity even if DNA is bound.

4.4.3 Conclusions and future directions

HDX–MS provides insight into the conformational change of MutM upon non-native metal binding leading to inhibition of the enzymatic activity. According to our data, Cd(II) binding protected and constrained the zinc finger and H2TH motifs, while increasing dynamic motions within the active site and hinge regions between the two domains. These changes can explain the absence of the Schiff base intermediate and decreased affinity for non-specific DNA we observed in Chapter 3. As expected, Co(II) binding does not cause significant change in the MutM structure. Thus, conformational changes caused by Cd(II) are mostly likely due to a longer ionic radius, even though Cd(II) is considered an isostructural substitute for Zn(II) and binds a variety of zinc finger proteins. It could also be the electronic properties of Cd(II) (*e.g.*, polarization, p*K*a effects, *etc.*), but these aspects require further investigation.

Overall, this work verifies that Cd(II) coordination to the zinc finger can trigger local conformational changesin the *E. coli* MutM DNA repair protein, which lead to lossof activity. We would expect similar results with the human homologue hOGG1.[10] This gives support for one proposed mechanism of Cd(II) co-carcinogenesis. In this case, Cd(II) could be a co-carcinogen with oxidative stress.[11,12]Through mechanisms unknown, Cd(II) induces oxidative stress in the cell, which leads to increased damage of DNA bases such as 8-oG. Due to the structural perturbation of DNA glycosylases by Cd(II), 8-oG modifications will accumulate from

lack of repair. Depending on where these unrepaired mutations occur in the genome, they could eventually lead to cancer.

4.5 REFERENCES

(1) Asmuss, M., Mullenders, L. H., Eker, A., and Hartwig, A. (2000) Differential effects of toxic metal compounds on the activities of Fpg and XPA, two zinc finger proteins involved in DNA repair. *Carcinogenesis21,* 2097–2104.

(2) Sugahara, M., Mikawa, T., Kumasaka, T., Yamamoto, M., Kato, R., Fukuyama, K., Inoue, Y., and Kuramitsu, S. (2000) Crystal structure of a repair enzyme of oxidatively damaged DNA, MutM (Fpg), from an extreme thermophile, Thermus thermophilus HB8. *EMBO J.19*, 3857–3869.

(3) Fromme, J. C., Bruner, S. D., Yang, W., Karplus, M., and Verdine, G. L. (2003) Product-assisted catalysis in base-excision DNA repair. *Nat. Struct. Biol.10,* 204–211.

(4) Busenlehner, L. S., and Armstrong, R. N. (2005) Insights into enzyme structure and dynamics elucidated by amide H/D exchange mass spectrometry. *Arch. Biochem. Biophys.433*, 34–46.

(5) Asuru, A. P., An, M., and Busenlehner, L. S. Dissection of porphyrin-induced conformational dynamics in the heme biosynthesis enzyme ferrochelatase. *Biochemistry51,* 7116–7127.

(6) Larkin, M. A., Blackshields, G., Brown, N. P., Chenna, R., McGettigan, P. A., McWilliam, H., Valentin, F., Wallace, I. M., Wilm, A., Lopez, R., Thompson, J. D., Gibson, T. J., and Higgins, D. G. (2007) Clustal W and Clustal X version 2.0. *Bioinformatics23,* 2947–2948.

(7) Gilboa, R., Zharkov, D. O., Golan, G., Fernandes, A. S., Gerchman, S. E., Matz, E., Kycia, J. H., Grollman, A. P., and Shoham, G. (2002) Structure of formamidopyrimidine-DNA glycosylase covalently complexed to DNA. *J. Biol. Chem.277,* 19811–19816.

(8) Buchko, G. W., Hess, N. J., and Kennedy, M. A. (2000) Cadmium mutagenicity and human nucleotide excision repair protein XPA: CD, EXAFS and $^{(1)}H/^{(15)}N$-NMR spectroscopic studies on the zinc(II)- and cadmium(II)-associated minimal DNA-binding domain (M98-F219). *Carcinogenesis21,* 1051–1057.

(9) Zharkov, D. O., Shoham, G., and Grollman, A. P. (2003) Structural characterization of the Fpg family of DNA glycosylases. *DNA Repair (Amst)2,* 839–862.

(10) Hamm, M. L., Gill, T. J., Nicolson, S. C., and Summers, M. R. (2007) Substrate specificity of Fpg (MutM) and hOGG1, two repair glycosylases. *J. Am. Chem. Soc.129*, 7724–7725.

(11) Arita, A., and Costa, M. (2009) Epigenetics in metal carcinogenesis: nickel, arsenic, chromium and cadmium. *Metallomics1*, 222–228.

(12) S., M., P., D. S., and B., S. R. (2010) A review of epigenetic effect of heavy metal carcinogens on human health. *The Open Nutraceuticals Journal 3*, 188–193.

CHAPTER 5

SUMMARY AND PERSPECTIVE

5.1 SUMMARY.

Although non-native metals including Co(II), Cd(II), As(III), and Pb(II) are well established carcinogens, the mechanism of the carcinogenesis is still not fully understood.[1,2] In this dissertation research, we investigated one of the proposed mechanisms: that these non-native metals substitute for the native metals in proteins and disrupt protein function. DNA repair proteins that contain zinc finger motif(s) are potential targets for these metals. In this work, we investigated whether two metals, Cd(II) and Co(II), could inhibit the DNA glycosylase MutM, which contains a Cys_4 zinc finger. We determined that Cd(II) and Co(II) form a 1:1 complex with MutM and that the metal ions are coordinated by cysteine thiolates in the zinc finger. In terms of metal binding affinity, MutM zinc finger prefers Zn(II) over Cd(II) and Co(II). Cd(II)–MutM has altered conformational dynamics that disable 8-oG recognition and inhibit excision activity (Figure 1.1). In comparison, Co(II)–MutM retains most of the properties of Zn(II)–MutM and little structural change is observed.

5.1.1 Inhibition of zinc finger proteins by Cd(II). According to the hard/soft–acid/base theory, Zn(II) is classified as a borderline metal ion that binds sulfur, oxygen, and nitrogen equally well, while Cd(II) is a soft metal ion which prefers thiolate ligands. Therefore, the Cys_4

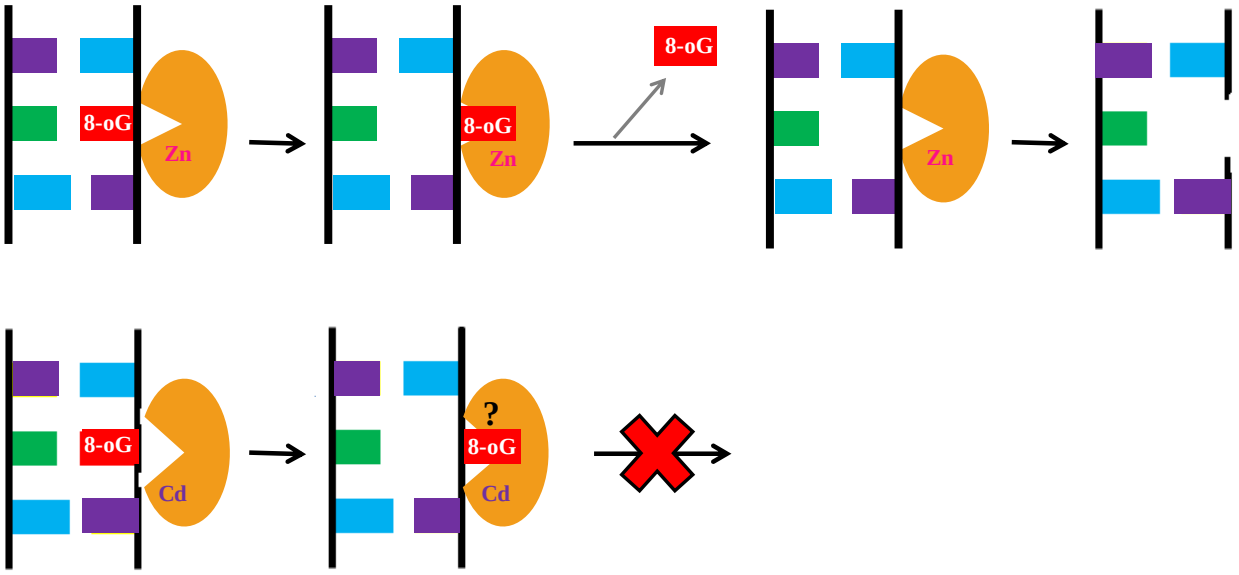

Figure 5.1. Schematic of the inhibition of MutM by Cd(II). Cd(II) coordination to the zinc finger causes conformational change at the active site of MutM and inhibits its glycosylase activity. It is not clear whether the 8-oG base is extruded from the helix in the Cd(II)-bound enzyme.

zinc finger is the most probable target for Cd(II) substitutionamong the commonly encountered zinc finger types. This has been confirmed by a previous study with truncated zinc finger motif peptides.[3] Zinc finger peptides with *both* Cys and His residues prefer Zn(II), while the Cys_4 type prefers Cd(II) over Zn(II) by a factor of $10^{3.3}$.[3] However, we observed a higher preference for Zn(II) over Cd(II) by MutM through both optical absorbance spectroscopy and activity assays under our experimental conditions. This contradiction indicates the importance of investigating the full-length zinc finger proteins since the hydrogen bonding network, as well as the hydrophobic interactions between zinc finger and other motifs, may stabilize the zinc finger. In this case, the ability of Cd(II), and potentially other non-native metals, to replace Zn(II) in a zinc finger protein is more dependent on the amino acid sequence, structure, and environment of the zinc finger instead of the type of zinc finger.

On the other hand, the replacement of Zn(II) by non-native metal ions is more likely to happen *in vivo* because the Cd(II)/MutM ratio could be much higher in the cell than in our experiments. Cd(II) concentrations in the cell could reach the micromolar range,[4] which is similar to that in our *in vitro* experiments; however, due to the detection limitations, we require the MutM concentration to be low micromolar. There is still discussion about the intracellular concentration of Cd(II) that is available to interact with zinc finger proteins since Cd(II) could be bound to metallothionein proteins in the cell. Metallothioneins (MT) are Cys–rich Zn(II) storage proteins that compete with zinc finger motifs for metal binding. MTs are known to bind many heavy metals including Cd(II) and Hg(I).[5] Although inhibition of MutM by MT-bound Cd(II) was observed,[6] a complete picture of competition among Zn(II), Cd(II), zinc finger, DNA and metallothioneins is necessary to elucidate the ability of Cd(II) to compete for Zn(II) in zinc fingers *in vivo*.

DNA repair proteins containing similar zinc finger motifs may perform completely different functions in the cell. For example, XPA and MutM are both Cys_4 type zinc finger proteins. While MutM is a tri-functional glycosylase/AP-lyase enzyme,[7] XPA is a DNA binding protein that recruits the nucleotide excision repair machinery to damaged DNA and has no enzymatic activity.[8] Therefore, it is necessary to point out the specific function or catalytic step that is inhibited by non-native metals in order to clarify the inhibition mechanism. We clearly determined that Cd(II) binding disables the first stage of MutM catalyzed reaction, namely, the damaged base (8-oG) recognition and excision; however, Co(II) did not. While the Cd(II) experiments support that non-native metals disrupt DNA binding of the zinc finger DNA repair proteins, care must be taken in making broad assumptions about all metals since Co(II) was not inhibitory.

5.1.2 The secondary Cd(II) binding site of MutM. In Chapter 4, we showed the protection of the beginning of αF (peptide 193–197) for Cd(II)–MutM. The αF is a flexible region during DNA binding.[9] This region includes Cys195, one of the two Cys residues outside the zinc finger. If this peptide is buried into the protein, Cys195 might be pulled closer to Cys147 in αC. The distance between the two sulfur groups from the Cys side chain is ~4.8 Å. (Figure 5.2). Compared with the distances between the zinc finger thiolates, normally 3–4 Å, these two Cys residues outside the zinc finger could potentially form a secondary metal binding site. In Chapter 2, a second Cd(II) binding on Cd(II)–MutM, but not on Zn(II)–MutM, was observed. Whether this secondary metal binding is due to the change in orientation of Cys195 upon Cd(II) binding is not known. To confirm the secondary Cd(II) binding site, we can compare the structure of the 2Cd(II)–MutM preparation and Cd(II)–MutM preparation through HDX–MS. If this secondary

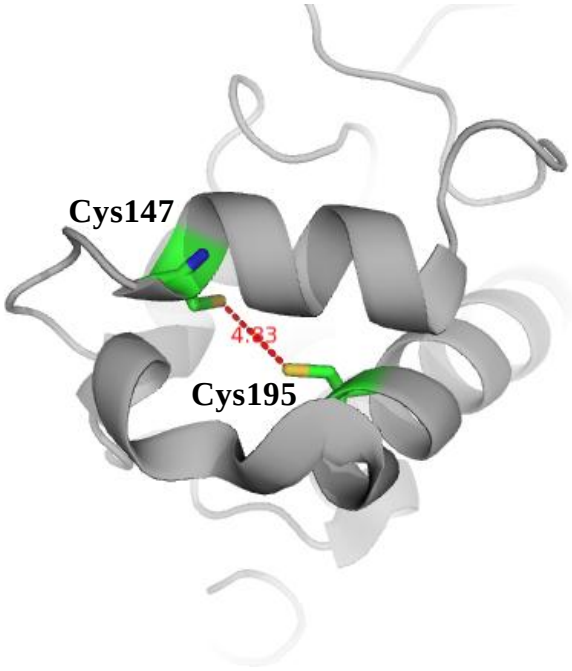

Figure 5.2. Orientation of Cys195 and Cys147. Distance between the thiolates is 4.8 Å, compared to that in a normal Cys_4 zinc finger (3–4 Å). As peptide 193–197 is protected upon Cd(II) binding to the zinc finger, these two Cys residues might be brought closer to each other.

Cd(II) binding site does exist, we should be able to observe further conformational change caused by the second Cd(II) binding.

5.1.3 Inhibition of zinc finger proteins by other non-native metals. Other metals that interfere with zinc finger DNA repair proteins include Cu(II), Hg(II), Co(II), Ni(II), As(III) and Pb(II).[6] Except for Cd(II), Pb(II) and Co(II), the competition of these metals with Zn(II) for zinc fingers has not been systematically studied. It is possible that the non-native metals could be inserted into the zinc finger during protein synthesis, when hydrogen bond networks are not fully formed. However, not all metals will be able to outcompete Zn(II). For example, Pb(II) is not adopted by MutM when provided in culture media or during purification. Whether Pb(II) is more preferred by the other types of zinc fingers is not known.Most zinc finger proteins which are inhibited by Pb(II) are DNA binding proteins but are not directly involved in DNA repair.[10]In addition, both Pb(II) and Hg(II) are consideredsoft acids, which prefer soft bases, (*i.e.*, thiolates). Unlike Pb(II), the simultaneous treatment of MutM with Zn(II) and Hg(II) did not prevent the inhibition of MutM by Hg(II). This indicated that the Hg(II)–S bond is thermodynamically strong.[11] Surprisingly, Hg(II) does not interfere with DNA binding by XPA, which also contains a Cys_4type zinc finger.[11]It is possible that the XPA zinc finger structure is more protected such that Hg(II) substitution is less likely to occur or the conformational changesin XPA caused by Hg(II) binding does not disturb DNA binding. In total, this means that not all Cys_4 zinc fingers behave similarly despite their inherent affinities for soft metals.

Cu(II), Ni(II), and Co(II) are borderline acids, which are not particularly preferred by any ligand. According to the ligand field stabilization energy (LFSE) theory, Co(II) is less preferred by all type of zinc fingers, compared to Zn(II).Co(II) is an isostructural substitute for Zn(II), with

very similar metal–ligand bond lengths. These observations are all supported by our workwith MutM, which is not inhibited by Co(II). In contrast, Co(II) interferes with XPA DNA binding, clearing demonstrating that the protein environment around the zinc finger is important to determining whether a metal will inhibit or not.[3]

5.1.4 Biological implications. As mentioned previously, although the metal ion/protein ratio is much higher in the cell than in our experiments, Zn(II) substitution in a full length protein is not as easy as people thought. The only way to ensure non-native metal incorporation by MutM was to provide the metals during protein expression and purification. To obtain the 1:1 metal–MutM complex, roughly a 20-fold excess of Cd(II) wasrequired, while >100- fold of Co(II) was required. Whether metal incorporation during protein synthesis accounts for inhibition of zinc finger proteins*in vivo* is something we can explore in the future.

Moreover, the two domain structure of MutM permits these domains to move during DNA binding. The αA and αF of the free MutM are flexible enough for accommodation of DNA. Also, the C-terminal loop that serves as a "wall" of the DNA binding pocket is crystallographically disordered in the MutM–DNA complex but ordered in the free protein.[12] As mentioned in our structural study, change in the metal–S bond length triggers a conformational change of the DNA binding pocket and the active site. Thus, conformational changes in the binding pocket following the DNA binding may also alter the metal binding environment of the zinc finger. It is interesting to explore the metal binding properties of DNA–bound MutM because a large fraction of MutM is complexed with DNA in the cell. Additionally, MutM adopts different conformational states for specific and non–specific DNA binding.[12] Consequently, a series of DNA–MutM complexes

could be tested for metal substitution. This will give us a better idea about how and when Zn(II) is replaced.

Demonstrating that non-native metal ions inhibit the DNA repair pathways by replacing Zn(II) from the zinc finger of DNA repair proteins is a complicated issue. The first point to consider is whether the metal ion can be adopted by the zinc finger under reasonable conditions. This is dependent on the specific metal ion considered, the zinc finger type, and the overall folding of the full length protein. Also, any motion of the protein, especially during DNA binding or catalytic action, may change Zn(II) accessibility. Secondly,one must consider whether the incorporation of a non-native metal ion inhibits the protein and, for multi-functional proteins, which step or steps are disturbed. This is determined by the mechanism of substitution and more importantly, the local/globular conformational change caused by the substitution. Take Cd(II) as an example; even though it is isostructural to Zn(II) in Cys_4 zinc fingers, it inhibits MutM glycosylase activity due to conformational changes at the active site but does not disturb a similar Cys_4 zinc finger protein XPA. Therefore, the inhibition of DNA repair proteins by non-native metals is different from case to case. It is not easy to figure out general trends as to which metals are toxic, and what type of zinc finger is likely to be inhibited.

Nevertheless, proteins with conserved motifs and functions might have similar metal inhibition patterns. Enzymes in the Fpg family, for example, have conserved zinc finger and H2TH motifs. These enzymes are all two-domain structured, with a DNA binding cleft between the two domains and a conserved active pocket at the bottom of the cleft. Thus, changes at the zinc finger may affect these enzymes in a similar way as in MutM. Neil2 and Neil3 are human glycosylases belonging to Fpg family (Figure 5.3).[13,14]These two enzymes share very similar zinc

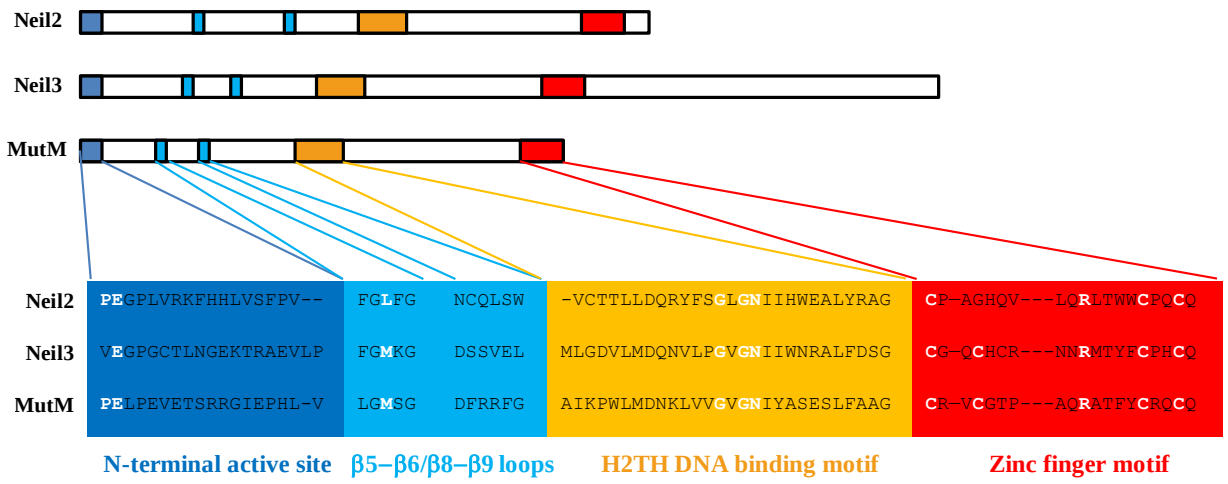

Figure 5.3. Alignment of MutM, Neil2 and Neil3. Neil2 and Neil3 are human glycosylases in the Fpg family. They share conserved active site, H2TH DNA binding motif and the zinc finger motif as MutM.

finger motifs with MutM. They both have the conserved Arg on the β-hairpin of the zinc finger, which is essential in 8-oG recognition. For Neil2, the zinc finger is located at the C- terminus of the protein similar to MutM whereas Neil3 has an extended C-terminal domain. Both enzymes have the H2TH DNA binding motif with conserved Gly and Asn residues, whose side chains form hydrogen bonding networks with the zinc finger to maintain the relative arrangement between the motifs. There is also a conserved hydrophobic amino acid residue on one of the loops of the N-terminal domain analogous to Met73 between β5–β6 in MutM. This amino acid residue inserts into the DNA helix and interrupts base–stacking. Finally, they share the N-terminal active site, which is at the bottom of the DNA binding cleft. A conserved Glu is responsible for accommodating the leaving 8-oG while Pro (conserved in Neil3 but not in Neil2) makes a nucleophilic attack on the C1′ of the pentose to open the ring.[12] Thus, conformational changes of the zinc finger, H2TH motif, and the active pocket as well as the loss of glycosylase activity caused by Cd(II) coordination to zinc finger are very likely to apply to Neil2 and Neil3. We can infer that since Zn(II) could be replacedby an excess amount of Cd(II) in MutM, glycosylase activity of similar enzymes are probably inhibited as well. This is likely due to changes in orientation of essential amino acid residues and hydrogen bonding network. Co(II)–Neil2 and Co(II)–Neil3, like Co(II)–MutM, should perform normal glycosylase activity.

5.2 CONCLUSION

Our work with MutM provides the first insight into the structural and dynamic changes of a full length zinc finger protein upon Cd(II) binding. We reveal that Cd(II) coordination in the zinc finger led to small but important conformational changes detected by HDX–MS. The

Cd(II)−MutM zinc finger adopts a slightly longer metal–S bond, and that could account for the loss of sequence specific DNA binding, as well as catalytic activity. However, no such conformational changes were observed for Co(II), which may be related to the shorter Co(II)–S bond. The overall structural analysis of MutM again demonstrates the importance of investigation of full length zinc finger proteins when exploring the non-native metal inhibition. Studies of truncated zinc fingers shed light on the general trend of their metal binding preference; however, these trends may not be observed in the full length proteins.

5.3 REFERENCES

(1) Hamilton, J. W., Kaltreider, R. C., Bajenova, O. V., Ihnat, M. A., McCaffrey, J., Turpie, B. W., Rowell, E. E., Oh, J., Nemeth, M. J., Pesce, C. A., and Lariviere, J. P. (1998) Molecular basis for effects of carcinogenic heavy metals on inducible gene expression. *Environ. Health Perspect.106 Suppl 4*, 1005−1015.

(2) Beyersmann, D., and Hartwig, A. (2008) Carcinogenic metal compounds: Recent insight into molecular and cellular mechanisms. *Arch. Toxicol.82*, 493–512.

(3) Witkiewicz-Kucharczyk, A., and Bal, W. (2006) Damage of zinc fingers in DNA repair proteins, a novel molecular mechanism in carcinogenesis. *Toxicol. Lett.162*, 29–42.

(4) Ahlgren, L., and Mattsson, S. (1981) Cadmium in man measured in vivo by X-ray fluorescence analysis. *Phys. Med. Biol.26*, 19–26.

(5) Klaassen, C. D., Liu, J., and Choudhuri, S. (1999) Metallothionein: An intracellular protein to protect against cadmium toxicity. *Annu. Rev. Pharmacol. Toxicol.39*, 267–294.

(6) Hartwig, A., Asmuss, M., Blessing, H., Hoffmann, S., Jahnke, G., Khandelwal, S., Pelzer, A., and Burkle, A. (2002) Interference by toxic metal ions with zinc-dependent proteins involved in maintaining genomic stability. *Food. Chem. Toxicol.40*, 1179–1184.

(7) Morland, I., Rolseth, V., Luna, L., Rognes, T., Bjoras, M., and Seeberg, E. (2002) Human DNA glycosylases of the bacterial Fpg/Mutm superfamily: An alternative pathway for the repair of 8-oxoguanine and other oxidation products in DNA. *Nucleic Acids Res.30*, 4926–4936.

(8) Li, L., Lu, X., Peterson, C. A., and Legerski, R. J. (1995) An interaction between the DNA repair factor XPA and replication protein a appears essential for nucleotide excision repair. *Mol. Cell Biol.15*, 5396–5402.

(9) Gilboa, R., Zharkov, D. O., Golan, G., Fernandes, A. S., Gerchman, S. E., Matz, E., Kycia, J. H., Grollman, A. P., and Shoham, G. (2002) Structure of formamidopyrimidine-DNA glycosylase covalently complexed to DNA. *J. Biol. Chem.277*, 19811–19816.

(10) Hanas, J. S., Rodgers, J. S., Bantle, J. A., and Cheng, Y. G. (1999) Lead inhibition of DNA-binding mechanism of $Cys_{(2)}His_{(2)}$ zinc finger proteins. *Mol. Pharmacol.56*, 982–988.

(11) Asmuss, M., Mullenders, L. H., Eker, A., and Hartwig, A. (2000) Differential effects of toxic metal compounds on the activities of Fpg and XPA, two zinc finger proteins involved in DNA repair. *Carcinogenesis21*, 2097–2104.

(12) Zharkov, D. O., Shoham, G., and Grollman, A. P. (2003) Structural characterization of the Fpg family of DNA glycosylases. *DNA Repair (Amst)2*, 839–862.

(13) Dou, H., Mitra, S., and Hazra, T. K. (2003) Repair of oxidized bases in DNA bubble structures by human DNA glycosylases Neil1 and Neil2. *J. Biol. Chem.278*, 49679–49684.

(14) Sejersted, Y., Hildrestrand, G. A., Kunke, D., Rolseth, V., Krokeide, S. Z., Neurauter, C. G., Suganthan, R., Atneosen-Asegg, M., Fleming, A. M., Saugstad, O. D., Burrows, C. J., Luna, L., and Bjoras, M. Endonuclease VIII-like 3 (Neil3) DNA glycosylase promotes neurogenesis induced by hypoxia-ischemia. *Proc. Natl. Acad. Sci. U. S. A.108*, 18802–18807.